

AD 746834

WANL-FR-M-72-003

MODIFICATION AND CONTROL OF OXIDE STRUCTURES
ON METALS AND ALLOYS: (PHASE II)

Final Report
(20 November 1970 - 20 December 1971)
February, 1972

This document is subject to special export controls
and each transmittal to foreign governments or
foreign nationals may be made only with the approval
of the Naval Air Systems Command.

APPROVED FOR PUBLIC RELEASE;
DISTRIBUTION UNLIMITED

by

R. C. Svedberg

Prepared Under Contract N00019-71-C-0089

for

NAVAL AIR SYSTEM COMMAND

Department of the Navy
Washington, D. C. 20360

Attn: I. Machlin
NASC-AIR 52031 B



ASTRONUCLEAR LABORATORY
WESTINGHOUSE ELECTRIC CORPORATION

Westinghouse Electric Corporation - P. O. Box 10864 - Pittsburgh, Pa. 15236

Reproduced by
NATIONAL TECHNICAL
INFORMATION SERVICE
U S Department of Commerce
Springfield VA 22151

106

Unclassified

Security Classification

DOCUMENT CONTROL DATA - R&D

(Security classification of title, body of abstract and indexing annotation must be entered when the overall report is classified)

1. ORIGINATING ACTIVITY (Corporate author) Westinghouse Astronuclear Laboratory P. O. Box 10864 Pittsburgh, Pennsylvania 15236		2a. REPORT SECURITY CLASSIFICATION Unclassified	
		2b. GROUP N/A	
3. REPORT TITLE Modification and Control of Oxide Structures on Metals and Alloys: (Phase II)			
4. DESCRIPTIVE NOTES (Type of report and inclusive dates) Final Technical Report - 20 November 1970 to 20 December 1971			
5. AUTHOR(S) (Last name, first name, initial) Svedberg, Robert C.			
6. REPORT DATE February, 1972		7a. TOTAL NO. OF PAGES 106	7b. NO. OF REFS 33
8a. CONTRACT OR GRANT NO. N00019-71-C-0089		9a. ORIGINATOR'S REPORT NUMBER(S) WANL-FR-M-72-003	
b. PROJECT NO. APPROVED FOR PUBLIC RELEASE; DISTRIBUTION UNLIMITED		9b. OTHER REPORT NO(S) (Any other numbers that may be assigned this report)	
10. AVAILABILITY/LIMITATION NOTICES This document is subject to special export controls and each transmittal to foreign governments or foreign nationals may be made only with the approval of the Naval Air Systems Command			
11. SUPPLEMENTARY NOTES		12. SPONSORING MILITARY ACTIVITY Naval Air Systems Command Washington, D. C. 20360	
13. ABSTRACT The chemical diffusion coefficient of oxygen in Nb ₂ O ₅ at 967°C, in 1.67/1.00 mole ratio TiO ₂ :Nb ₂ O ₅ niobate at 819°C and in a 2.85/1.00 mole ratio HfO ₂ :Nb ₂ O ₅ niobate at 786, 983, and 1192°C were determined using a thermogravimetric technique whereby the rate of change of oxygen composition was measured as a function of time as equilibrium was being achieved with a constant oxygen partial pressure. The chemical diffusion coefficients measured were dependent on the deviation from stoichiometry as well as temperature. The variation of the chemical diffusion coefficient is thought to be the result of the formation of various equilibrium phases formed as a result of the oxygen deficiency of the niobates. NiO-Nb ₂ O ₅ and Al ₂ O ₃ -Nb ₂ O ₅ systems did not show indications of nonstoichiometric behavior as did the niobates containing TiO ₂ and HfO ₂ . The oxidation behavior of niobium alloy B-1 (Nb-15Ti-10Ta-10W-2Hf-3Al) is reported for temperatures of 800, 1000, and 1200°C. The parabolic rate constant for the B-1 alloy was found to be $k_p = (4.24 \pm 1.6 \times 10^{-7}) \exp \left[\frac{48,000 \pm 9,500 \text{ cal}}{RT} \right] \text{ mg}^2/\text{cm}^4/\text{min}$ Chemically active Ti was found in one of the reaction layers between the oxide and metal substrate using electron microprobe techniques. Oxidation behavior of Nb in air is shown to be a function of preoxidation treatment in low oxygen partial pressures and can be related to the amount of NbO formed during the pretreatment exposure.			

Security Classification

14. KEY WORDS	LINK A		LINK B		LINK C	
	ROLE	WT	ROLE	WT	ROLE	WT
Oxide						
Defect Structure						
Oxygen Diffusion Coefficient						
Niobates						
Niobium Alloy Oxidation						
Oxygen Transport in Niobates						

INSTRUCTIONS

1. **ORIGINATING ACTIVITY:** Enter the name and address of the contractor, subcontractor, grantee, Department of Defense activity or other organization (*corporate author*) issuing the report.

2a. **REPORT SECURITY CLASSIFICATION:** Enter the overall security classification of the report. Indicate whether "Restricted Data" is included. Marking is to be in accordance with appropriate security regulations.

2b. **GROUP:** Automatic downgrading is specified in DoD Directive 5200.10 and Armed Forces Industrial Manual. Enter the group number. Also, when applicable, show that optional markings have been used for Group 3 and Group 4 as authorized.

3. **REPORT TITLE:** Enter the complete report title in all capital letters. Titles in all cases should be unclassified. If a meaningful title cannot be selected without classification, show title classification in all capitals in parenthesis immediately following the title.

4. **DESCRIPTIVE NOTES:** If appropriate, enter the type of report, e.g., interim, progress, summary, annual, or final. Give the inclusive dates when a specific reporting period is covered.

5. **AUTHOR(S):** Enter the name(s) of author(s) as shown on or in the report. Enter last name, first name, middle initial. If military, show rank and branch of service. The name of the principal author is an absolute minimum requirement.

6. **REPORT DATE:** Enter the date of the report as day, month, year, or month, year. If more than one date appears on the report, use date of publication.

7a. **TOTAL NUMBER OF PAGES:** The total page count should follow normal pagination procedures, i.e., enter the number of pages containing information.

7b. **NUMBER OF REFERENCES:** Enter the total number of references cited in the report.

8a. **CONTRACT OR GRANT NUMBER:** If appropriate, enter the applicable number of the contract or grant under which the report was written.

8b, 8c, & 8d. **PROJECT NUMBER:** Enter the appropriate military department identification, such as project number, subproject number, system numbers, task number, etc.

9a. **ORIGINATOR'S REPORT NUMBER(S):** Enter the official report number by which the document will be identified and controlled by the originating activity. This number must be unique to this report.

9b. **OTHER REPORT NUMBER(S):** If the report has been assigned any other report numbers (*either by the originator or by the sponsor*), also enter this number(s).

10. **AVAILABILITY/LIMITATION NOTICES:** Enter any limitations on further dissemination of the report, other than those

imposed by security classification, using standard statements such as:

- (1) "Qualified requesters may obtain copies of this report from DDC."
- (2) "Foreign announcement and dissemination of this report by DDC is not authorized."
- (3) "U. S. Government agencies may obtain copies of this report directly from DDC. Other qualified DDC users shall request through _____."
- (4) "U. S. military agencies may obtain copies of this report directly from DDC. Other qualified users shall request through _____."
- (5) "All distribution of this report is controlled. Qualified DDC users shall request through _____."

If the report has been furnished to the Office of Technical Services, Department of Commerce, for sale to the public, indicate this fact and enter the price, if known.

11. **SUPPLEMENTARY NOTES:** Use for additional explanatory notes.

12. **SPONSORING MILITARY ACTIVITY:** Enter the name of the departmental project office or laboratory sponsoring (paying for) the research and development. Include address.

13. **ABSTRACT:** Enter an abstract giving a brief and factual summary of the document indicative of the report, even though it may also appear elsewhere in the body of the technical report. If additional space is required, a continuation sheet shall be attached.

It is highly desirable that the abstract of classified reports be unclassified. Each paragraph of the abstract shall end with an indication of the military security classification of the information in the paragraph, represented as (TS), (S), (C), or (U).

There is no limitation on the length of the abstract. However, the suggested length is from 150 to 225 words.

14. **KEY WORDS:** Key words are technically meaningful terms or short phrases that characterize a report and may be used as index entries for cataloging the report. Key words must be selected so that no security classification is required. Identifiers, such as equipment model designation, trade name, military project code name, geographic location, may be used as key words but will be followed by an indication of technical context. The assignment of links, roles, and weights is optional.

WANL-FR-M-72-003

**MODIFICATION AND CONTROL OF OXIDE STRUCTURES
ON METALS AND ALLOYS: (PHASE II)**

Final Report
(20 November 1970 - 20 December 1971)
February, 1972

This document is subject to special export controls and each transmittal to foreign governments or foreign nationals may be made only with the approval of the Naval Air Systems Command.

by

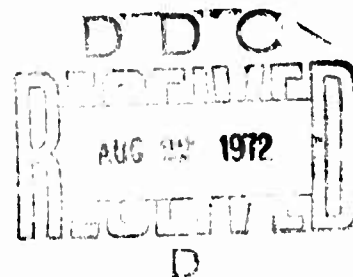
R. C. Svedberg APPROVED FOR PUBLIC RELEASE
DISTRIBUTION UNLIMITED

Prepared Under Contract N00019-71-C-0089

for

NAVAL AIR SYSTEM COMMAND

Department of the Navy
Washington, D. C. 20360
Attn: I. Machlin
NASC-AIR 52031 B



ASTRONUCLEAR LABORATORY
WESTINGHOUSE ELECTRIC CORPORATION

Westinghouse Electric Corporation - P. O. Box 10864 - Pittsburgh, Pa. 15236

TABLE OF CONTENTS

<u>Section</u>	<u>Page No.</u>
1 INTRODUCTION AND SUMMARY	1
2 REVIEW OF OXYGEN TRANSPORT IN HIGH TEMPERATURE OXIDES	6
2.1 Relating D Values to Metal Consumed	6
2.2 Compilation of Diffusion Data	8
3 OXYGEN DIFFUSION THROUGH MIXED NIOBATES	19
3.1 Thermogravimetric Techniques for Determining the Oxygen Diffusion Coefficient	19
3.1.1 Rationale for Sample Geometry	19
3.1.2 Solutions to Fick's Second Law	21
3.2 Experimental Materials	23
3.3 Experimental Apparatus	26
3.3.1 Furnace	26
3.3.2 Balance	26
3.3.3 Gas	28
3.4 Procedure for Use of the Cahn Microbalance	28
3.5 Experimental Results and Discussion	30
3.5.1 Nb_2O_5	36
3.5.2 $TiO_2-Nb_2O_5$	44
3.5.3 $HfO_2-Nb_2O_5$	47
4 ANALYSIS OF THE OXIDATION BEHAVIOR OF A Nb-15Ti-10W-10Ta-2Hf-3Al ALLOY B-1	52
4.1 Experimental Apparatus and Procedure	52
5 EFFECTS OF LOW OXYGEN PARTIAL PRESSURE PREOXIDATION EXPOSURE ON THE AIR OXIDATION BEHAVIOR OF Nb	74

TABLE OF CONTENTS (continued)

<u>Section</u>		<u>Page No.</u>
6	CONCLUSIONS	77
7	REFERENCES	78
	APPENDIX A - DATA COMPILATION	80

LIST OF TABLES

<u>Table No.</u>	<u>Title</u>	<u>Page</u>
1	Preliminary Values of the Chemical Diffusion Coefficients of Oxygen in Nb_2O_5 and Other Niobates	5
2	Diffusion Coefficients for Various Oxidation Times and Oxide Thickness	9
3	List of Mobile Species in Matrices Which Have Shown Low Transport Rates	13-14
4	List of D_0 and Q Values for Diffusion of Species in Oxides Listed in Table 3	15-16
5	Chemical Diffusion Coefficients for $\alpha - \text{Nb}_2\text{O}_5$ at 900°C (Ref. 9)	17
6	Comparative Parameters Used to Evaluate Oxide Geometry	20
7	Experimental Materials for Making Mixed Niobates and the Experimental Composition	24
8	Validity Test for the Application of the Diffusion Models	38-39
9	Comparison of the Chemical Diffusion Coefficients Calculated from the Slope of $\log \left(\frac{1 - M(t)}{Q} \right)$ vs t with that Calculated from the Parabolic Constant	41
10	Parabolic Oxidation Constants for the Initial Oxidation of B-1 Alloys	68
11	Oxides Found on Pre-oxidized Nb Before Air Exposure	75

LIST OF FIGURES

<u>Figure No.</u>	<u>Title</u>	<u>Page No.</u>
1	Iso-diffusion Coefficient Plot Showing Metal Consumed as a Function of Time for Various Values of the Chemical Diffusion Coefficient Through the Oxide	10
2	Diffusion Coefficients for Cations and Anions Through Oxides Suitable for Elevated Temperature Service	11
3	Diffusion Coefficients for Cations and Anions Through Oxides Suitable for Elevated Temperature Service	12
4	Pellets Sintered in H ₂ Furnace for 16 Hours at 1420°C. (All Pellets were 7/8 in. dia. Before Sintering.)	25
5	Modified Vacuum Microbalance Used for Flowing Gas Studies	27
6	Weight Losses for Nb ₂ O ₅ as a Function of Time for Various Oxygen Partial Pressure Differentials at 967°C	31
7	Weight Losses for 1.67:1 Molar Ratio TiO ₂ -Nb ₂ O ₅ as a Function of Time for Various Oxygen Partial Pressure Differentials at 819°C	32
8	Weight Losses for 2.85:1 Molar Ratio HfO ₂ -Nb ₂ O ₅ as a Function of Time for Various Oxygen Partial Pressure Differentials at 786°C	33
9	Weight Losses for 2.85:1 Molar Ratio HfO ₂ -Nb ₂ O ₅ as a Function of Time for Various Oxygen Partial Pressure Differentials at 983°C	34
10	Weight Losses for 2.85:1 Molar Ratio HfO ₂ -Nb ₂ O ₅ as a Function of Time for Various Oxygen Partial Pressure Differentials at 1192°C	35
11	Plot of $-\log (1-M(t)/Q)$ vs Time Used to Determine the Chemical Diffusion Coefficients of Oxygen in Nb ₂ O ₅ at 967°C	37
12	Plot of $(M(t)/A)^2$ vs Time Used to Determine the Chemical Diffusion Coefficients of Oxygen in Nb ₂ O ₅ at 967°C for Short Times	40
13	Nonstoichiometry in α -Nb ₂ O ₅ as a Function of Oxygen Partial Pressure	43
14	Plot of $-\log (1-M(t)/Q)$ vs Time Used to Determine the Chemical Diffusion coefficients of Oxygen in a 1.67:1 TiO ₂ -Nb ₂ O ₅ Oxide at 819°C	45
15	Nonstoichiometry in 1.67:1 TiO ₂ -Nb ₂ O ₅ as a Function of Oxygen Partial Pressure	46

LIST OF FIGURES (Continued)

<u>Figure No.</u>	<u>Title</u>	<u>Page No.</u>
16	Plot of $-\log (1-M(t)/Q)$ vs Time Used to Determine the Chemical Diffusion Coefficients of Oxygen in a 2.85:1 $\text{HfO}_2\text{-Nb}_2\text{O}_5$ Oxide at 786°C	48
17	Plot of $-\log (1-M(t)/Q)$ vs Time Used to Determine the Chemical Diffusion Coefficients of Oxygen in a 2.85:1 $\text{HfO}_2\text{-Nb}_2\text{O}_5$ Oxide at 983°C	49
18	Plot of $-\log (1-M(t)/Q)$ vs Time Used to Determine the Chemical Diffusion Coefficients of Oxygen in a 2.85:1 $\text{HfO}_2\text{-Nb}_2\text{O}_5$ Oxide at 1192°C	50
19	Nonstoichiometry in 2.85:1 $\text{HfO}_2\text{-Nb}_2\text{O}_5$ as a Function of Oxygen Partial Pressure	51
20	Effects of Al Content on the Oxidation Rate of B-1 Alloys	54
21	Comparison of the Oxidation Rate of B-1 at 1100°C After One Hour at 1300°C with B-1 Oxidation at 1000°C	55
22	Photomicrograph of the Oxide Scale Formed on B-1 After One Hour at 1300°C and 3 Hours at 1100°C	56
23	Weight Gain as a Function of Time for B-1 Alloys with 3.42 Al Oxidized at 800, 1000, and 1200°C in Air	58
24	Oxide Scales on a B-1 Alloy Oxidized in Air at 800°C for the Times Indicated	59
25	Oxide Scales on a B-1 Alloy Oxidized in Air at 1000°C for the Times Indicated	60
26	Oxide Scales on a B-1 Alloy Oxidized in Air at 1200°C for the Times Indicated	61
27	Microprobe Scan of Ti, Nb, and Ta Across the Structure Formed During Oxidation of a B-1 Alloy at 1060°C for 3 Hours	62
28	Rate of Growth of Various Zones in B-1 as a Function of Time at 800°C	63
29	Rate of Growth of Various Zones in B-1 as a Function of Time at 1000°C	64
30	Rate of Growth of Various Zones in B-1 as a Function of Time at 1200°C	65
31	Plot of $(M(t)/A)^2$ vs Time Used to Determine the Parabolic Oxidation Constant for B-1 at 800°C	67
32	Plot of $(M(t)/A)^2$ vs Time Used to Determine the Parabolic Oxidation Constant for B-1 at 1000°C	69

LIST OF FIGURES (Continued)

<u>Figure No.</u>	<u>Title</u>	<u>Page No.</u>
33	Plot of $(M(t)/A)^2$ vs Time Used to Determine the Parabolic Oxidation Constant for B-1 at 1200°C	70
34	Plot of $(M(t)/A)^2$ vs Time Used to Determine the Parabolic Oxidation Constant for B-1 at 1260°C	71
35	Plot of the Parabolic Rate Constant vs $1/T$ Used to Calculate the Activation Energy for the Initial Diffusion Controlled Oxidation Process Found in B-1 Alloys	73
36	Effect of Pre-exposure to Low Partial Pressure Oxygen on the Air Oxidation Rate of Nb	76

DEFINITION OF TERMS

\tilde{D}	=	Chemical Diffusion Coefficient (cm^2/sec)
t	=	Time (sec)
Q	=	Total weight loss between two equilibration conditions (grams)
A	=	Cross sectional area (cm^2)
k_p	=	Parabolic rate constant ($\text{mg}^2/\text{cm}^4\text{-min}$)
T	=	Temperature ($^{\circ}\text{C}$)
J_o	=	Oxygen flux ($\text{grams}/\text{cm}^2/\text{sec}$)
P_m	=	Density of structural material (grams/cm^3)
k	=	ratio $\frac{\text{moles of oxygen}}{\text{moles of metal}}$
T	=	Thickness of structural material consumed (cm)
J_m	=	Cation Flux Through Oxide ($\text{grams}/\text{cm}^2/\text{sec}$)
Φ	=	Pilling-Bedworth ratio
l	=	1/2 thickness of oxide (cm)
X	=	Diffusion Distance (cm)
P_{O_2}	=	Partial pressure of oxygen (atm)
D_i^s	=	Self-diffusion Coefficient (cm^2/sec)
J_i	=	Flux of ith species ($\text{grams}/\text{cm}^2/\text{sec}$)
C	=	Concentration (grams/cm^3)
$M(t)$	=	Weight loss at any time t (grams)
\tilde{D}_{k_p}	=	Chemical diffusion coefficient derived for the condition $\tilde{D}t/l^2 \leq .15$ using a parabolic model (cm^2/sec)

FOREWORD

The work described herein was performed at the Astronuclear Laboratory of the Westinghouse Electric Corporation under Navy Contract N00019-71-C-0089. This report is a continuation of the work started under Navy Contract N00019-70-C-0148. Mr. I. Machlin of the Naval Air Systems Command served as Project Manager. Program supervision at WANL was by Mr. R. W. Buckman, Jr., Manager, Materials Science.

The author wishes to acknowledge additional personnel contributing to this program. These are Mr. S. S. Laciak for metallography, Messrs. R. W. Conlin and A. W. Danko for x-ray and microprobe studies, and Mr. C. S. Fitterer for heat treating and general assistance.

ABSTRACT

The chemical diffusion coefficient of oxygen in Nb_2O_5 at 967°C , in 1.67/1.00 mole ratio $\text{TiO}_2:\text{Nb}_2\text{O}_5$ niobate at 819°C and in a 2.85/1.00 mole ratio $\text{HfO}_2:\text{Nb}_2\text{O}_5$ niobate at 786, 983, and 1192°C were determined using a thermogravimetric technique whereby the rate of change of oxygen composition was measured as a function of time as equilibrium was being achieved with a constant oxygen partial pressure. The chemical diffusion coefficients measured were dependent on the deviation from stoichiometry as well as temperature. The variation of the chemical diffusion coefficient is thought to be the result of the formation of various equilibrium phases formed as a result of the oxygen deficiency of the niobates. $\text{NiO}-\text{Nb}_2\text{O}_5$ and $\text{Al}_2\text{O}_3-\text{Nb}_2\text{O}_5$ systems did not show indications of nonstoichiometric behavior as did the niobates containing TiO_2 and HfO_2 . The oxidation behavior of niobium alloy B-1 ($\text{Nb}-15\text{Ti}-10\text{Ta}-10\text{W}-2\text{Hf}-3\text{Al}$) is reported for temperatures of 800, 1000, and 1200°C . The parabolic rate constant for the B-1 alloy was found to be

$$k_p = (4.24 \pm 1.6 \times 10^{-7}) \exp \left[\frac{48,000 \pm 9,500 \text{ cal}}{RT} \right] \text{ mg}^2/\text{cm}^4/\text{min}$$

Chemically active Ti was found in one of the reaction layers between the oxide and metal substrate using electron microprobe techniques. Oxidation behavior of Nb in air is shown to be a function of preoxidation treatment in low oxygen partial pressures and can be related to the amount of NbO formed during the pretreatment exposure.

I. INTRODUCTION AND SUMMARY

This study was initiated to investigate the feasibility of modifying oxide defect structures to enhance oxidation protection of elevated temperature structural materials. Materials capable of performing at temperatures in excess of 2000°F in oxidizing environments without degradation are being demanded for use in air breathing propulsion engines and power generation systems. The great majority of the research effort to provide materials capable of fulfilling the requirements of structural integrity at elevated temperatures and in oxidizing environments have involved attempts to increase oxidation resistance by adding additional alloying elements to the basic structural material or by coating the basic structural alloy with an oxidation resistant material. However, alloying to obtain oxidation resistance, in most cases, alters the mechanical strength and ductility of the base structural material while coating to obtain oxidation resistance requires the application of a foreign refractory compound which must adhere to but not react with the structural substrate. In addition, coatings are also subject to damage by thermal shock and physical impact. It is generally held that coatings, which are necessary to insure structural integrity, are not acceptable; only coatings which will prolong lifetimes are currently used in most applications.

The approach for providing oxidation protection being investigated in this program is considered rather unique in light of the prior research and development programs reported in the literature. Techniques are being investigated which are designed to modify the defect structure of equilibrium oxides which are characteristic of the parent structural material. In this way an improvement in oxidation resistance can be realized without changing the structural and mechanical properties of the substrate or adding additional phases or compounds to the system. Modifying the parent oxide to decrease the transport of anions and cations through the lattice, or to improve the adherence between the oxide and the substrate by stabilizing a denser oxide phase will improve the oxidation resistance.

The Phase I study has shown that high pressure high temperature exposure of Nb_2O_5 does produce a denser phase that maintains its characteristics after quenching to room temperature⁽¹⁾. However, it has not yet been possible to investigate the stability or the transport properties of the quenched phases. In addition, two different preexposure treatments have been shown to result in reduced oxidation rates in air for alloy B-1 (Nb-15Ti-10W-10Ta-2Hf-3Al). The first preexposure in 20 torr oxygen at 650°C caused a decrease in the oxidation rate in air at 1040°C when compared to an untreated B-1 alloy. The second method of pretreatment involved an oxidation exposure at 2400°F in air for one hour which improved the oxidation during exposure to air at 2200°F ⁽²⁾. Also, during Phase I the ability to form mixed oxide structures on Nb, Ta, and the B-1 alloy at low temperatures was demonstrated. A tapiolite (rutile) structure was formed on these materials in an aqueous autoclave doped with Fe^{3+} (ferric) ions. While these experiments have shown that altering the oxide structure is possible, the maximum potential of these various techniques has yet to be demonstrated.

The literature was also reviewed during Phase I to determine if any measurements describing the rate of diffusion of oxygen through mixed refractory metal oxide scales had been reported. This review showed that this kind of information does not exist. Concurrent with this lack of diffusion data is an incomplete understanding of the defect structures and transport mechanisms which control the diffusion of oxygen through these scales. Resulting from this review, the published compilations^(3,4) of transport properties of oxygen through the oxides of various high temperature structural materials were brought up to date.

Much of the available oxide diffusion data has been compiled and calculated for purposes of direct comparison and is presented in a later section. In analyzing this data, one must consider the experimental techniques used as well as the degree of refinement used to characterize the material under investigation. In addition, there are large discrepancies between investigations on the same oxide material. However, the data available does give a good indication of the relative transport properties of the oxides.

It becomes necessary to know and understand the transport processes in these oxides if one is to engineer a protective oxide. In addition, the plasticity of oxides must be controlled, and work in this area is being actively pursued⁽⁵⁾. One must know whether an ideal oxide structure possesses sufficiently slow oxygen transport properties to provide a protective film; for if one can achieve a degree of adherence between an oxide and its substrate, the rate of anion or cation transport through the oxide still determines the rate of oxidation protection afforded by the oxide. A knowledge of this transport rate is therefore essential when choosing systems for further investigation; for even if one could guarantee and achieve a coherent oxide-substrate system, oxygen transport rates will ultimately determine the rate of oxidation.

As a result, primary effort during Phase II was therefore directed toward examining the chemical diffusion coefficient of oxygen in mixed niobates, namely $\text{Nb}_2\text{O}_5 + \text{TiO}_2$, ZrO_2 , HfO_2 , Al_2O_3 , Cr_2O_3 , NiO , Co_3O_4 , Fe_3O_4 , and V_2O_5 . Binary oxide compositions were selected to form single phase compounds based on the work of Goldschmidt⁽⁶⁾. Mixed oxide discs were prepared by mixing, cold pressing, and sintering the elemental oxide powders. Transport rates were measured at 800, 1000, and 1200°C in oxygen partial pressures between 0.20 atm. and 10^{-22} atm.

The rate of change of weight due to oxygen removal was determined continuously using a Cahn RH recording microbalance. Of the oxides mentioned above, $\text{TiO}_2\text{-Nb}_2\text{O}_5$, $\text{HfO}_2\text{-Nb}_2\text{O}_5$, and Nb_2O_5 exhibited deviations from stoichiometry as a function of oxygen partial pressure. Two separate $\text{NiO-Nb}_2\text{O}_5$ systems showed no deviation from stoichiometry until an apparent reduction reaction began and then very large weight losses were recorded. $\text{Al}_2\text{O}_3\text{-Nb}_2\text{O}_5$ exhibited a mixed behavior which has yet to be rationalized. The remaining systems will be evaluated during Phase III of this continuing program. The phases, which exhibited regions of nonstoichiometry, also exhibited sufficiently large oxygen diffusion coefficients to disqualify them from consideration as an oxygen diffusion barrier.

In the case of $\text{NiO-Nb}_2\text{O}_5$ the oxygen partial pressure at which reduction began indicated that the oxide phase would not be stable, i. e. , would give up oxygen when in equilibrium with Nb. In systems where no weight change due to oxygen pressure was measurable, the thermogravimetric technique could not be used to determine the oxygen diffusion coefficient.

Values of the chemical diffusion coefficient \tilde{D} measured during Phase II are listed in Table 1. These values must be considered as preliminary values until the reproducibility of the blank runs can be rechecked. The power dependence of the deviation from stoichiometry on the oxygen partial pressure can be used to illuminate the defect structure and oxygen transport mechanism if it can be established that the system is single phased over the experimental range of oxygen partial pressure and temperature.

A series of B-1 alloy samples were oxidized in air at 800, 1000, and 1200°C for various time periods. Microprobe traces of the Ti profile across the oxide-metal interface were made, the results of which depended on the metallographic sample preparation. Oxidation kinetics for these conditions are presented.

X-ray studies of preoxidation scales on Nb and subsequent air oxidation results indicate that slowest oxidation rates are dependent on the formation of NbO structure.

TABLE 1. Values of the Chemical Diffusion Coefficients for Oxygen
in Nb_2O_5 and Other Niobates

System Mole Ratio	\bar{D} (10^{-7} cm ² /sec)	Time Interval Over Which D Was Measured (sec)	Deviation From Stoichiometry $\text{Nb}_2\text{O}_{5-x}$ (moles oxygen)	Initial Equilibrium Oxygen Pressure (atm.)	Final Equilibrium Oxygen Pressure (atm.)	Temperature (°C)
Nb_2O_5	36.6	280	0.00177	4.35×10^{-2}	3.7×10^{-12}	967
	6.99	3520	0.00325			
	27.0	400	0.00843	3.7×10^{-12}	6.45×10^{-15}	967
	36.8	1100	0.0112			
	9.8	1100	0.02713	6.45×10^{-15}	3.3×10^{-17}	967
	2.03	10,900	0.0360			
			Deviation From Stoichiometry Milligrams of Oxygen			
1.67:1.00 $\text{TiO}_2:\text{Nb}_2\text{O}_5$	2.00	53,000	1.86	5.75×10^{-2}	4.6×10^{-15}	819
	62.80	500	2.12			
	27.70	700	2.20	4.6×10^{-15}	6.06×10^{-18}	819
	13.30	4800	2.332			
	33.3	500	2.592			
	25.6	1700	2.812	6.06×10^{-18}	4.9×10^{-20}	819
	10.3	3800	3.004			
2.85:1.00 $\text{HfO}_2:\text{Nb}_2\text{O}_5$	7.7	7000	0.276	6.6×10^{-16}	8.69×10^{-22}	786
	36.6	600	0.072	3.1×10^{-2}	8.11×10^{-12}	983
	10.3	650	0.202	8.11×10^{-12}	2.24×10^{-14}	983
	29.4	550	0.254			
	7.0	850	0.744	2.24×10^{-14}	7.98×10^{-17}	983
	1.05	11,150	0.944			
	18.1	250	--	4.6×10^{-2}	1.2×10^{-8}	1192
	1.17	6250	0.268			
	15.3	500	0.408			
	0.529	4900	0.792	1.2×10^{-8}	2.92×10^{-11}	1192
	6.12	7200	0.844			

II. REVIEW OF OXYGEN TRANSPORT IN HIGH TEMPERATURE OXIDES

The search for oxygen transport rates of oxygen through mixed binary niobates resulted in the following compilation of the data collected from the literature. In addition to reporting the data in tabular form, several graphs were constructed to enable the reader to quickly compare the data and relate diffusion rates to oxide thickness, the thickness of the metallic substrate consumed and to determine the equivalent scale thicknesses for given combinations of diffusion rates and time.

The transport properties are being compared by plotting the value of D vs. $1/T$ for the high temperature oxides. The data has been gathered from the compilations of Bernard published in 1962⁽³⁾, Brett and Seigle⁽⁴⁾ published in 1968, and up dated from the series Diffusion Data⁽⁷⁾, published quarterly since 1967.

2.1 RELATING D VALUES TO METAL CONSUMED

The oxidation of a high temperature structural material causes a reduction in the cross sectional area of the load bearing members because of the material reacted to form the oxide. In addition, oxygen dissolved in the structural material may have an adverse effect on low temperature ductility.

If one considers only the thickness of the material consumed to form an oxide in the simplified case of a pure metal, then the thickness of the structural material consumed $T(\text{cm})$ in a unit of time for an oxide where anions diffuse from the gas-oxide interface to the oxide metal interface is given by

$$T = \frac{J_o}{P_m} \times \frac{(\text{molecular wt} - M)}{(\text{molecular wt} - O)} \times k \quad (1)$$

where J_o is the oxygen flux through the oxide scale, P_m is the density of structural material, and k is the ratio of the number of moles of oxygen to the number of moles of metal in a

stoichiometric oxide, i. e., for MO , $k = 1$ and for M_2O_5 , $k = 2/5$. The rate of degradation (rate of thickness change) of the structural member is directly proportional to the flux of oxygen through the oxide layer, the oxidation state of the oxide, and the molecular weight of the substrate, but is inversely proportional to the density of the metal.

If one considers an oxide-metal system where cation diffusion is the predominant transport process, then equation 1 simplifies to:

$$T = \frac{J_m}{P_m} \quad (2)$$

where J_m is the flux of cations ions through the oxide. Equations 1 and 2 will give the thickness of the metal consumed if one has a knowledge of the diffusion coefficient D and the gradient representing the driving force for the transport of anions or cations through the lattice.

Estimating the actual oxide thickness based on the amount of metal consumed is more difficult because the density of the growing oxide is difficult to determine. However, if one uses the Pilling-Bedworth criterion where the volume ratio ϕ is given by

$$\phi = \frac{\text{molecular volume of oxide } \text{MeX}_x}{\text{atomic volume of metal}} \quad (3)$$

where both volumes refer to equivalent amounts of metal, i.e.,

$$\phi \text{Nb}_2\text{O}_5 = \text{MV}_{\text{Nb}_2\text{O}_5} / 2 \text{AV}_{\text{Nb}} \quad (4)$$

where MV is molecular volume and AV is atomic volume. Then from the values listed in Kubaschewski and Hopkins⁽⁸⁾, (i.e. $\phi \approx 2.68$ for Nb_2O_5) the thickness of the oxide formed will be 2.68 times the thickness of the metal consumed for a given area of coverage.

Table 2 lists the values of D calculated from the relationship

$$D = \frac{X^2}{5t}$$

where $X^2 = kt$ and $k = 5D$ based on the work of Brett and Seigle⁽⁴⁾, and the values are plotted in Figure 1 showing the rate of metal loss as a function of time for various values of the chemical diffusion coefficient. This plot is dependent on temperature only in that D depends on temperature. The average linear rate in Table 2 is dependent on the diffusion time selected.

This analysis does not consider the effects of the oxidizing media dissolving into the substrate and affecting the mechanical properties over and above the effect caused by the metal loss.

2.2 COMPILATION OF DIFFUSION DATA

The diffusion coefficients are shown in Figures 2 and 3 as plots of $\log_{10} D$ vs. $1/T$. Superimposed on the graphs are the values of D and their respective rate of metal consumption by oxide formation. Tables 3 and 4 list the oxides, the diffusing species, the melting points of the oxides, and the structures where available, the values for D_0 and Q , and the temperature range over which the data is valid. In most cases the oxide compounds which possess the slowest transport properties are spinels. However, it is generally accepted that the oxidation protection for most coatings and alloys is due to the ability of the system in question to form a protective layer of Al_2O_3 , SiO_2 , or Cr_2O_3 as a barrier between the oxidizing environment and the structural substrate. The diffusion coefficient for oxygen in $\alpha - Nb_2O_5$ has been shown to be a function of oxygen pressure⁽⁹⁾. These values are shown in Table 5 and are quite large even at the lower temperatures.

TABLE 2. Diffusion Coefficients for Various Oxidation Times and Oxide Thickness

D(Cm ² /sec)	Diffusion t Time (Hrs.)	Tolerated Metal Loss (mil)	X Oxide Thickness (mils)	Linear Average Rate
3.23 x 10 ⁻¹²	1000	1.0	3.0	0.01 mil/hr
3.23 x 10 ⁻¹¹	100	1.0	3.0	0.01 mil/hr
3.23 x 10 ⁻¹⁰	1000	10.0	30.0	0.01 mil/hr
3.23 x 10 ⁻¹⁰	10	1.0	3.0	0.1 mil/hr
3.23 x 10 ⁻⁹	100	10.0	30.0	0.1 mil/hr
3.23 x 10 ⁻⁸	1000	100.0	300.0	1.0 mil/hr
	10	10.0	30.0	1.0 mil/hr

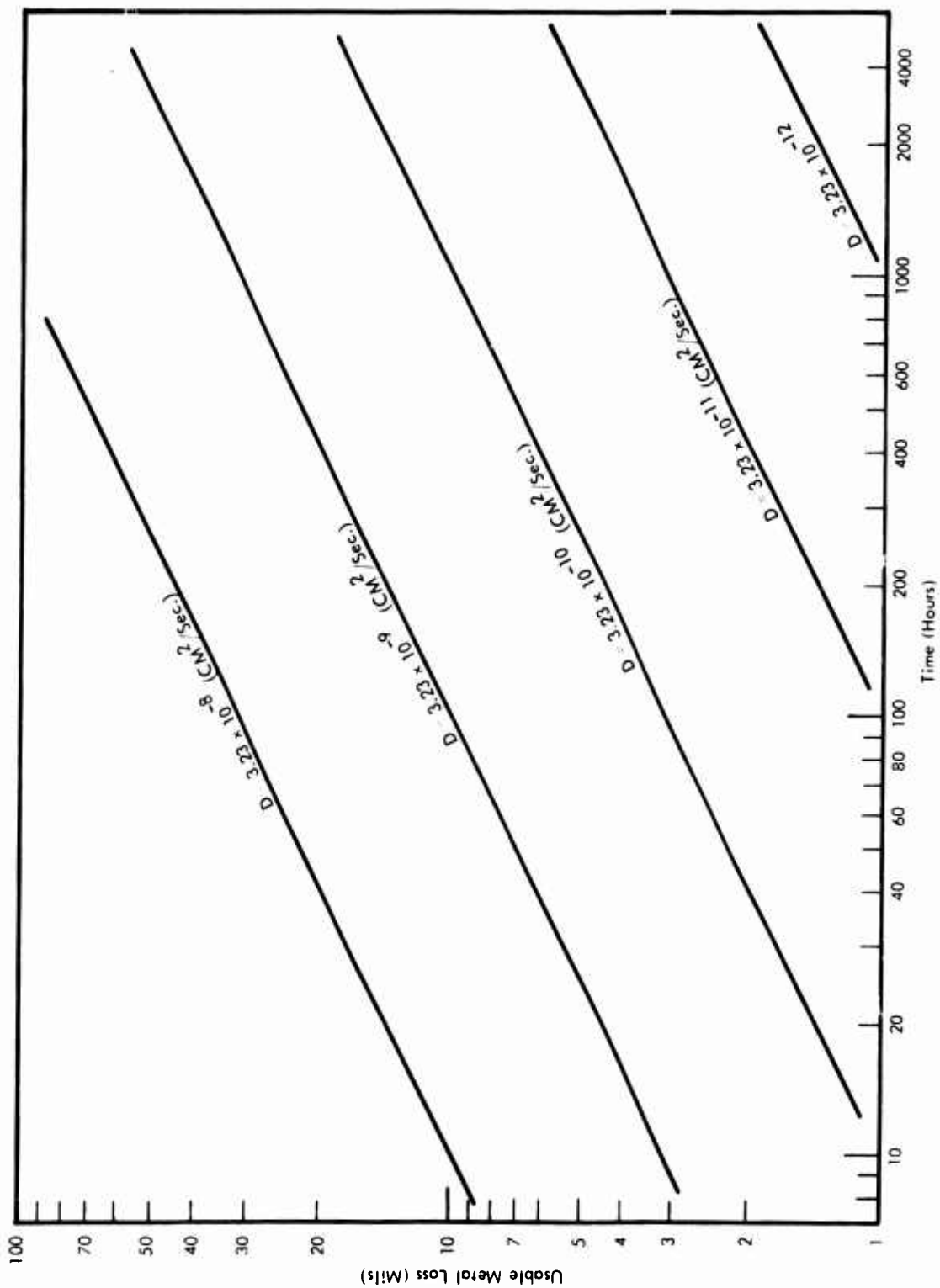


Figure 1. Iso-diffusion Coefficient Plot Showing Metal Consumed as a Function of Time for Various Values of the Chemical Diffusion Coefficient Through the Oxide

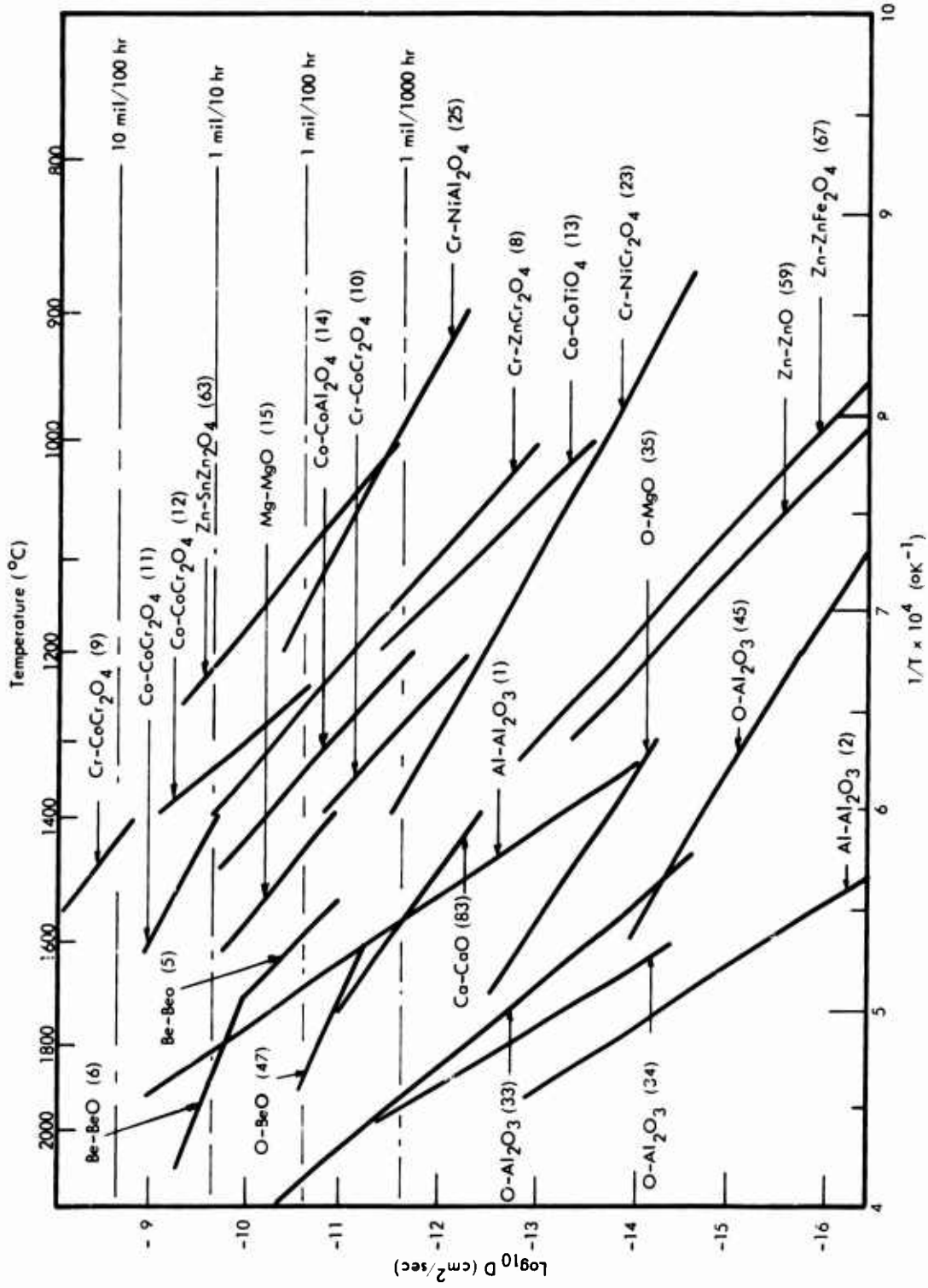


Figure 2. Diffusion Coefficient for Cations and Anions Through Oxides Suitable for Elevated Temperature Service

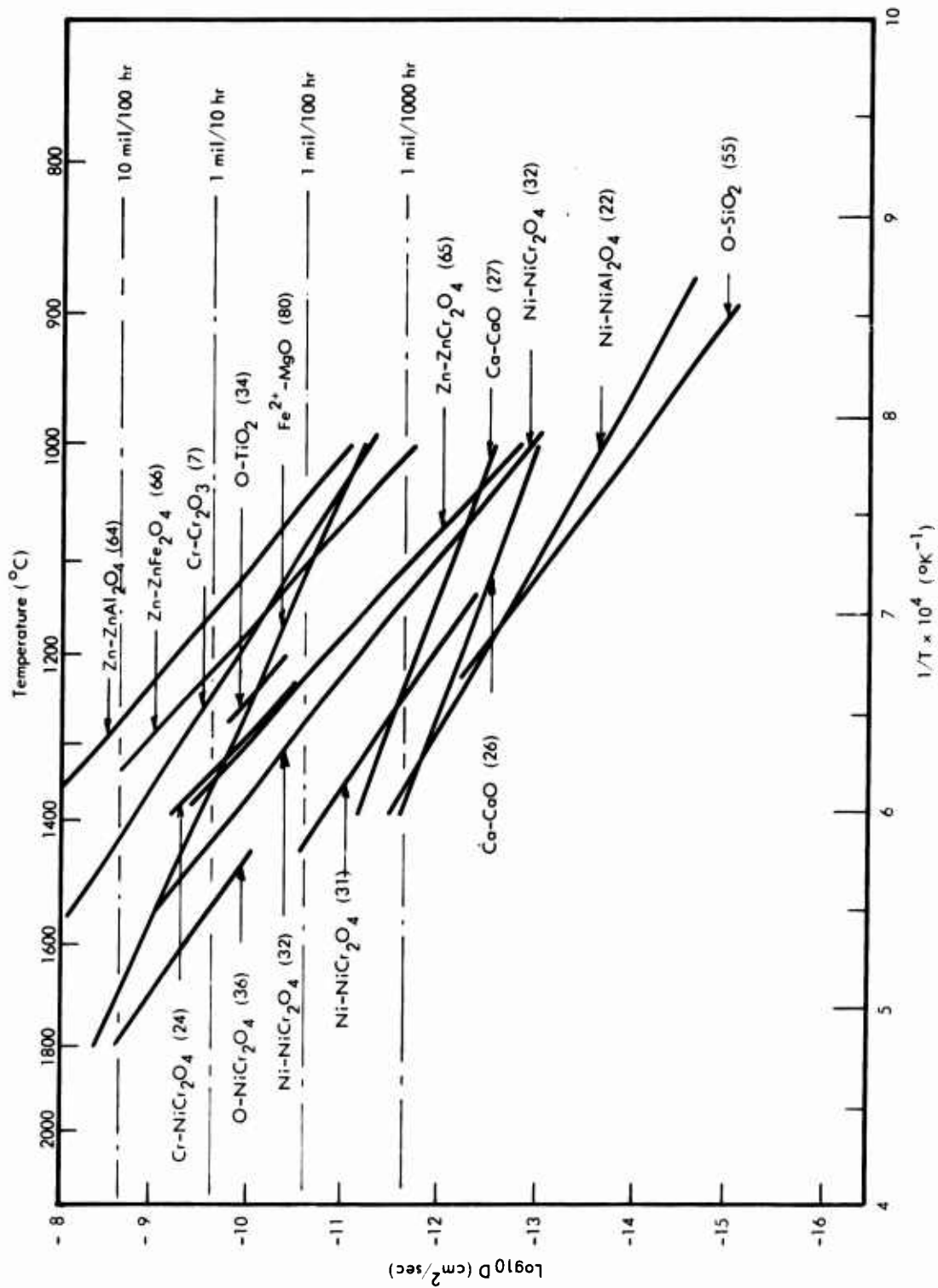


Figure 3. Diffusion Coefficient for Cations and Anions Through Oxides Suitable for Elevated Temperature Service

TABLE 3. List of Mobile Species in Matrices Which Have Shown Low Transport Rates

Mobile Species	Matrix	Melting Point (°C)	Structure	Identification No. for Graph	Reference
O	MgO	2800	NaCl	35	5
Mg				15	4
Fe ²⁺				80	6
O	Al ₂ O ₃	2015-2050	Cr ₂ O ₃	33	5
O				34	4
O				45	4
Al				1	4
Al				2	5
Cr	CoCr ₂ O ₄	N.A.	Spinel	10	5
Cr				9	4
Co				12	5
Co				11	4
Ni	NiCr ₂ O ₄	N.A.	Spinel	31	4
*Ni				32	5
Cr				23	4
Cr				24	5
Co	CoAl ₂ O ₄	1955	Spinel	14	5
Co	CoTiO ₃	N.A.	Cr ₂ O ₃	13	5
Cr	ZnCr ₂ O ₄	N.A.	Spinel	8	4
Zn				65	4
Zn	SnZn ₂ O ₄	N.A.	Spinel	63	4
Zn	ZnFe ₂ O ₄	1720	Spinel	66	4
Zn				67	4
Ni	NiAl ₂ O ₄	2020	Spinel	22	4
Cr				25	4
Cr	Cr ₂ O ₃	2000-2440	rhombohed:DS _i	7	5

*Corrected Data from Ref. 4 .

TABLE 3 (Cont'd.)

Mobile Species	Matrix	Melting Point (°C)	Structure	Identification No. for Graph	Reference
O	BeO	2520-2550	Wurtzite	47	4
Be				5,6	4
O	TiO ₂	1870	tetrag:C4 (rutile)	39	5
Zn	ZnO	1970	Wurtzite	59	4
Ca	CaO	2545-2570	NaCl	33, 26, 27	6
O	SiO ₂	1700	Quartz (hexagonal)	55	5

TABLE 4. List of D_o and Q Values for Diffusion of Species in Oxides Listed in Table 3

Matrix	Mobile Species	I. D. Coefficient	D_o (cm^2/sec)	Q kcal/mole	Temperature Range $^{\circ}\text{C}$
MgO	O	35	2.5×10^{-6}	62.4	(1300 - 1700)
	Mg	15	0.23	78.7	(1400 - 1600)
	Fe ²⁺ *	80	8.8×10^{-5}	41.7	(1000 - 1850)
Al ₂ O ₃	O	33	0.2	110.0	< 1450
	O	34	1900	152.0	> 1600
	O	45	6.3×10^{-8}	57.6	< 1600
	Al	1	25,000	135.0	----
	Al	2	28	144.0	----
CoCr ₂ O ₄	Cr	10	300	85.0	(1200 - 1400)
	Cr	9	2	70.0	(1400 - 1600)
	Co	12	80	90.0	(1250 - 1400)
	Co	11	10^{-3}	51.0	(1400 - 1600)
NiCr ₂ O ₄	Ni	31	1.5×10^{-3}	61.4	(1130 - 1450)
	Ni*	32	0.85	75.0	----
	Cr	23	0.75	73.0	(950 - 1450)
	Cr	24	200	89.0	(1250 - 1400)
CoAl ₂ O ₄	Co	14	8	85	(1200 - 1500)
CoTiO ₃	Co	13	500	95	(1000 - 1200)
Zr ₁ Cr ₂ O ₄	Cr	8	9	81	(1000 - 1400)
	Zr	65	60	85	(1000 - 1400)
SnZn ₂ O ₄	Zn	63	37	76.3	(1000 - 1250)
ZnFe ₂ O ₄	Zn	66	1000	86.0	(900 - 1350)
	Zn	67	8.8×10^{-2}	86.0	----
NiAl ₂ O ₄	Ni	22	2.9×10^{-5}	53.3	(880 - 1388)
	Cr	25	1.17×10^{-3}	50.0	(900 - 1200)
Cr ₂ O ₃	Cr	7	0.137	61.1	(1045 - 1550)

* Corrected Data from Ref. 4.

TABLE # . (Cont' d.)

Matrix	Mobile Species	I. D. Coefficient	D_o (cm ² /sec)	Q kcal/mole	Temperature Range °C
BeO	O	47	5.2×10^{-7}	42.9	(1600 - 1900)
	Be	5	1.37	91.9	1500 - 1725
	Be	6	1.1×10^{-6}	36.15	1725 - 2000
TiO ₂	O	39	1.6	74.0	(1200 - 1275)
ZnO	Zn	59	0.1	89.0	(800 - 1300)
CaO	Ca	83	1.125×10^{-4}	64.3	(1455 - 1760)
		26	8.75×10^{-8}	34.6	(1000 - 1400)
		27	1.95×10^{-7}	34.02	(1000 - 1400)
SiO ₂	O	55	1.51×10^{-2}	71.2	(925 - 1225)

TABLE 5. Chemical Diffusion Coefficients of α -Nb₂O₅ at 900°C (Ref. 9)

Oxygen Pressure (atm.)	\tilde{D} Oxygen in Nb ₂ O ₅ (cm ² /sec)
1 to 10 ⁻⁵	6 x 10 ⁻⁶
10 ⁻⁶ to 10 ⁻¹⁰	~10 ⁻⁸

No data has been found for the effect of binary oxide additions to Nb_2O_5 on the rate of diffusion of oxygen in the mixed oxides. Much work has been presented which show the effects of alloying on the oxidation behavior. The alloy additions must oxidize along with niobium to form mixed oxide scales and reduce the transport rate of oxygen through the scales.

III. OXYGEN DIFFUSION THROUGH MIXED NIOBATES

3.1 THERMOGRAVIMETRIC TECHNIQUES FOR DETERMINING THE OXYGEN DIFFUSION COEFFICIENT

Oxidation-reduction kinetics and nonstoichiometry of metal oxides have been studied primarily by thermogravimetric⁽¹⁰⁻¹⁵⁾ and electrical conductivity techniques⁽¹⁶⁻²¹⁾. To date all of the published kinetic data for nonstoichiometric oxides utilizing thermogravimetric techniques have involved oxides in which the predominant defect was the singly ionized cation vacancy. This work involves oxides whose structure is thought to be contained on the anion lattice in the form of single or double charged anion vacancies.

In these studies, the driving force for diffusion is provided by the partial pressure of oxygen established in the gaseous phase adjacent to the oxide. By equilibrating the oxide with a known oxygen partial pressure and then abruptly changing the oxygen partial pressure, the rate of weight change with time indicates the mobility of oxygen as it is being removed from or diffused into the sample. By assuming that the surface of the specimen equilibrates immediately with the surrounding atmosphere, the chemical diffusion coefficient \tilde{D} can be obtained from an integrated solution of Fick's second law assuming a constant diffusion coefficient. Once the geometry of the sample is established, the proper solution of Fick's law can be applied.

3.1.1 Rationale for Sample Geometry

Table 6 shows a comparison of the three sample geometries considered for this investigation, the flat disc, the cylinder, and the sphere. Solutions to the appropriate diffusion equations presented by Crank⁽²²⁾ were utilized to determine the optimum geometry for the diffusion samples. The following factors were considered in the analysis to select the best geometry:

- 1) Weight of the material required to achieve a measurable weight change during the experimental exposure. (For pure Nb_2O_5 , a ΔX of 0.01 will give a weight change of 0.6 mg/gram of Nb_2O_5).

TABLE 6. Comparative Parameters Used to Select Oxide Geometry

	Flat Plate		Cylinder		Sphere	
Dimension	2 cm dia x 0.1 cm thick		0.5 cm dia x 2 cm long		1 cm dia	
Volume	.314 cm ³		.393 cm ³		0.523 cm ³	
Surface/Edge	10/1		8/1		--	
Diffusion Times	D cm ² /sec	t (sec)*	D cm ² /sec	t (sec)	D cm ² /sec	t (sec)
	10 ⁻⁸	3.75x10 ⁵	10 ⁻⁸	5x10 ⁶	10 ⁻⁸	10 ⁷
	10 ⁻¹⁰	3.75x10 ⁶	10 ⁻¹⁰	5x10 ⁸	10 ⁻¹⁰	10 ⁹
	10 ⁻¹²	3.75x10 ⁷	10 ⁻¹²	5x10 ¹⁰	10 ⁻¹²	10 ¹¹

* 1 year = 3.16 x 10⁷ sec.

- 2) Time to achieve equilibrium.
- 3) Ease of analysis of results.
- 4) Ease of fabrication.

The shapes considered were spheres, cylinders, and flat plates. Spheres would be the ideal shape based on considerations of edge effects when compared to flat plates or cylindrical samples. However, the diameter of a sphere with sufficient volume to enable a meaningful weight gain would require extremely long equilibration times. This left the comparison of the flat plate and cylinder. Again, the equilibration times for cylinder would be long. Analysis showed that a disc 2 cm dia. by 0.1 cm thickness would be the best configuration based on the restraints imposed.

3.1.2 Solutions to Fick's Second Law

Chemical diffusion is used to denote diffusion which as the result of a concentration or chemical potential gradient. This is not to be confused with self-diffusion or tracer diffusion, which does not occur as the result of a chemical potential or concentration gradient. After Wagner⁽²³⁾

$$D_i^s = \lim_{(\partial c_i / \partial x) \rightarrow 0} \left[\frac{J_i}{(\partial c_i / \partial x)} \right] c_i \quad (5)$$

D_i^s = self diffusion coefficient

J_i = flux

x = distance

c = concentration

The self-diffusion coefficient on the i th species, D_i^s , is proportional to the diffusion coefficient for the defect responsible for the migration of the i th species. The chemical diffusion coefficient \tilde{D} is the proportionality constant in Fick's Law

$$J = \tilde{D} (d\tilde{c}/dx) \quad (6)$$

We use the integrated thin plate solution for Fick's second law

$$\frac{\partial c}{\partial t} = -\tilde{D} \frac{\partial^2 c}{\partial x^2} \quad (7)$$

after Crank⁽²²⁾

$$\frac{M(t)}{Q} = 1 - \sum_{n=0}^{\infty} \frac{8}{(2n+1)^2 \pi^2} e^{-D(2n+1)^2 \pi^2 t / 4l^2} \quad (8)$$

where t = times (seconds)

l = half thickness of the plate.

For values of $\tilde{D}t/l^2 \geq 0.15$ only the first term ($n = 0$) of the series is required, therefore equation (8) simplifies to

$$\frac{M(t)}{Q} = 1 - \frac{8}{\pi^2} (e^{-\tilde{D} \pi^2 t / 4l^2}) \quad (9)$$

or

$$\log (1 - M(t)/Q) = \log \frac{8}{\pi^2} + \frac{D \pi^2 t}{(9.2)l^2} \quad (10)$$

By plotting $\log (1 - M(t)/Q)$ vs t , the slope of the line can be measured and \tilde{D} can be calculated; this analysis is valid for $\frac{\tilde{D}t^2}{l^2} \geq 0.15$.

For $\frac{\tilde{D}t}{l^2} \leq 0.25$ the following relationship can be used to evaluate D .

$$\left(\frac{M(t)}{A}\right)^2 = k_p \cdot t \quad (11)$$

and

$$k_p = \frac{4\tilde{D}}{\pi} (\Delta c)^2 \quad (12)$$

where Δc is the concentration of oxygen removed from the oxide during reduction or the amount added during oxidation in grams/cc.

3.2 EXPERIMENTAL MATERIALS

Solid oxides for the diffusion kinetic evaluation were fabricated from powders of the separate oxides by mixing, cold pressing, and sintering. Table 7 lists the starting purities of the oxides as specified by the seller, the composition of the oxide mixtures, the sintering temperatures and times, and the densities measured for the samples thus far.

The as-received oxide powders were weighted and mixed together in an agate mortar and pestle with acetone saturated with stearic acid, a lubricant. It was found that by dissolving the stearic acid in acetone a more uniform distribution of stearic acid was obtained in the powders. The mixed samples were allowed to dry and then a methyl-methacrylate binder was added (about 20 to 30 drops to a 10 gram mixture) and mixed again in a vial. This oxide powder was cold pressed into 0.875 inch (2.22 cm) diameter pellets at 30,000 pounds (49,000 psi). These oxides were then sintered in air for 16-20 hours at the temperatures shown in Table 7. Prior to the establishment of the air-firing procedure, several other sintering environments were tried. 1) Sintering at 1420°C in H_2 2) Sintering at 1300°C in vacuum and 3) Sintering in air at 1350°C . Alumina ceramics were used to support the oxides in each of these environments during sintering.

A series of pellets sintered in H_2 are shown in Figure 4. These pellets were sintered overnight in an H_2 furnace at 1420°C . They were dark gray in color, indicating an oxygen deficiency. On heating these samples to 1300°C in an air furnace all but the $\text{TiO}_2\text{-Nb}_2\text{O}_5$ pellet broke into small fragments. These samples were either heated too fast, or the volume change on adding oxygen was significant enough to shatter the samples. Subsequently, the pressed samples have been successful sintered in air.

TABLE 7. Experimental Materials Used for Making Mixed Niobates and Experimental Compositions

Oxide	Purity	Experimental Composition Mole %	Sintering Temperature °C	Densities*
Nb ₂ O ₅	99.95	100	1420	3.19
Al ₂ O ₃	99.995	73	1360	3.28
V ₂ O ₅	99.9	57.3	Vaporizes	----
TiO ₂	A. R.	62.6	1420	3.61
ZrO ₂	99.9	74.0	1420	---
Cr ₂ O ₃	A. R.	62.5	1210 - 1360	---
Co ₃ O ₄	99.5	59.5	1207	---
NiO	99.0	87	1420	4.58
Fe ₂ O ₃	99.5	62.5	1210	---
HfO ₂	98.0	74	1420	5.99

* From weight and volume measurements.

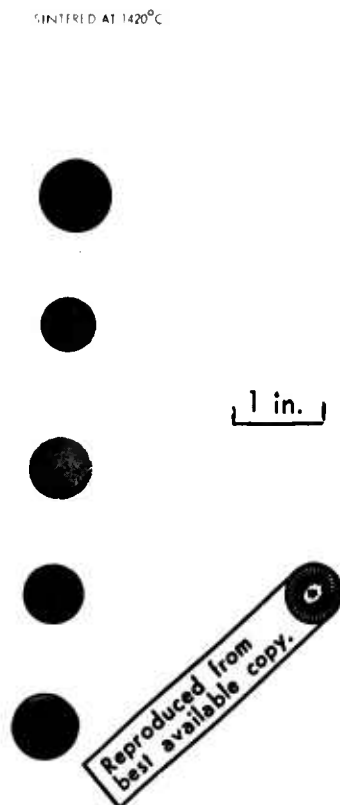


Figure 4. Pellets Sintered in H_2 Furnace for 16 Hours at 1420°C.
All pellets were initially 7/8" Dia. Before Sintering

After the initial sintering, the oxides were ground to pass through a (105) mesh sieve, binder was added, and 2.5 gram pellets were cold pressed from the samples and resintered in air. After the second sintering, the volume change noted was much smaller indicating that only sintering was occurring.

3.3 EXPERIMENTAL APPARATUS

The experimental apparatus is shown schematically in Figure 5. The entire apparatus was constructed from stainless steel. The furnace tube was mullite and was connected to the system using O-ring seals in a compression fitting. A brief description of the components follows.

3.3.1 Furnace

A vertical non-inductively wound, resistance heated 3 zone Lindberg Hevi-Duty Clam Shell Furnace having one 12-inch long center heater and a 6-inch long guard heater at each end was used to heat the sample. The reaction chamber in the furnace was constructed from a 38 mm mullite tube attached to the system O-ring compression fittings.

Temperature was measured and controlled using a Pt-Pt/13Rh thermocouple suspended in the vacuum system. The bead of the thermocouple was shielded from direct radiation by an alumina protection tube. The temperature was corrected for position and radiation effects by comparison with thermocouples directly attached to a sample in the hot zone during a separate calibration run.

3.3.2 Balance

Continuous weight change measurements were made using a Cahn UHV-RH microbalance with a 100 gram capacity and a 2 microgram sensitivity. The balance is housed in a stainless steel chamber constructed from a standard 8-inch Varian flanged nipple. Varian 2-3/4 inch nipples were cut and welded to the 8-inch nipple to provide appendages for the sample

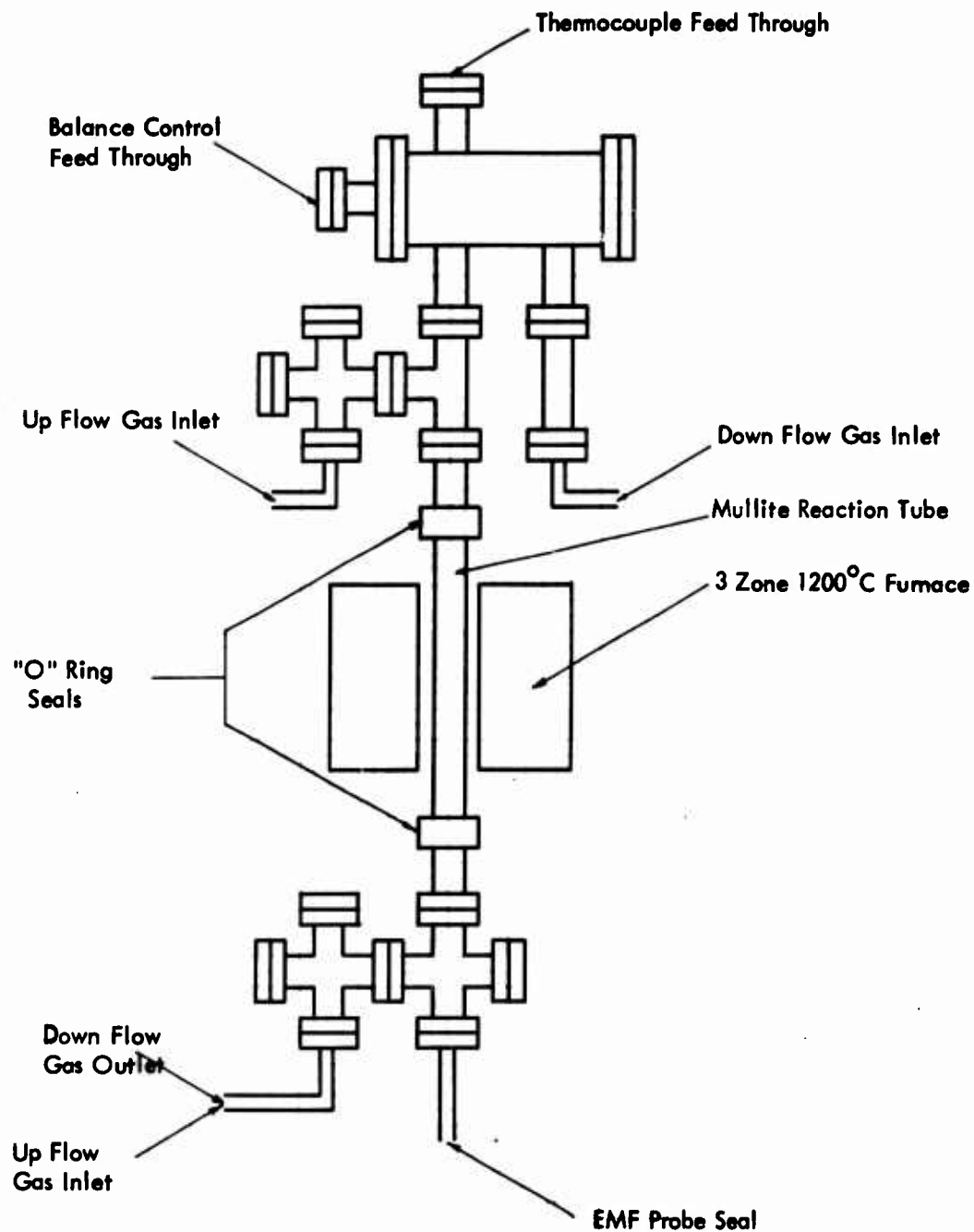


Figure 5. Modified Vacuum Microbalance Used for Flowing Gas Studies

and counterweight hangdowns and for thermocouple feedthroughs. The microbalance was mounted on a standard Varian rotatable 8-inch blankoff along with the vacuum feedthrough containing the electrical connections for the balance. The samples were suspended from the balance by 20 mil (0.5 mm) platinum-rhodium wire.

Weight changes were continuously recorded on a dual pen recorder with a potentiometric input system. A one mv full scale recorder range was used for all continuous weight-gain records.

3.3.3 Gas

High purity oxygen, argon, and chemically pure CO and CO₂ gases were used directly from the cylinder and admitted into the system through glass pressure drop flow meters. These flow meters issue a constant flow of gases through the furnace independent of the effect of temperature fluctuations on the gas bottle pressure regulators.

3.4 PROCEDURE FOR USE OF THE CAHN MICROBALANCE

The niobate discs were cradled in a Pt-Rh wire support and suspended from the balance hang-down hook by a 20 mil (0.5 mm) diameter Pt-Rh wire. Initially, 5 mil (0.127 mm) diameter wire was used. However, at 1200°C and at oxygen partial pressures greater than 0.20 atm, the cross section of the wire was reduced by both PtO₂ volatilization and creeping of the wire, and these 5 mil diameter supports broke. Subsequently, only 20 mil supports and oxygen partial pressures of 0.2 atm or less were used.

The sample was sealed in the furnace by lowering the microbalance chamber. The system was brought to temperature in an air environment to insure an equilibrium stoichiometric structure at the beginning of each run. The Ar/O₂ and CO/CO₂ gas mixtures were established through a bypass valve to insure that the gas metering system was completely purged. Then the gas mixtures were switched to flow through the furnace reaction tube to begin equilibration.

Equilibrations were made successively with a 20/1 argon/oxygen mixture, and with nominal 1/20, 1/1, and 20/1 CO/CO₂ mixtures. Flow rates were nominally 400 ml/min which gave a flow velocity through the tube of about 0.58 cm/sec. The microbalance indicated an initial weight change due to the flow velocity.

An EMF oxygen meter was used to verify the oxygen partial pressures, and also because of its fast response to measure the lapse time required for the front of the new gas mixture to reach the sample. This was chosen as zero time for the experiments. The EMF probe was of standard design and utilized a Co/CoO reference electrode, a Ca stabilized ZrO₂ solid electrolyte and platinum electrical connections. Although not used during each experiment, the EMF probe was used to substantiate the ability of the gas mixtures to maintain the calculated partial pressure of oxygen without taking special precautions to further purify the gases from the cylinders. The samples were equilibrated with a specific gas mixture until no weight changes were measurable for an hour.

A set of blank runs were made for each temperature and gas mixture using 99.9% pure sintered Al₂O₃ to determine the effect of time and gas flow on the weight measuring system.

There was a definite effect of time on weight change for the blank inert sample. This was attributed primarily to the differences between the densities and bouyancies of the various gas mixtures. As noted on Figure 5, the gas was introduced through the bottom of the system and exited just below the balance chamber. The gradual mixing of the newly introduced gas with the old gas mixture caused a time dependent, but reproducible drift in the weight readings. Each gas mixture successively introduced into the system caused a characteristic weight change with time. These weight changes, which were measured on a blank sample, were subtracted from the weight changes measured on the experimental samples to give the real weight loss of oxygen as a function of time.

For a given gas mixture at equilibrium with the sample, a slow drift of ± 20 micrograms over a 24 hour period was noted. It is not possible to ascertain as yet whether this drift is periodic with time or random. If it is periodic with time it could reflect cyclic temperatures, line voltages, and power demands at the laboratory.

3.5 EXPERIMENTAL RESULTS AND DISCUSSION

Results for the systems Nb_2O_5 , $\text{TiO}_2\text{-Nb}_2\text{O}_5$, and $\text{HfO}_2\text{-Nb}_2\text{O}_5$ will be presented in detail. The $\text{NiO-Nb}_2\text{O}_5$ system did not exhibit non-stoichiometric behavior until an oxygen partial pressure corresponding to approximately the dissociation pressure of NiO was present in the system. At this point rapid reduction of the $\text{NiO-Nb}_2\text{O}_5$ system began, occurring at a rate of about 124 micrograms per minute. These rapid reduction rates caused the balance to go off scale, and the equilibrium oxygen weight corresponding to the oxygen partial pressure could not be measured. The results obtained with the $\text{Al}_2\text{O}_3\text{-Nb}_2\text{O}_5$ system were erratic and inconsistent, and these results are being redone during Phase III.

The experimental data is presented in Appendix A in tabular form. The oxygen weight loss as a function of time for the oxides is presented in Figures 6 through 10. Associated with each curve on the graphs is the oxygen partial pressure gradient over which the weight loss was measured, and the temperature at which the measurements were made. The oxides were equilibrated with the highest partial oxygen pressure and then the lower oxygen partial pressure was established. The time rate of change of the weight of oxygen removed was measured continuously using the microbalance. Although the weight loss shown on the graphs for each partial pressure differential start at zero, the total weight loss for each oxide sample at a given temperature is cumulative

Figure 6 shows the weight loss results for Nb_2O_5 at 967°C . The largest weight loss occurred in the pressure range 10^{-15} to 10^{-17} atm O_2 . Figure 7 shows the rate of weight loss of

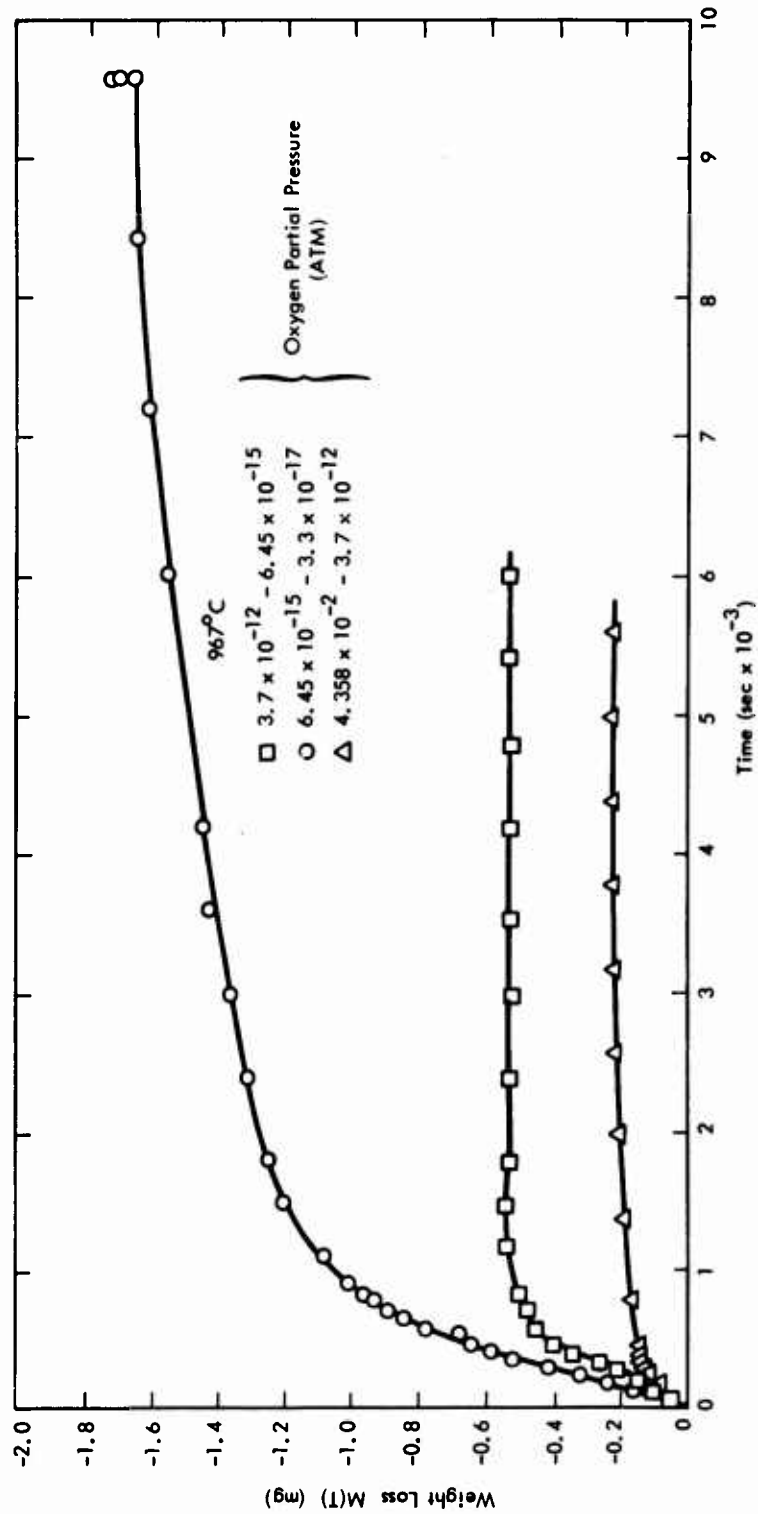


Figure 6. Weight Losses for Nb_2O_5 as a Function of Time for Various Oxygen Partial Pressure Differentials at 967°C

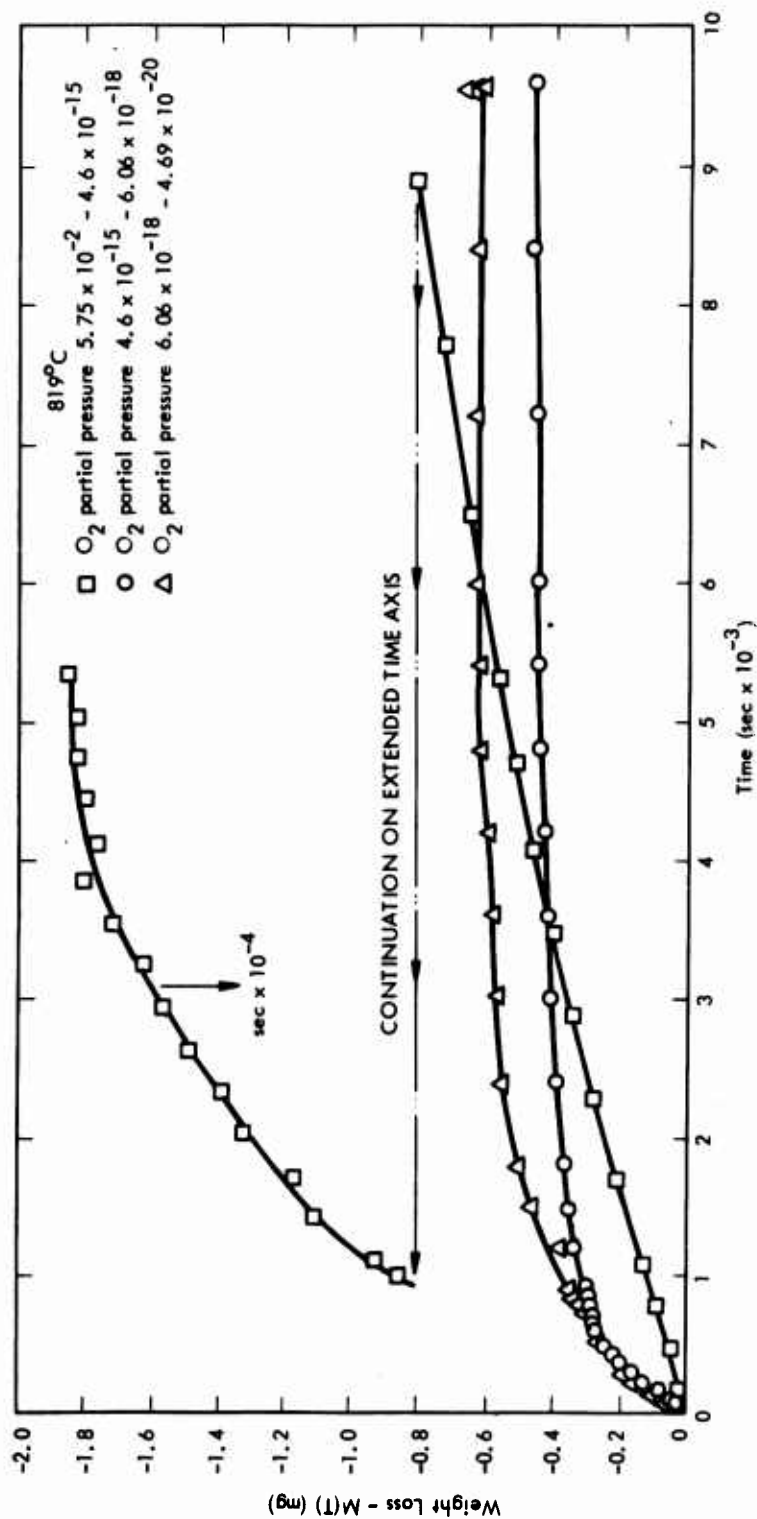


Figure 7. Weight Losses for 1.67:1 Molar Ratio TiO₂-Nb₂O₅ as a Function of Time for Various Oxygen Partial Pressure Differentials at 819°C

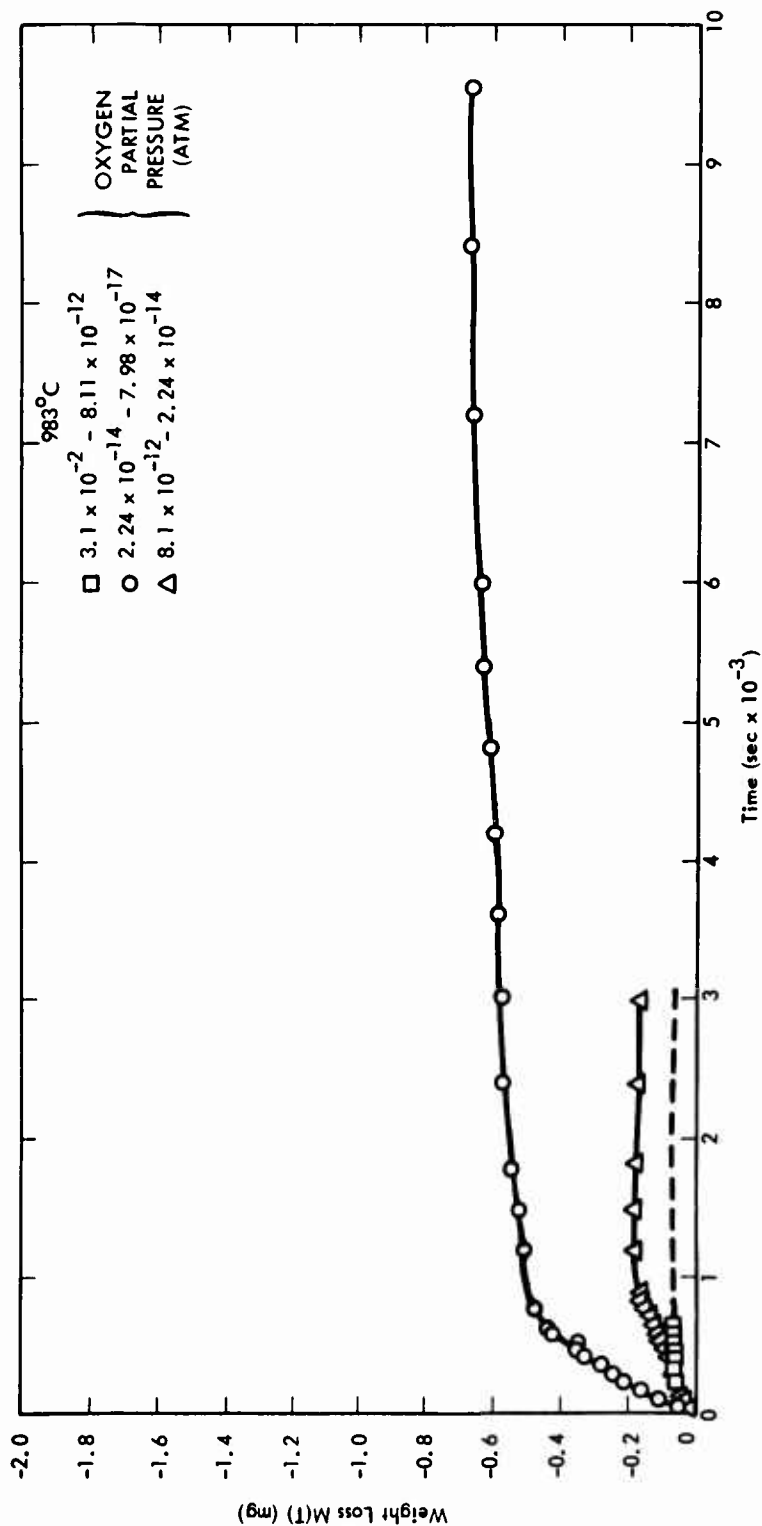


Figure 8. Weight Losses for 2.85:1 Molar Ratio $\text{HfO}_2\text{-Nb}_2\text{O}_5$ as a Function of Time for Various Oxygen Partial Pressure Differentials at 786°C

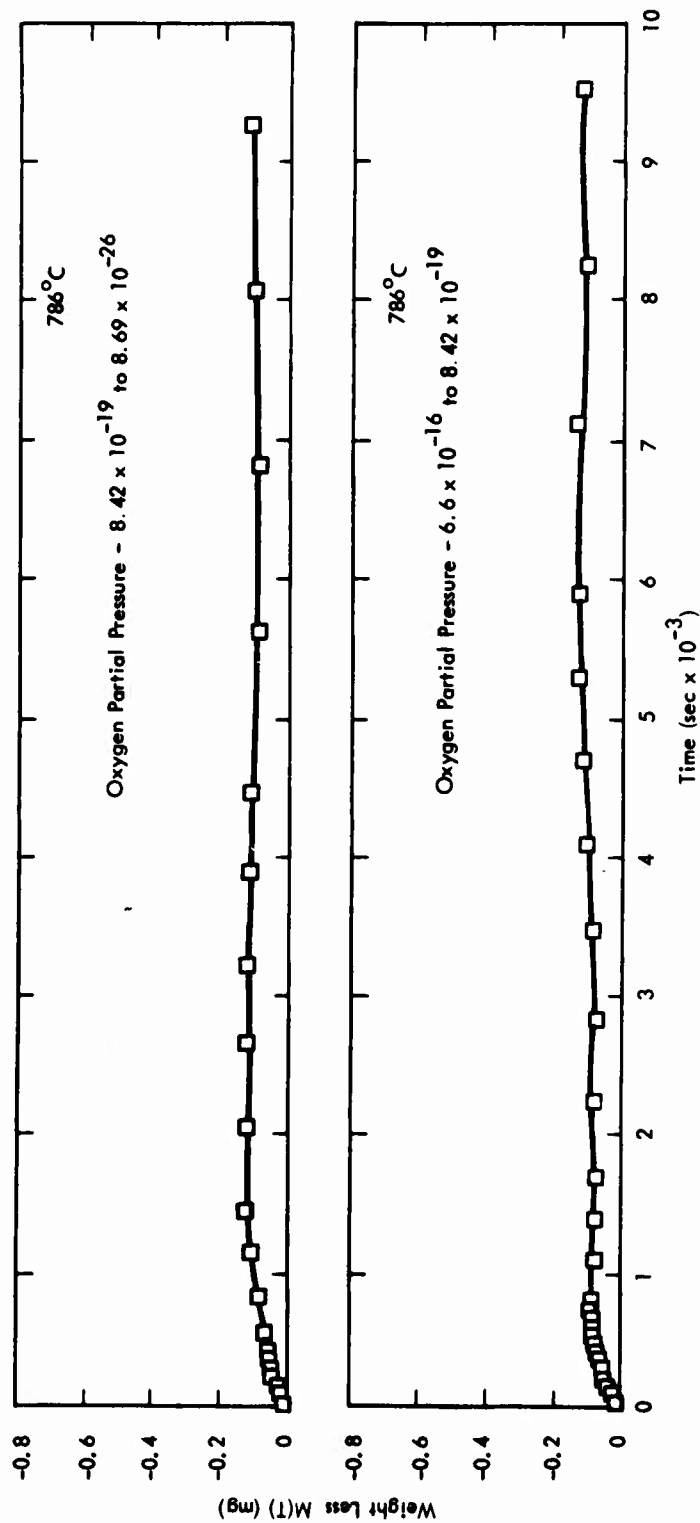


Figure 9. Weight Losses for 2.85:1 Molar Ratio $\text{HfO}_2\text{-Nb}_2\text{O}_5$ as a Function of Time for Various Oxygen Partial Pressure Differentials of 983°C

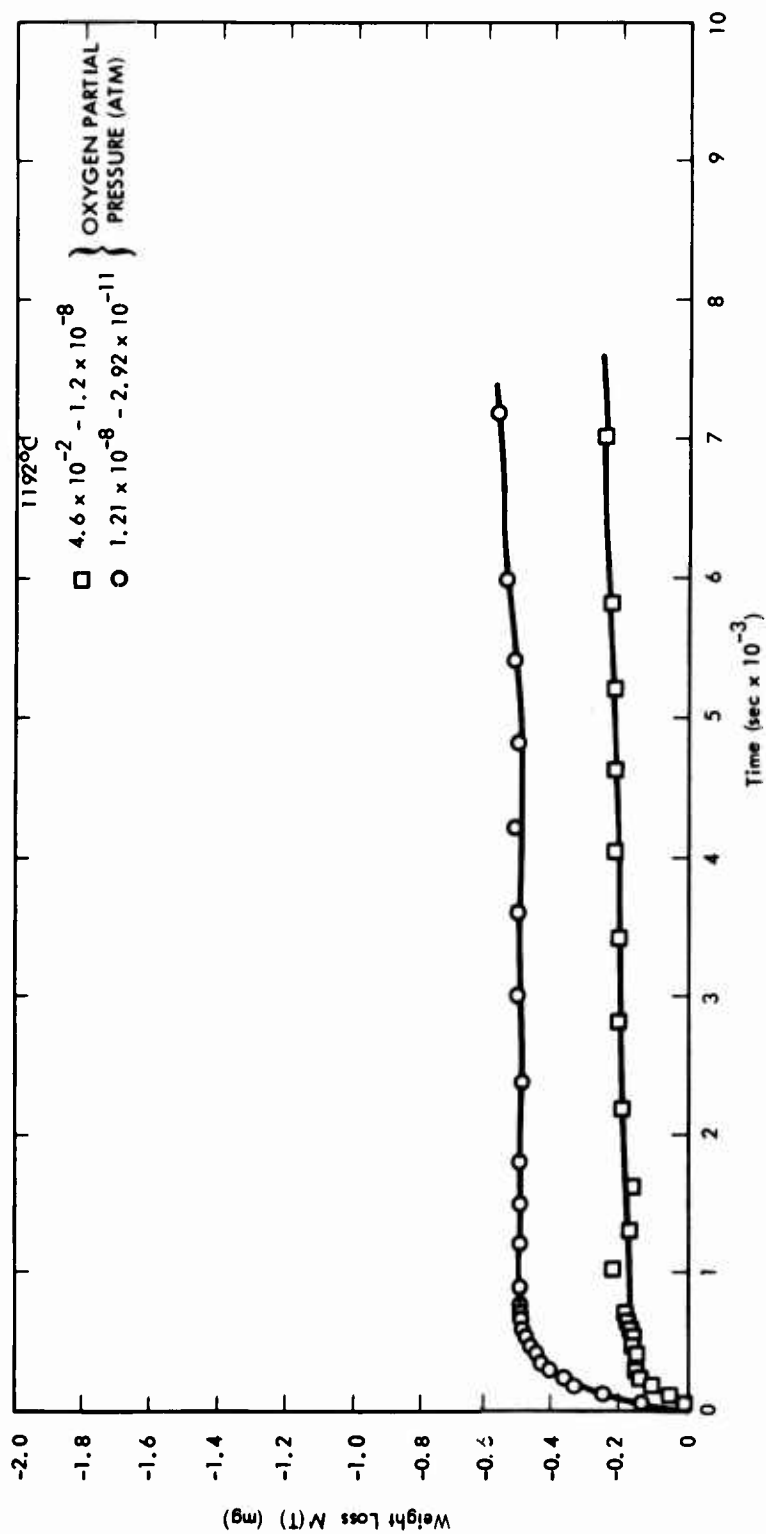


Figure 10. Weight Losses for 2.85:1 Molar Ratio $\text{HfO}_2\text{-Nb}_2\text{O}_5$ as a Function of Time for Various Oxygen Partial Pressure Differentials at 1192°C

$\text{TiO}_2\text{-Nb}_2\text{O}_5$ at 819°C . Because of the long time required to reach equilibrium at 4.6×10^{-15} , the data are plotted on two different time axes for the partial pressure region 10^{-2} to 10^{-15} . In the case of $\text{TiO}_2\text{-Nb}_2\text{O}_5$ the largest weight loss occurred between 10^{-2} and 10^{-15} atm. oxygen partial pressure.

Figures 8 through 10 show the weight loss as a function of time for $\text{HfO}_2\text{-Nb}_2\text{O}_5$. Compared to Nb_2O_5 and $\text{TiO}_2\text{-Nb}_2\text{O}_5$ the weight losses measured for $\text{HfO}_2\text{-Nb}_2\text{O}_5$ are relatively small especially at 786 and 983°C . At 786°C , there was no measurable weight loss due to reducing the oxygen partial pressure from 10^{-2} to 10^{-22} .

3.5.1 Nb_2O_5

Utilizing equation 10 the quantity $-\log (1-M(t)/Q)$ is plotted versus time to determine a slope from which to calculate the diffusion coefficients from the experimental results. Figure 11 shows this plot for Nb_2O_5 over the three oxygen partial pressure intervals. Table 1 lists the value of \tilde{D} calculated from these graphs. In each case there are distinct breaks in the curves, and two straight lines can be fitted to the curves. Values of \tilde{D} have been associated with each constant slope time interval. This solution of the diffusion equation 10 is valid for values of $\tilde{D}t/l^2 \geq 0.15$. Table 8 shows the values of $\tilde{D}t/l^2$ calculated from the derived diffusion coefficient and the time over which the linear behavior was noted.

Obtaining two different diffusion coefficients for a given oxygen partial pressure differential using this model is somewhat unique. In order to attempt to evaluate the initial diffusion coefficient to determine if it is the result of a breakdown in the model, or is in fact indicative of a phenomena occurring in the experiment, the short time model, valid for $\tilde{D}t/l^2 \leq 0.15$ and given in equation 11 was utilized. Figure 12 shows the graph of the plot $(M(t)/A)^2$ vs time. Table 9 lists the value of k_p , the parabolic rate constant, the value of the diffusion coefficient calculated for k_p as per equation 12 and the corresponding diffusion coefficient calculated from Figure 11. The results of \tilde{D}_{k_p} and \tilde{D} are in close agreement, indicating that there are two separate processes controlling diffusion during each reduction run.

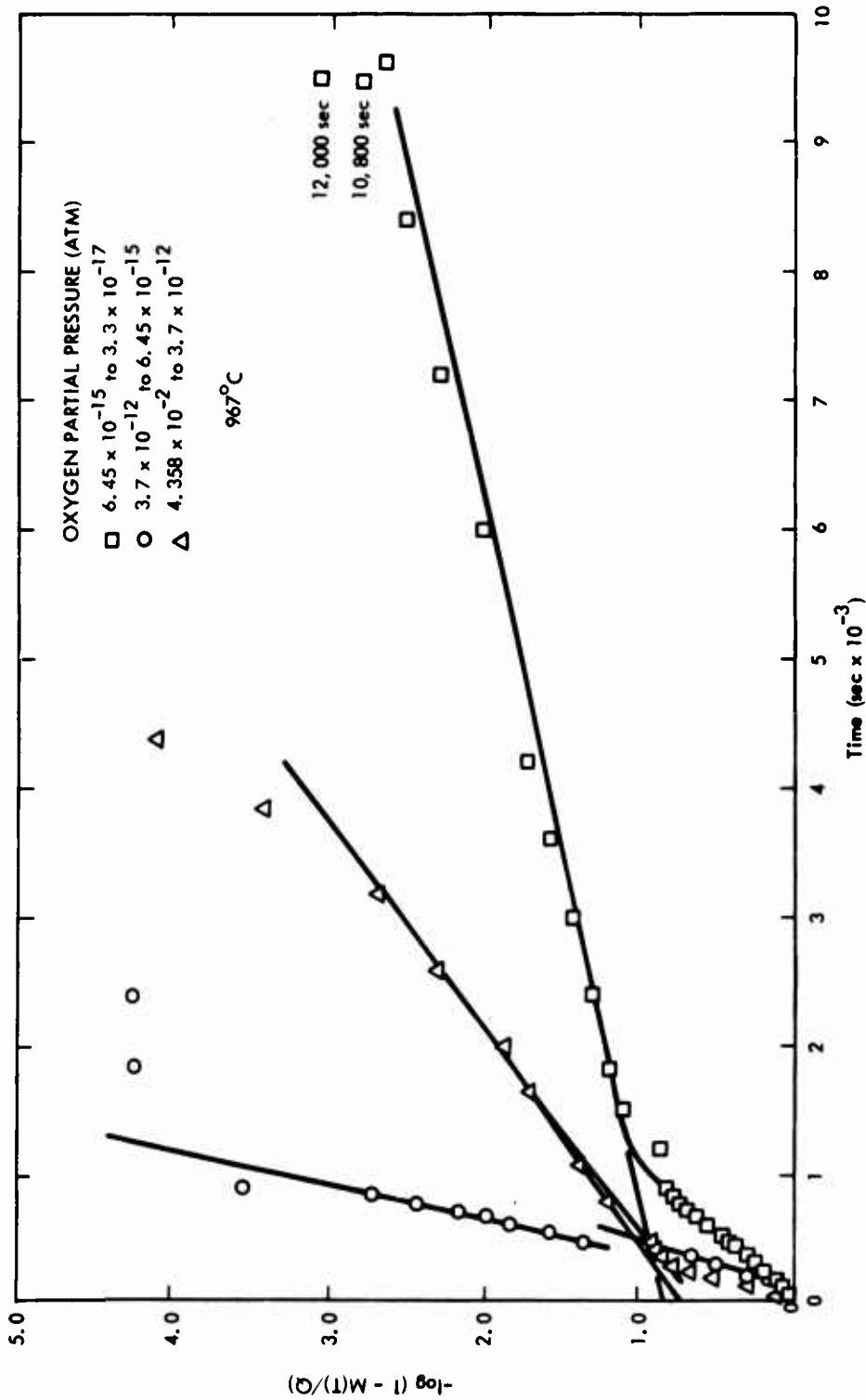


Figure 11. Plot of $-\log(1 - M(t)/Q)$ vs Time Used to Determine the Chemical Diffusion Coefficients of Oxygen in Nb_2O_5 at 967°C

TABLE 8. Validity Test for Application of the Diffusion Models

Nb ₂ O ₅		
\tilde{D} (10 ⁻⁷ cm ² /sec)	Temp. (°C)	\tilde{D}_t/l^2
36.6	967	.39
6.99	967	.93
27.00	967	.41
36.80	967	1.53
9.80	967	.41
2.03	967	.86

TiO ₂ -Nb ₂ O ₅		
\tilde{D} (10 ⁻⁷ cm ² /sec)	Temp. (°C)	\tilde{D}_t/l^2
2.	819	1.15
62.8	819	.34
27.7	819	.21
13.1	819	.70
33.3	819	.18
25.59	819	.48
10.3	819	.43

TABLE 8 (Cont'd.)

HfO ₂ -Nb ₂ O ₅		
\bar{D} (10 ⁻⁷ cm ² /sec)	Temp. (°C)	\bar{D}_t/l^2
7.5	786	4.82
36.6	983	2.02
10.2	983	0.61
29.4	983	1.48
7.0	983	.55
1.05	983	1.08
18.1	1192	4.16
1.17	1192	.67
15.3	1192	.70
.529	1192	.24
6.12	1192	1.01

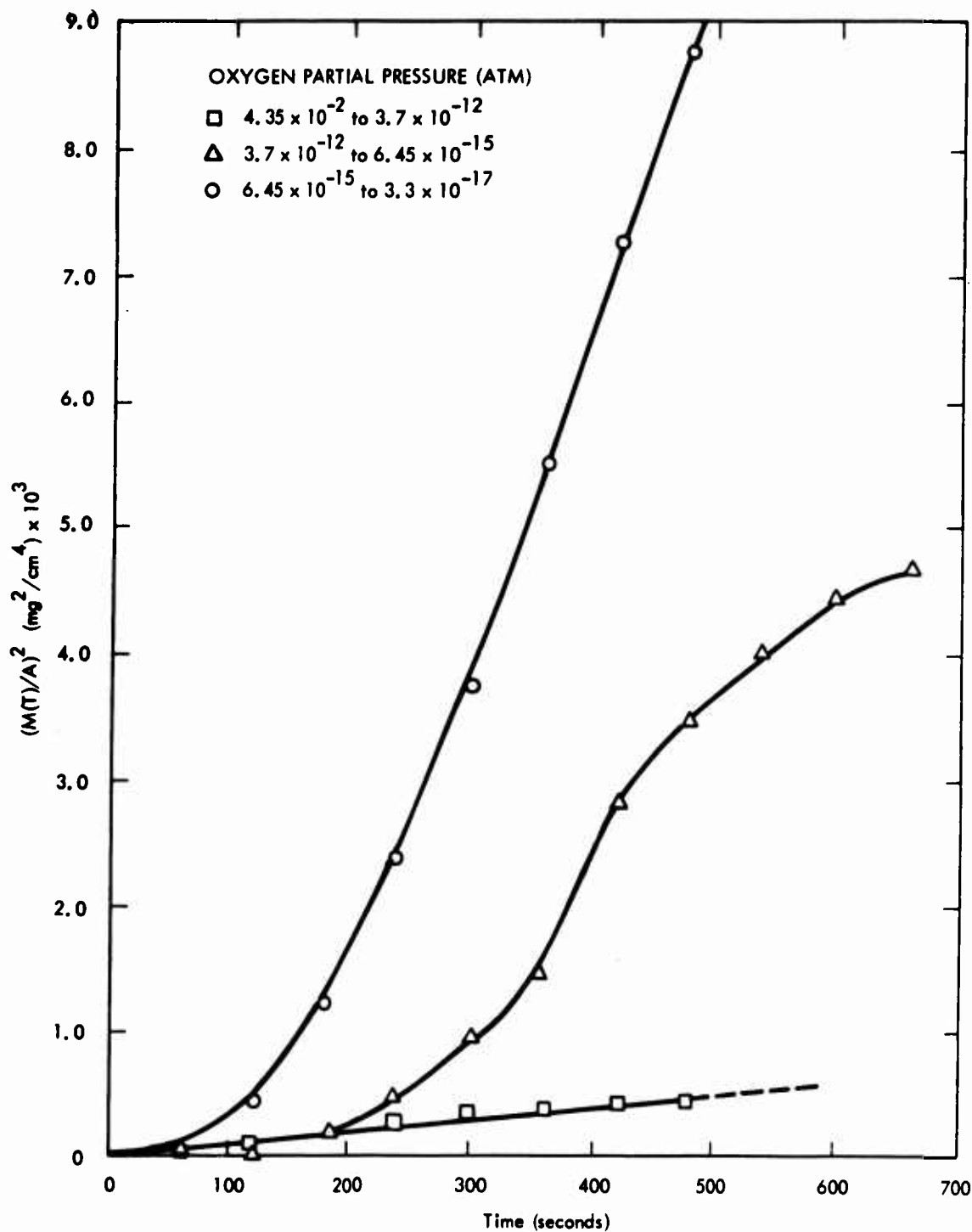


Figure 12. Plot of $(M(t)/A)^2$ vs Time Used to Determine the Chemical Diffusion Coefficients of Oxygen in Nb_2O_5 at 967°C for Short Times

TABLE 9. Comparison of the Chemical Diffusion Coefficient \tilde{D}_{kp} Calculated from the Parabolic Constant for Initial Stages of Reduction and \tilde{D} Calculated From the Slopes Shown in Figure 11.

Nb_2O_5					
Temp. (°C)	ΔP atm	k_p mg^2/cm^4-sec	ΔC mg/cm^3	\tilde{D}_{kp} cm^2/sec	\tilde{D} cm^2/sec
967	4.35×10^{-2} to 3.7×10^{-12}	1.43×10^{-6}	.681	2.46×10^{-6}	3.66×10^{-6}
967	6.45×10^{-5} to 3.3×10^{-17}	2.15×10^{-5}	5.10	10.4×10^{-7}	9.8×10^7

Schäfer⁽²⁴⁾ et al. have measured the thermodynamic stability of the system Nb-O-H-H₂O at 1300°C. O/Nb ratios over the range of 2.0 to 2.5 were investigated. This work definitely demonstrates the existence of 7 distinct equilibrium Nb₂O_{5-x} suboxide phases within this composition range. This evidence, as reported and correlated with other data by Streiff et al⁽²⁵⁾ precludes analyzing the diffusion data as if oxygen were diffusing through a homogeneous phase over all regions of non-stoichiometry. However, because the data of Schäfer⁽²⁴⁾ is reported at 1300°C and the diffusion data reported herein was done at 967°C, it is not possible to accurately determine the equilibrium phase boundaries of the lower temperature diffusion system. It is possible that the break in the plot of $\log (I-M(t)/Q)$ vs t could be the result of diffusion being controlled by different phases formed as the oxygen partial pressure gradient changes throughout the oxide sample. More detailed analysis of this phenomenon will be undertaken during Phase III.

Figure 13 shows a graph of the equilibrium oxygen non-stoichiometry as a function of the oxygen partial pressure. Graphs of this type are used to determine the oxygen partial pressure dependence of the defect structure. In a homogeneous oxide, it is possible to deduce the defect structure of an oxide by determining this power dependence⁽²⁶⁾. Along with the experimental data are several isotherms published by Kofstad⁽²⁶⁾ and Blumenthal⁽¹³⁾ et al. Over this pressure range a variable power dependence of the non-stoichiometric defect structure of Nb₂O₅ on oxygen partial pressure was obtained. The pressure dependence, determined during this experiment, agrees very well with the published results. Because of the strong indication that we can no longer consider defect structures in a homogeneous solid solution for Nb₂O₅, the diffusional processes reported in this work can be attributed to the various suboxide phases in equilibrium with the oxygen partial pressure gradients in the Nb₂O₅. More closely controlled measurements are required to exactly determine the effect of the various suboxides on oxygen diffusion rates.

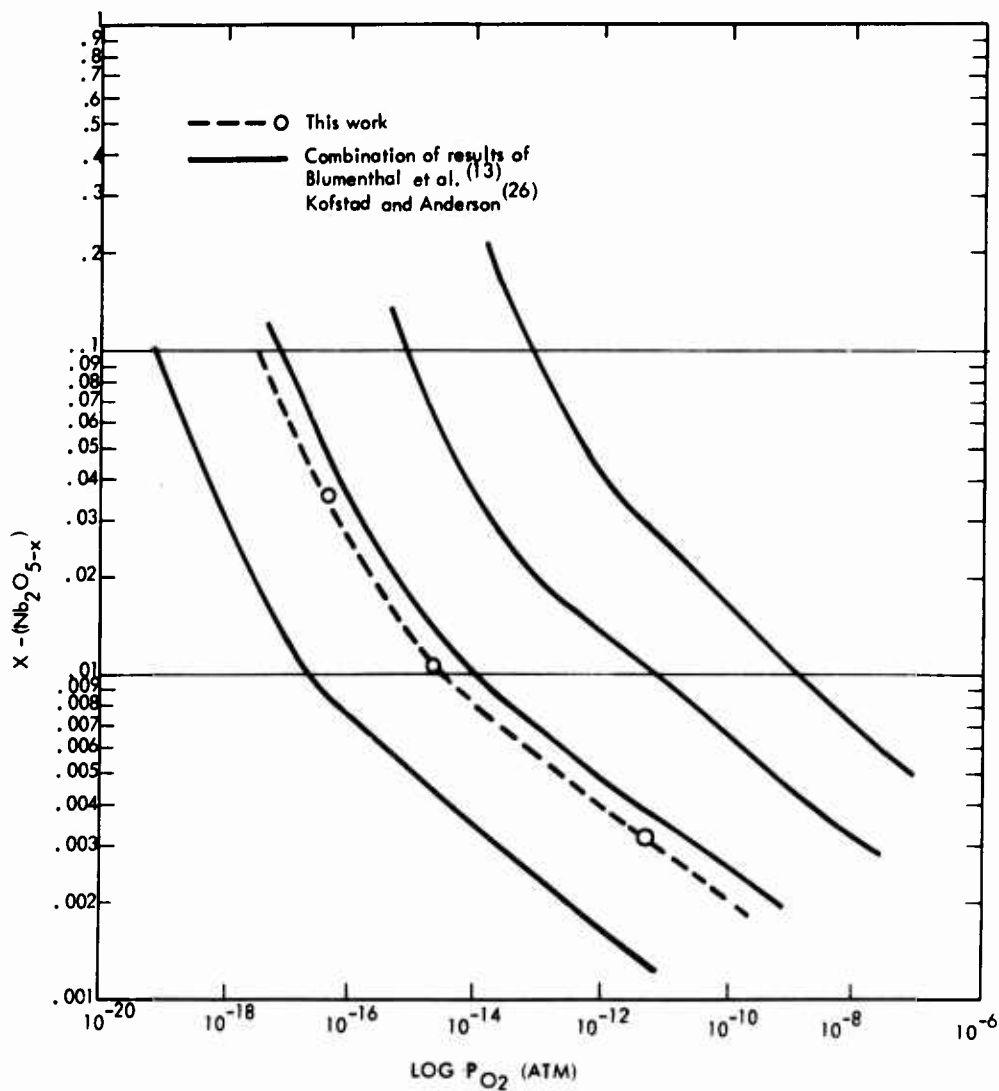


Figure 13. Nonstoichiometry in $\alpha\text{-Nb}_2\text{O}_5$ as a Function of Oxygen Partial Pressure

Relating the values for the chemical diffusion coefficient of oxygen determined in this work to that published in the literature supports the trend that the chemical diffusion coefficient is smaller at larger deviations from stoichiometry than in the near stoichiometric region. Sheasby and Cox⁽²⁷⁾ have reported that at 900°C and 10^{-17} atm oxygen partial pressure $\tilde{D}_{\text{Nb}_2\text{O}_5} = 1.4 \times 10^{-8}$. This work reports that at 967°C and 10^{-17} atm oxygen partial pressure $\tilde{D}_{\text{Nb}_2\text{O}_5}$ is 2.03×10^{-7} . Because of the presence of the suboxide phases, future work on determining the oxygen diffusion coefficient will also require that the suboxide structure through which diffusion occurs will have to be identified.

3.5.2 $\text{TiO}_2\text{-Nb}_2\text{O}_5$

Figure 7 shows the weight loss vs time for the $\text{TiO}_2\text{-Nb}_2\text{O}_5$ system (62.6 mole% TiO_2 - 37.4 mole% Nb_2O_5). This data was analyzed by the methods reported in Section 3.5.1 for Nb_2O_5 . Figure 14 shows a graph of $\log(1-M(t)/Q)$ vs time. Table I lists the values of \tilde{D} as determined from the slopes of these lines. Value of $\tilde{D}t/l^2$ as calculated from the derived diffusion coefficients are listed in Table 8; the dependence of the degree of non-stoichiometry on oxygen partial pressure is shown in Figure 15 for two conditions. It is assumed that this oxide is composed of $\text{TiNb}_2\text{O}_7 + \text{TiO}_2$ after Wadsley⁽²⁸⁾. Two conditions for the distribution of anion vacancies are postulated. The first is that the vacancies are associated only with TiO_{2-x} , and the second is that the vacancies are associated only with $\text{TiNb}_2\text{O}_{7-x}$.

In both cases the power dependencies, i.e., $x \propto \text{O}_2^{-1/20}$ is the same. This dependence of the degree of non-stoichiometry is exceptionally low, and no explanation for this behavior can be given at this time.

As was the case with Nb_2O_5 , TiNb_2O_7 can be identified with a homologous series $\text{Me}_{3n}\text{O}_{8n-3}$ ⁽²⁸⁾. Again it is possible to conclude that each of the reported diffusion values is indicative of the oxygen transport rate through several phases as oxygen is removed from

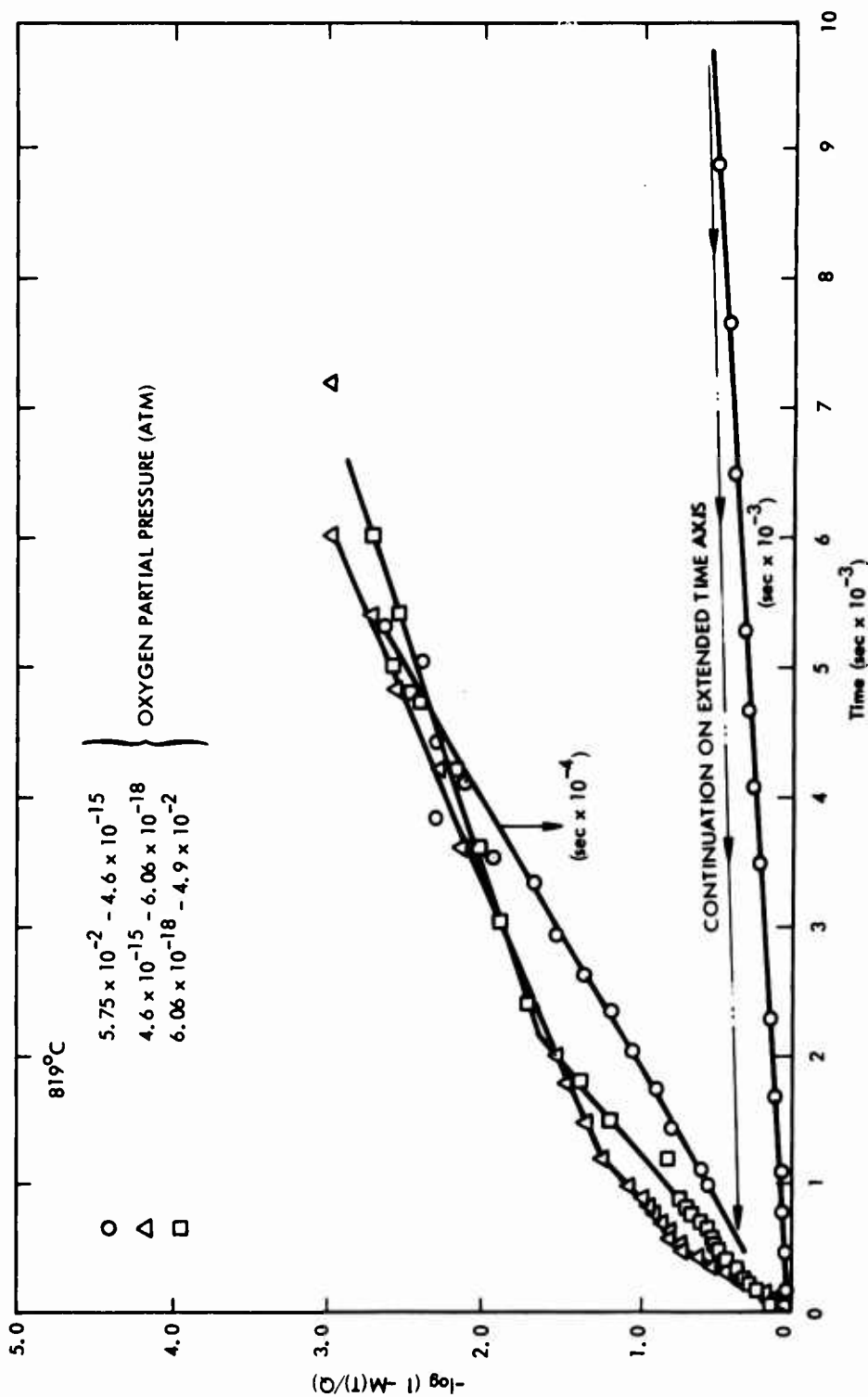


Figure 14. Plot of $-\log (1-M(t)/Q)$ vs Time Used to Determine the Chemical Diffusion Coefficients of Oxygen in a 1 67:1 $\text{TiO}_2\text{-Nb}_2\text{O}_5$ Oxide at 819°C

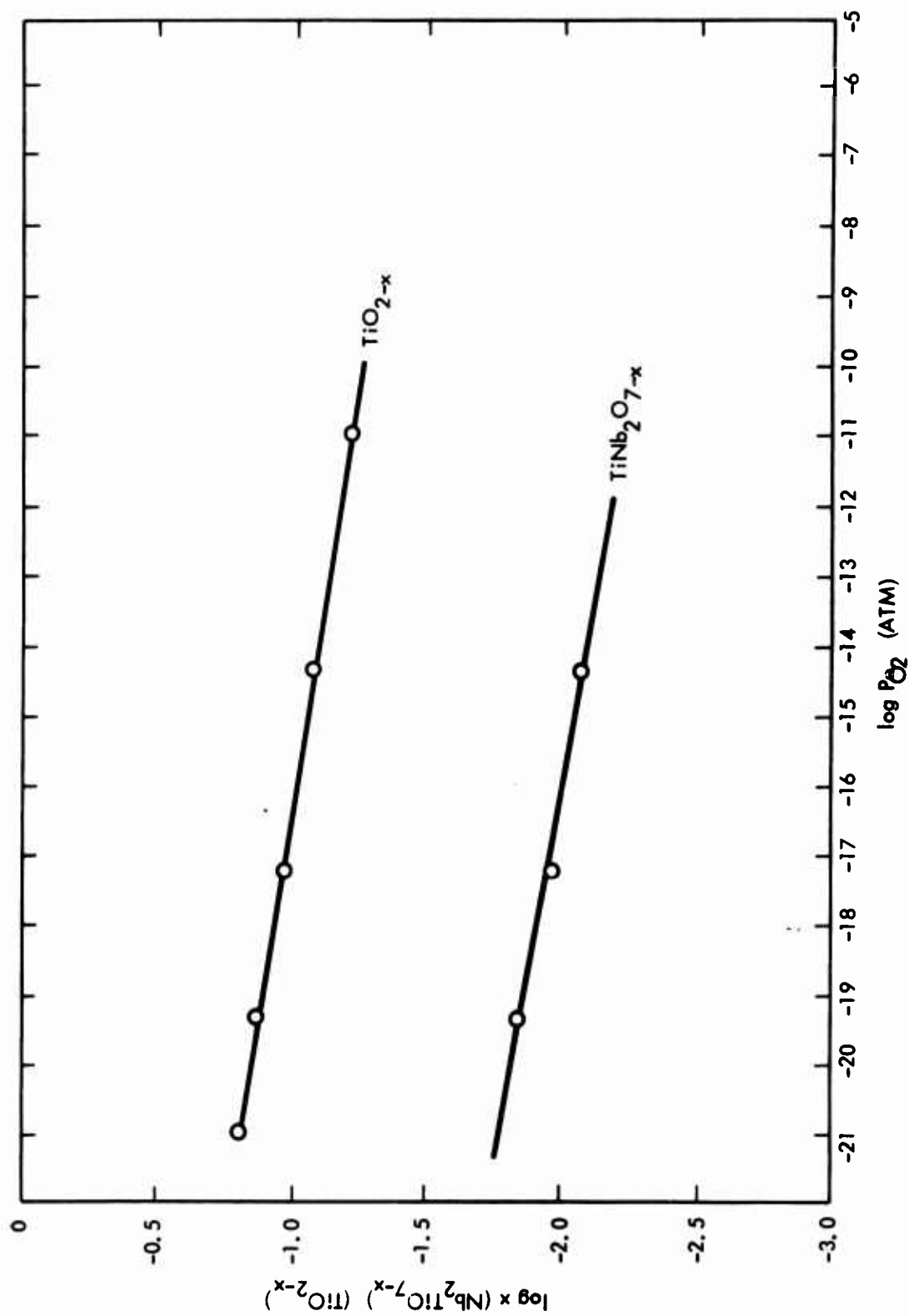


Figure 15. Nonstoichiometry in 1.67:1 $\text{TiO}_2\text{-Nb}_2\text{O}_5$ as a Function of Oxygen Partial Pressure

the sample during equilibration, and the comments applying to the experimental techniques required for Nb_2O_5 would also apply for this system. There is no comparable data for oxygen diffusion through $\text{TiO}_2\text{-Nb}_2\text{O}_5$ found in the literature for comparison. Excepting the equilibration between 10^{-2} and 10^{-15} atm, the transport rate of oxygen through this oxide is quite rapid even at 819°C . During Phase III the oxygen diffusion rate through the $\text{TiO}_2\text{-Nb}_2\text{O}_5$ oxide will be evaluated at 1000 and 1200°C .

3.5.3 $\text{HfO}_2\text{-Nb}_2\text{O}_5$

Figures 8-10 show the weight loss vs time for the oxygen partial pressure ranges studied. Again this data was analyzed by the techniques reported in Section 3.5.1 for Nb_2O_5 . Figures 16 through 18 show the graphs of $-\log \{1-M(t)/Q\}$ vs time for 786°C , 983°C , and 1192°C , respectively. Table 1 lists the values of D at the various conditions for $\text{HfO}_2\text{-Nb}_2\text{O}_5$. Values of $\tilde{D}t/l^2$ are tabulated in Table 8. The dependence on the degree of non-stoichiometry on oxygen partial pressure is plotted on Figure 19, assuming the oxygen is coming from excess HfO_{2-x} and the compound $\text{Hf Nb}_2\text{O}_7$ remains stoichiometric. No information concerning this mixed oxide system has been found in the literature. The $\text{HfO}_2\text{-Nb}_2\text{O}_5$ was not as thick as the Nb_2O_5 and $\text{TiO}_2\text{-Nb}_2\text{O}_5$ sample. Generally, equilibrium was achieved quite rapidly. In addition, the weight gains were very small. This data must be considered preliminary in nature.

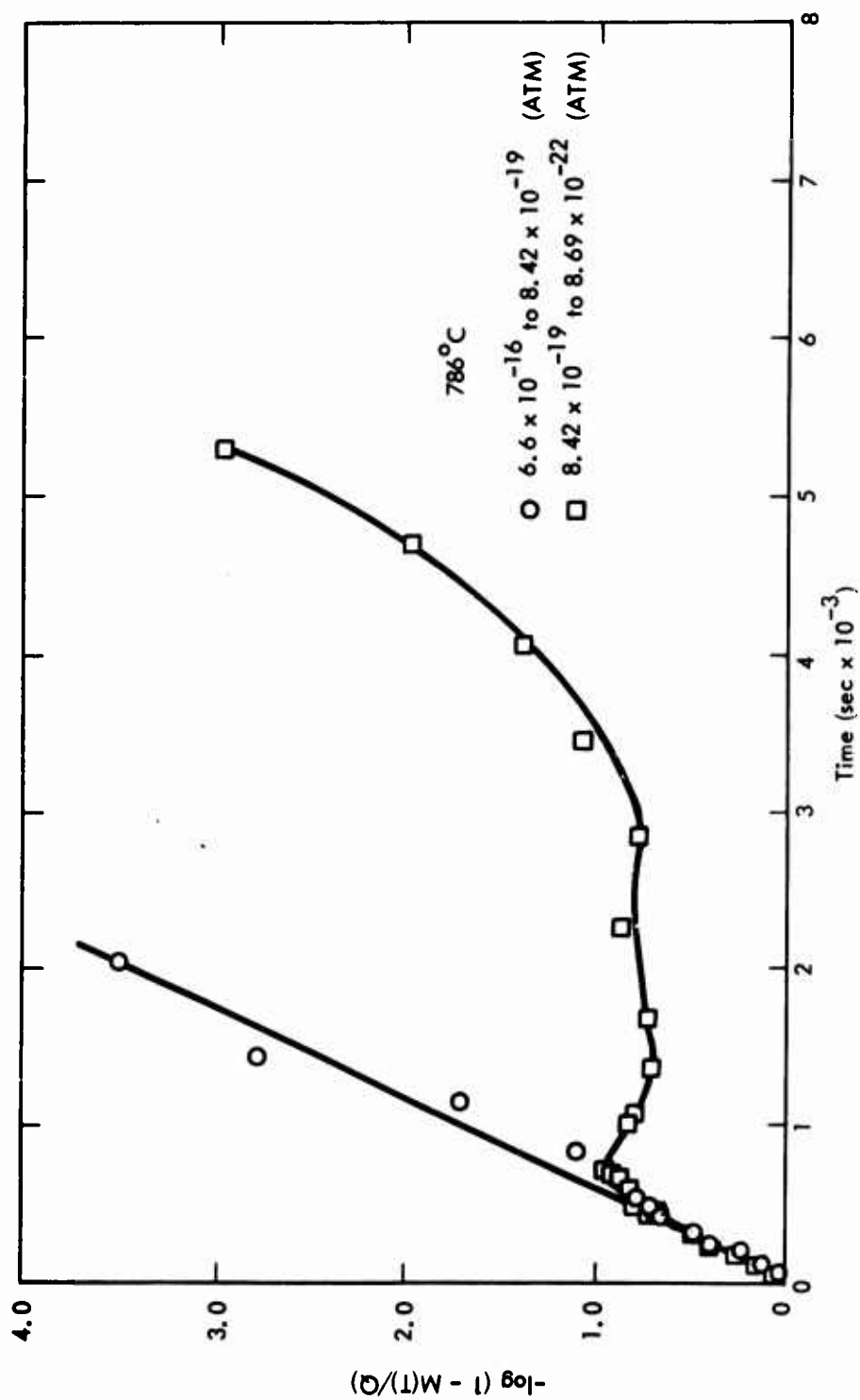


Figure 16. Plot of $-\log(1-M(t)/Q)$ vs Time Used to Determine the Chemical Diffusion Coefficients of Oxygen in a 2.85:1 $\text{HfO}_2\text{-Nb}_2\text{O}_5$ Oxide at 786°C

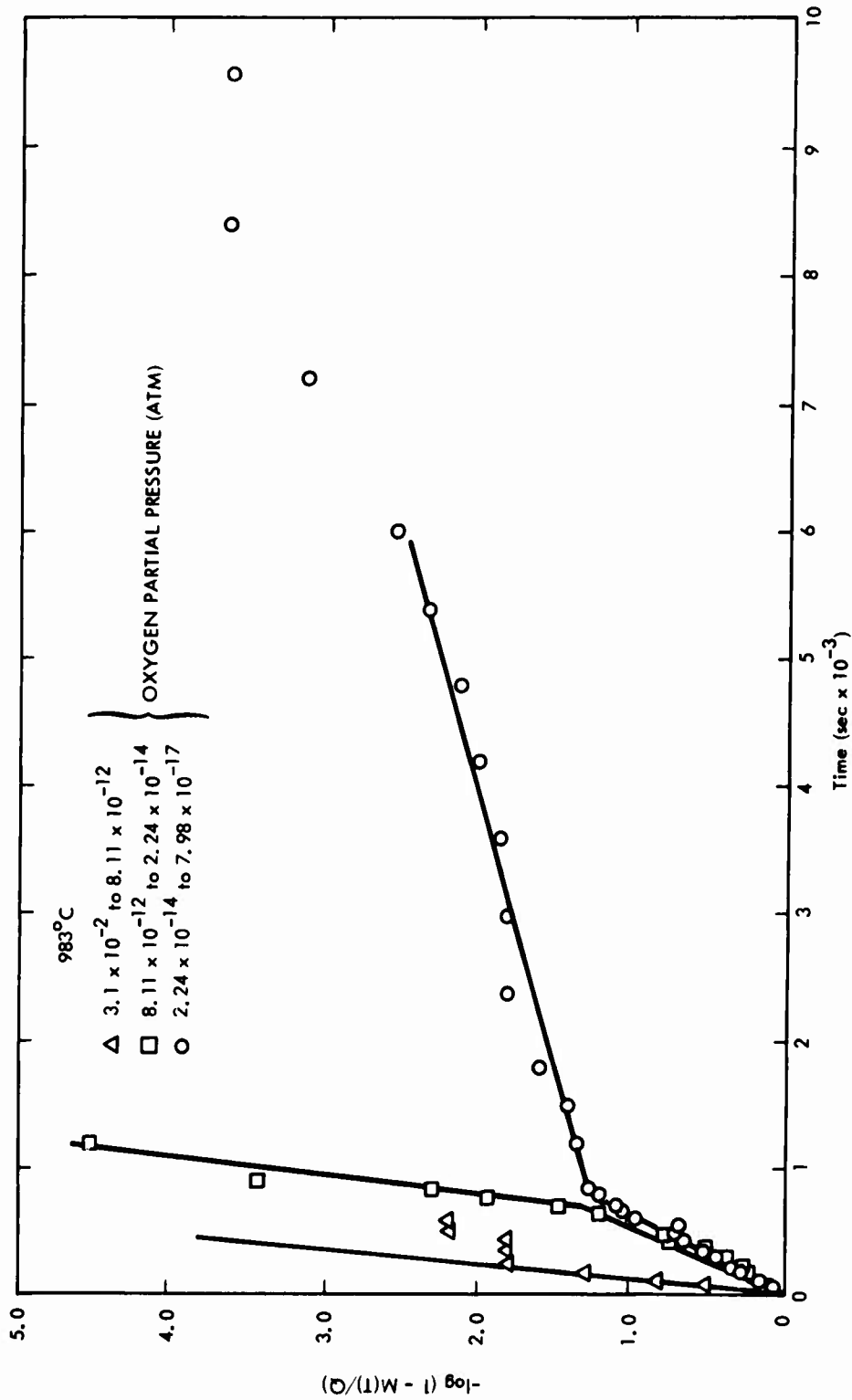


Figure 17. Plot of $-\log(1-M(t)/Q)$ vs Time Used to Determine the Chemical Diffusion Coefficients of Oxygen in a 2.85:1 $\text{HfO}_2\text{-Nb}_2\text{O}_5$ Oxide at 983°C

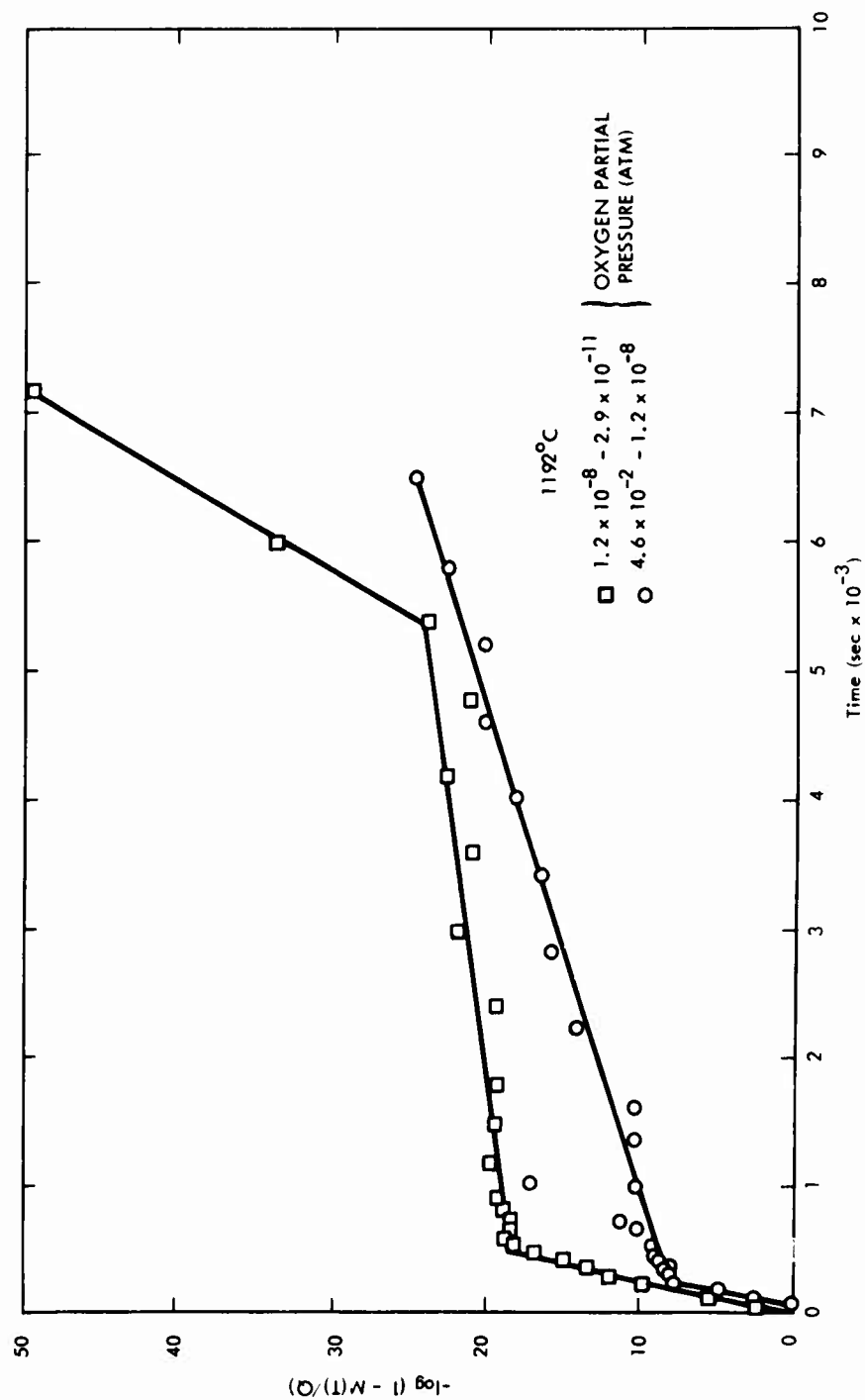


Figure 18. Plot of $-\log (1 - M(t)/Q)$ vs Time Used to Determine the Chemical Diffusion Coefficients of Oxygen in a 2.85:1 $\text{HfO}_2\text{-Nb}_2\text{O}_5$ Oxide at 1192°C

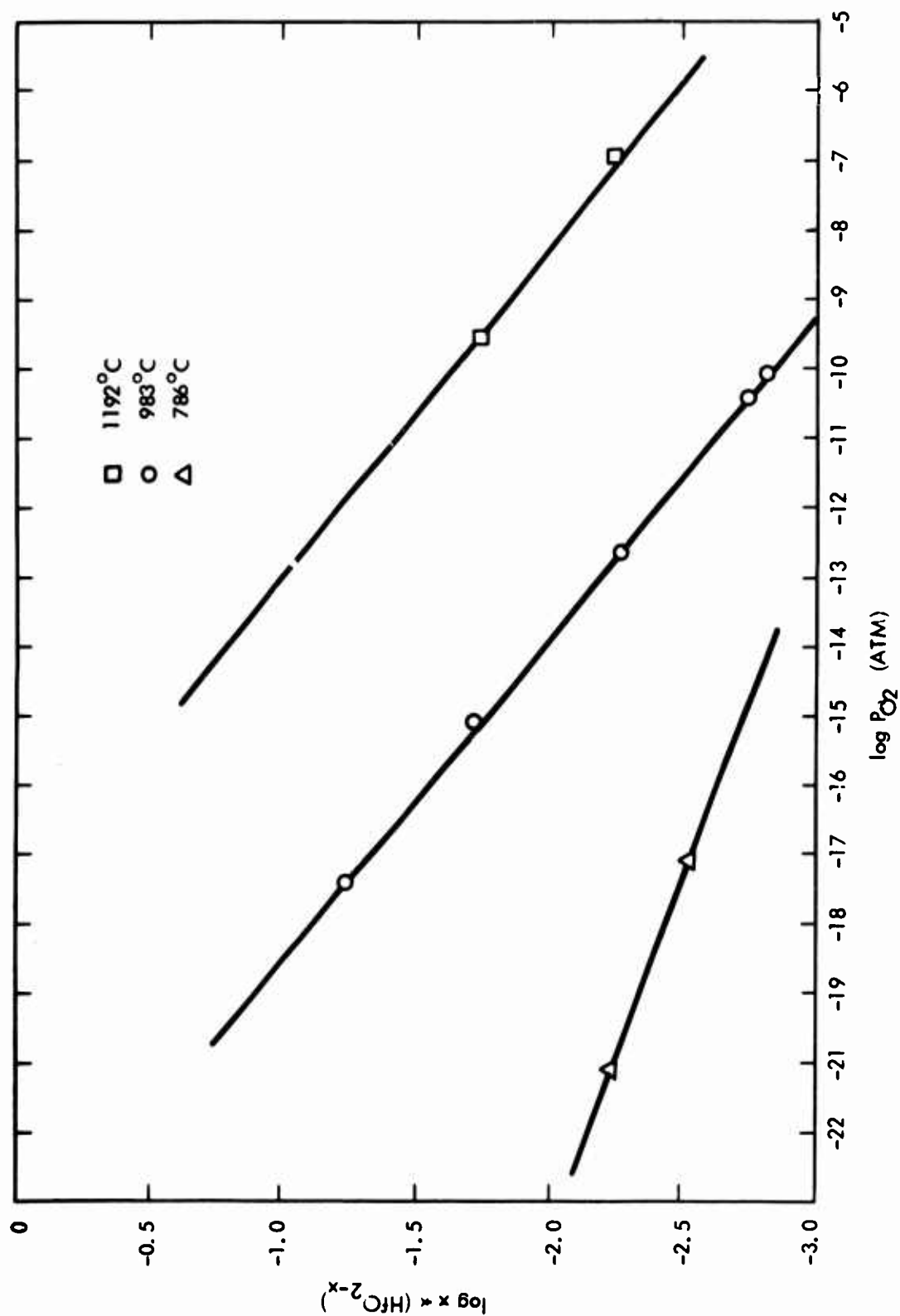


Figure 19. Nonstoichiometry in 2.85:1 $\text{HfO}_2\text{-Nb}_2\text{O}_5$ as a Function of Oxygen Partial Pressure²

IV. ANALYSIS OF THE OXIDATION BEHAVIOR OF A Nb-15Ti-10W-10Ta-2Hf-3Al ALLOY B-1

Very little work has been reported in the literature dealing with the oxidation behavior of complex columbium alloys utilizing x-ray, metallographic, and microprobe techniques^(29, 30). The B-1 alloy developed by WANL⁽³¹⁾ has been selected for a detailed evaluation. This alloy is currently being investigated by McDonnell-Douglas as a cladding material for a heat resistant leading edge material for one of the space shuttle concepts⁽³²⁾. It is a ductile alloy with moderate oxidation resistance. During the first phase of this program, B-1 was oxidized before and after exposure in a doped liquid autoclave. X-ray results for these oxides will be combined with kinetic, metallographic, and microprobe data to attempt to understand the complex oxidation behavior of this system.

4.1 EXPERIMENTAL APPARATUS AND PROCEDURE

B-1 alloy sheet samples .051 cm. thick were oxidized using a Stanton-Thermobalance. Heating was accomplished in a vertical platinum/rhodium wound furnace, with the natural convection current providing a fresh supply of air. Temperature was controlled to within $\pm 5^{\circ}\text{C}$ by the output of a platinum-platinum-rhodium thermocouple. The weight increase could be determined within ± 1 mg. Both weight and temperature were continuously recorded. The test samples were supported on Alumina supports with the sheet samples held in a vertical plane by slots cut into the Alumina refractory with a diamond saw. For the temperatures and environments under consideration, no discoloration or other reaction with the Al_2O_3 was noticed.

The samples were loaded onto the balance arm while the furnace, poised above the sample, was heated to the desired temperature. When the furnace was at temperature, the furnace was lowered over the sample. In less than 2 minutes, the sample was at temperature. The initial weight of the sample was corrected at each temperature for the weight changes caused

by the empty crucible mounting system due mainly to adsorbed moisture being lost.

Two series of experiments were made on the B-1 alloys. Two variations of the B-1 alloy were tested. One B-1 alloy contained 3.4 wt% Al and one B-1 alloy contained 2.2 wt% Al.

The first series of experiments involved the oxidation of both alloys at 1260°C to see if the small difference in aluminum content had any effect on the oxidation properties. The weight gain per unit area vs time, as shown on Figure 20, showed no difference in oxidation rate due to the difference in the aluminum concentration.

In order to duplicate the effects of a dual temperature exposure as reported by Goodspeed and Cornie⁽³¹⁾, B-1 samples were pre-oxidized for one hour at 1260°C and then furnace cooled and oxidized at 1100°C. Figure 21 shows the oxidation rate after the pre-oxidation treatment. On the same graph, the oxidation rate at 1000°C is plotted. This experiment verifies the results previously published by Goodspeed and Cornie⁽³¹⁾. The oxidation rate for at least 60 minutes at 1100°C after pre-oxidation at elevated temperature is as good as the oxidation rate of an untreated sample for the same time period but at a 100°C lower temperature. The oxidation rate after pre-oxidation at 1300°C was linear. Goodspeed and Cornie showed this improvement in oxidation rate for times up to 60 hours. There was a dual oxide layer formed as the result of this treatment (Figure 22); however, this layer was prone to spall as the sample was rapidly cooled to room temperature.

The second series of experiments were designed to measure the rate of growth of the various zones formed in the B-1 alloy during air oxidation. In Phase I, it was shown that a series of layers formed below the oxide layer form on the B-1 alloys. This layer formation was examined as a function of temperature and time at 800, 1000, and 1200°C.

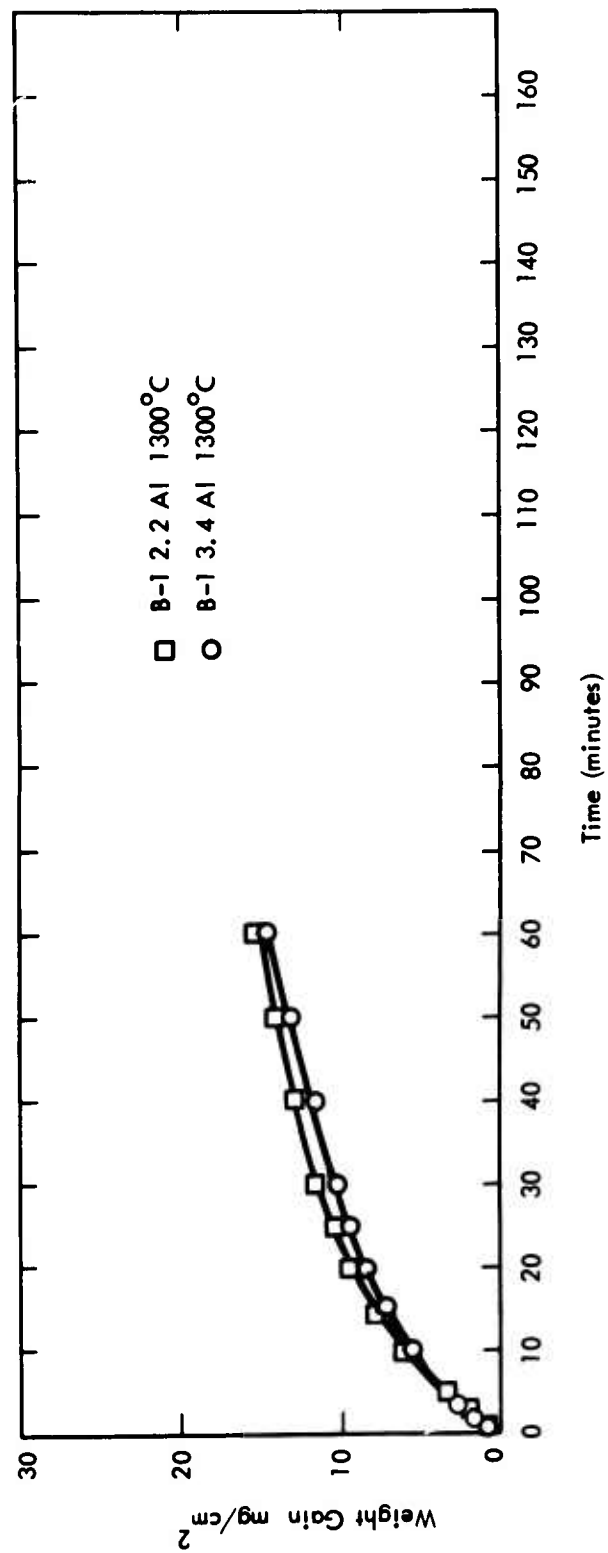


Figure 20. Effects of Al Content on the Oxidation Rate of B-1 Alloys

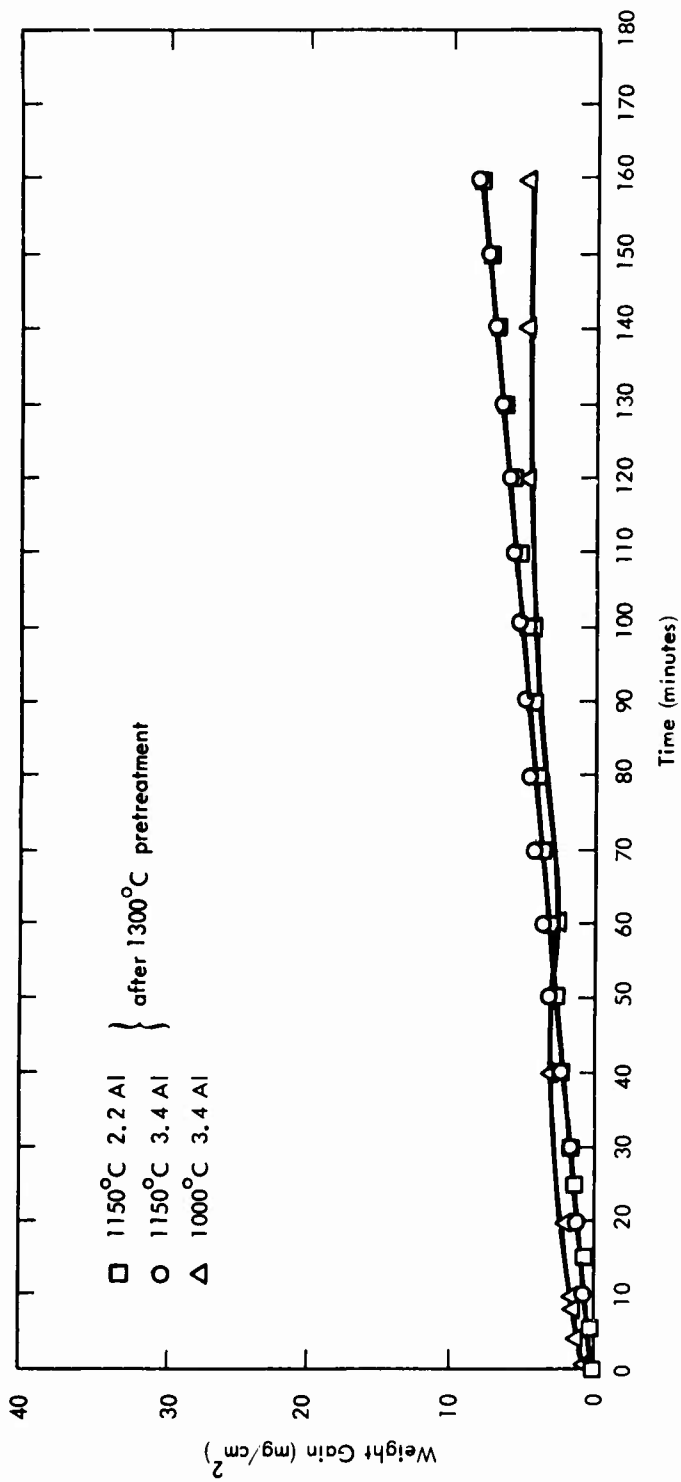
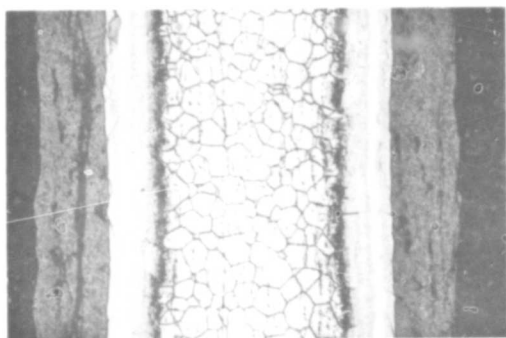
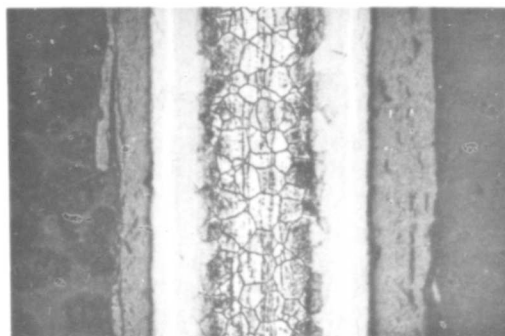


Figure 21. Comparison of the Oxidation Rate of B-1 at 1100°C After One Hour at 1300°C with B-1 Oxidation at 1000°C



100X

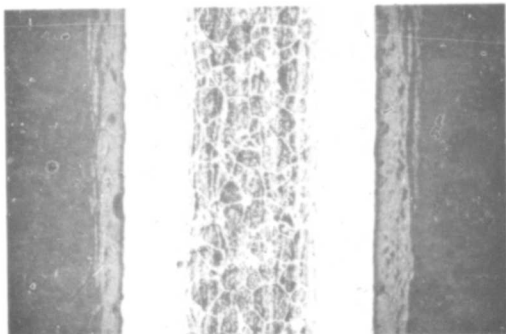
B-1 Alloy - 2.2 wt. % Al
1300°C - 1 hour



100X

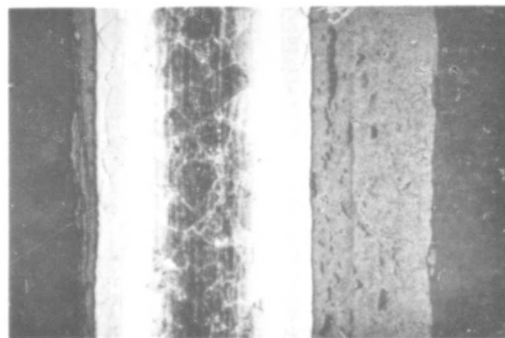
B-1 Alloy - 3.4 wt. % Al
1300°C - 1 hour

Reproduced from
best available copy.



100X

B-1 Alloy - 2.2 wt. % Al
1300°C - 1 hour



100X

B-1 Alloy - 3.4 wt. % Al
1300°C - 1 hour

Figure 22. Photomicrograph of the Oxide Scale Formed on B-1 After One Hour at 1300°C and 3 Hours at 1100°C



Figure 23 shows oxidation kinetics for the alloys at 800, 1000, and 1200°C. If one compares the oxidation rates at 1260°C and 1200°C (Figure 23 and Figure 20, respectively) there appears to be little difference in oxidation kinetics as a function of temperature.

Figure 24-26 shows the etched microstructure for these alloys after exposure to their respective oxidation environments in the etched condition. At 800°C the base metal is relatively unaffected and parabolic oxidation occurs. The only zone other than the oxide, which is visible, is that zone specified by the letters B and F. As the oxidation temperature is raised to 1000°C, an etched zone C and E begin to appear; however, some of the metallic zone D is still unaffected after 36 hours exposure. Even after 4 hours at 1200°C the metallic zone D does not exist. This zone has been affected during oxidation, and Ti is selectively etched out of the base metal because of the reaction with air.

This Ti depleted zone was illustrated by a qualitative microprobe scan made on samples of the B-1 alloy exposed in air for 3 hours at 1060°C. A microprobe trace of the elements Ti, Ta, and Nb is shown in Figure 27. The location of the microprobe trace is shown on the photomicrograph of the oxide structure. In the unetched condition, the "oxide", and "dark grain" and "light zone" are discernible from the metal matrix. The Ti depleted "dark zone" is revealed on etching.

Initially it was expected that this zone depleted in Ti was a direct result of Ti migration during oxidation. However, subsequent microprobe traces on the B-1 alloys shown in Figures 24 through 26 in the unetched condition revealed no such Ti depleted zone. It is apparent that during oxidation the chemical stability of Ti in the depleted zone is altered so that it becomes chemically active with the etchant and is leached away.

Figure 28 through 30 shows the rate of zone growth for the B-1 alloys. The various zone thicknesses, as determined from filar optical microscope measurements, are plotted vs $t^{1/2}$.

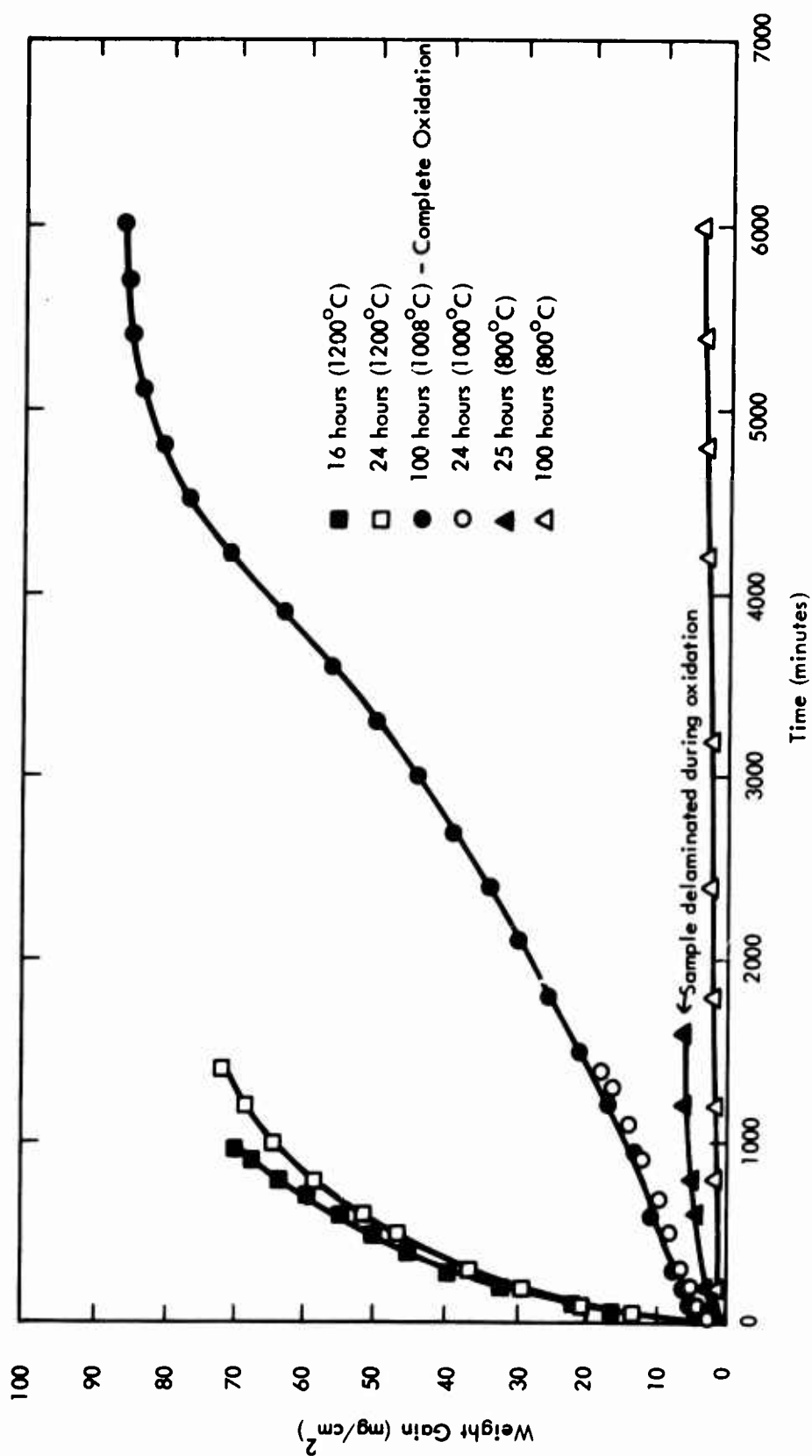


Figure 23. Weight Gain as a Function of Time for B-1 Alloys with 3.42 Al Oxidized at 800, 1000, and 1200°C in Air

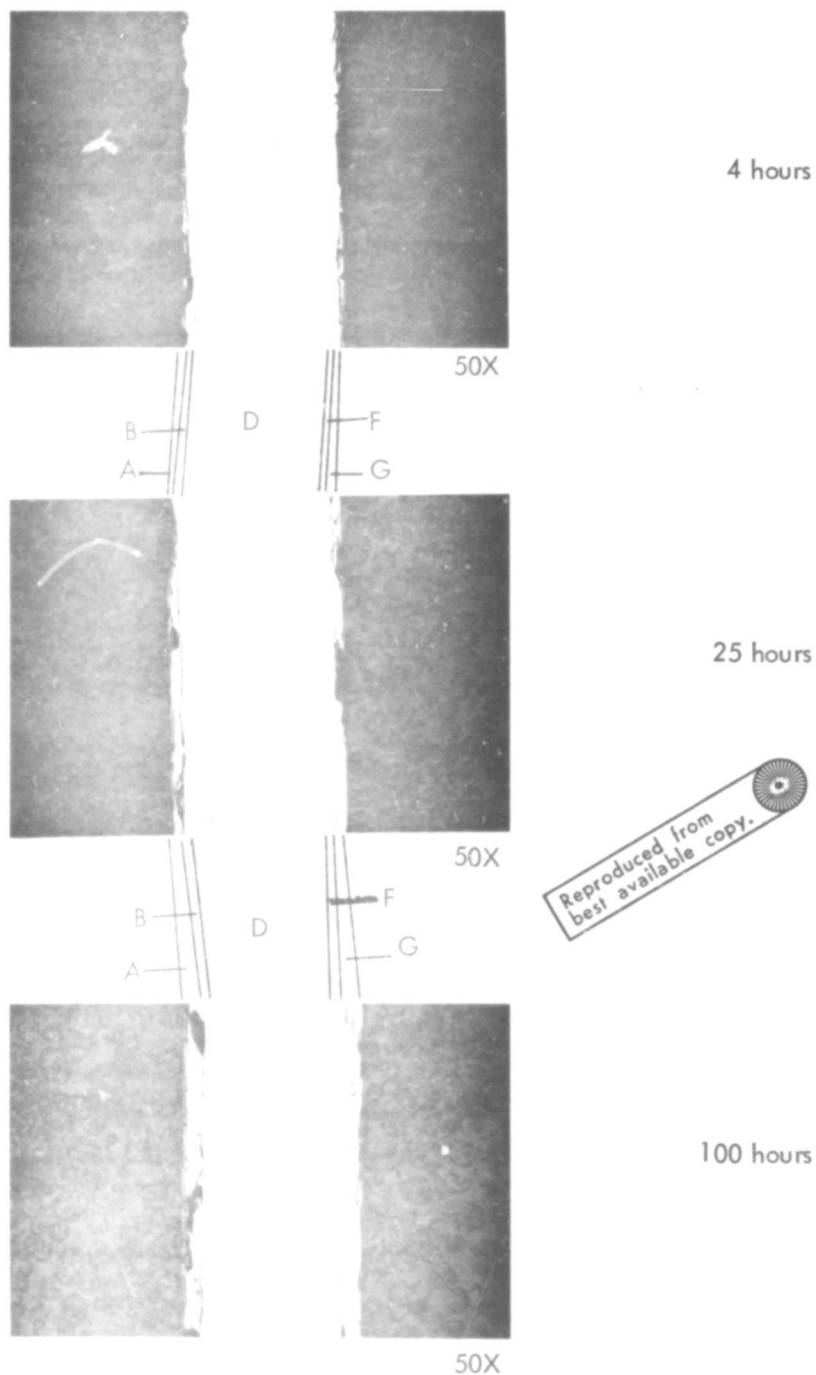
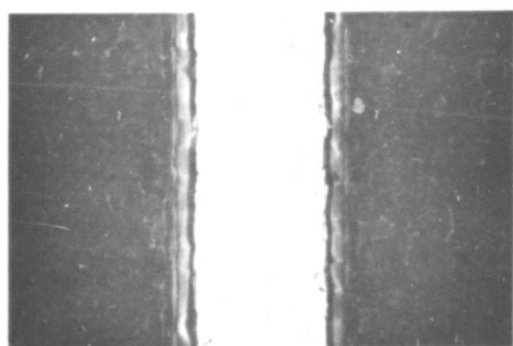


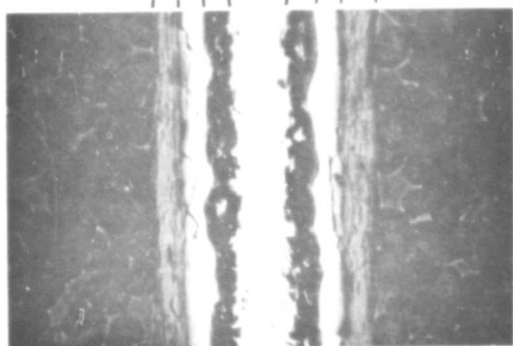
Figure 24. Oxide Scales on a B-1 Alloy Oxidized in Air at 800°C for Times Indicated.
(0.05 cm thick) Etchant (1:1:1 - HNO_2 -HF-Glycerin)



4 hours

50X

A B C D E F G

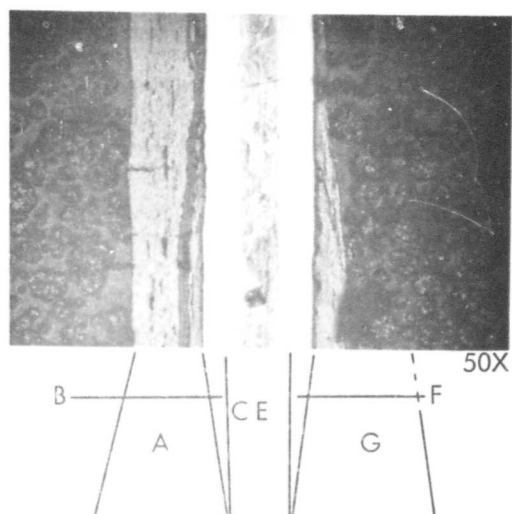


36 hours

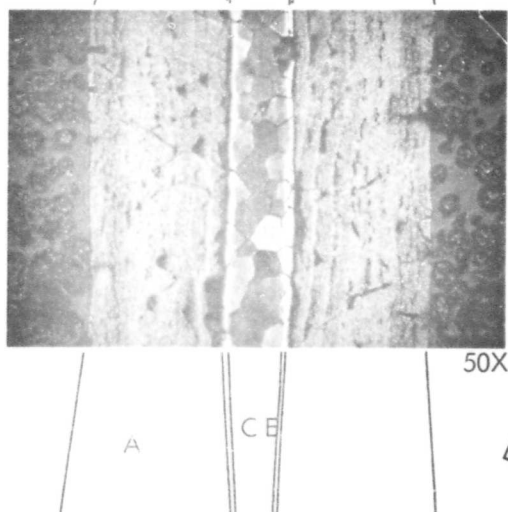
50X

100 hour sample
was completely oxidized

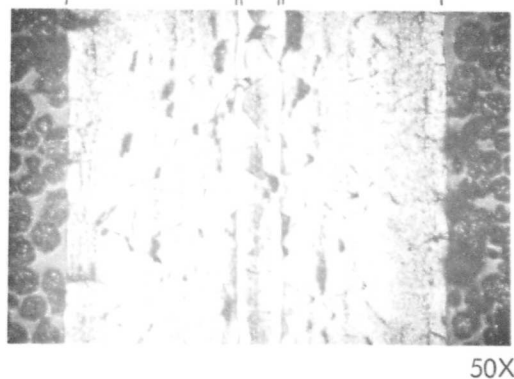
Figure 25. B-1 Alloy Oxidized in Air at 1000°C for Times Indicated
(0.05 cm thick) Etchant (1:1:1 - Glycerin-Hf-HNO₃)



4 hours



16 hours



24 hours



Reproduced from
best available copy.

Figure 26. B-1 Alloy Oxidized in Air at 1200°C for Times Indicated.
(0.05 cm thick) Etchant (1:1:1 - Glycerin-HF-HNO₃)

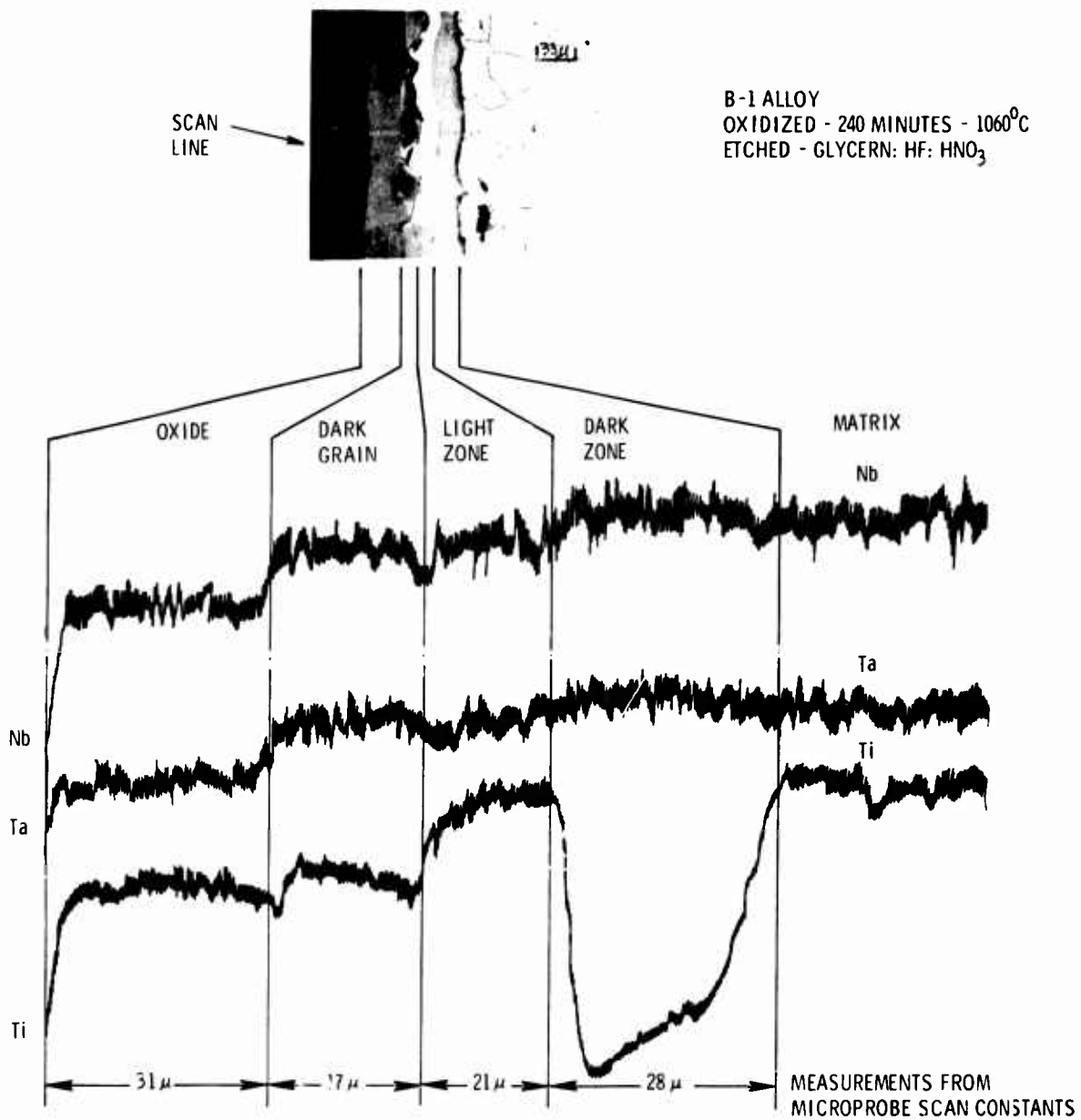


Figure 27. Microprobe Scan of Ti, Nb, and Ta Across Sample 20 B-1 Alloy

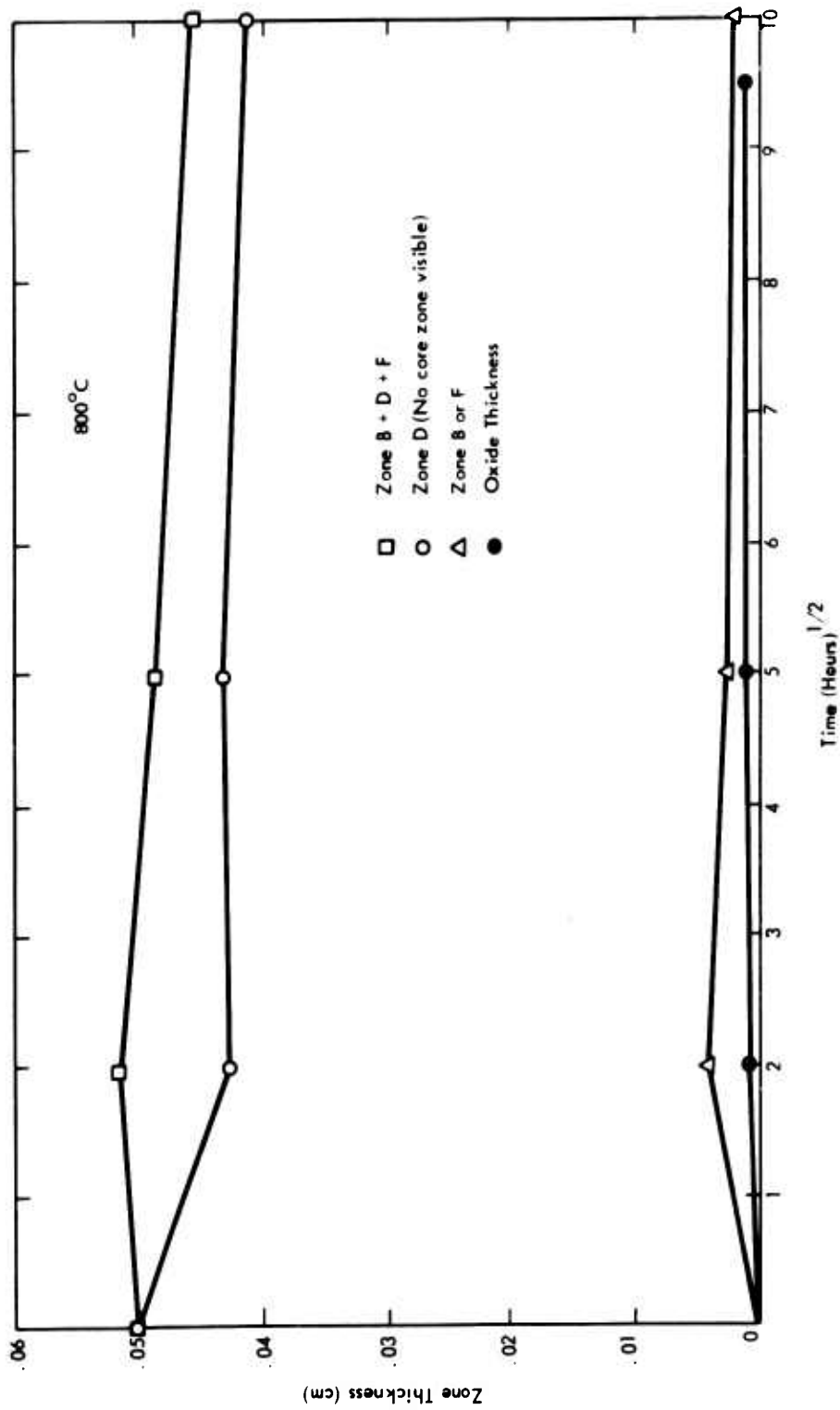


Figure 28. Rate of Growth of Various Zones in B-1 as a Function of Time at 800°C

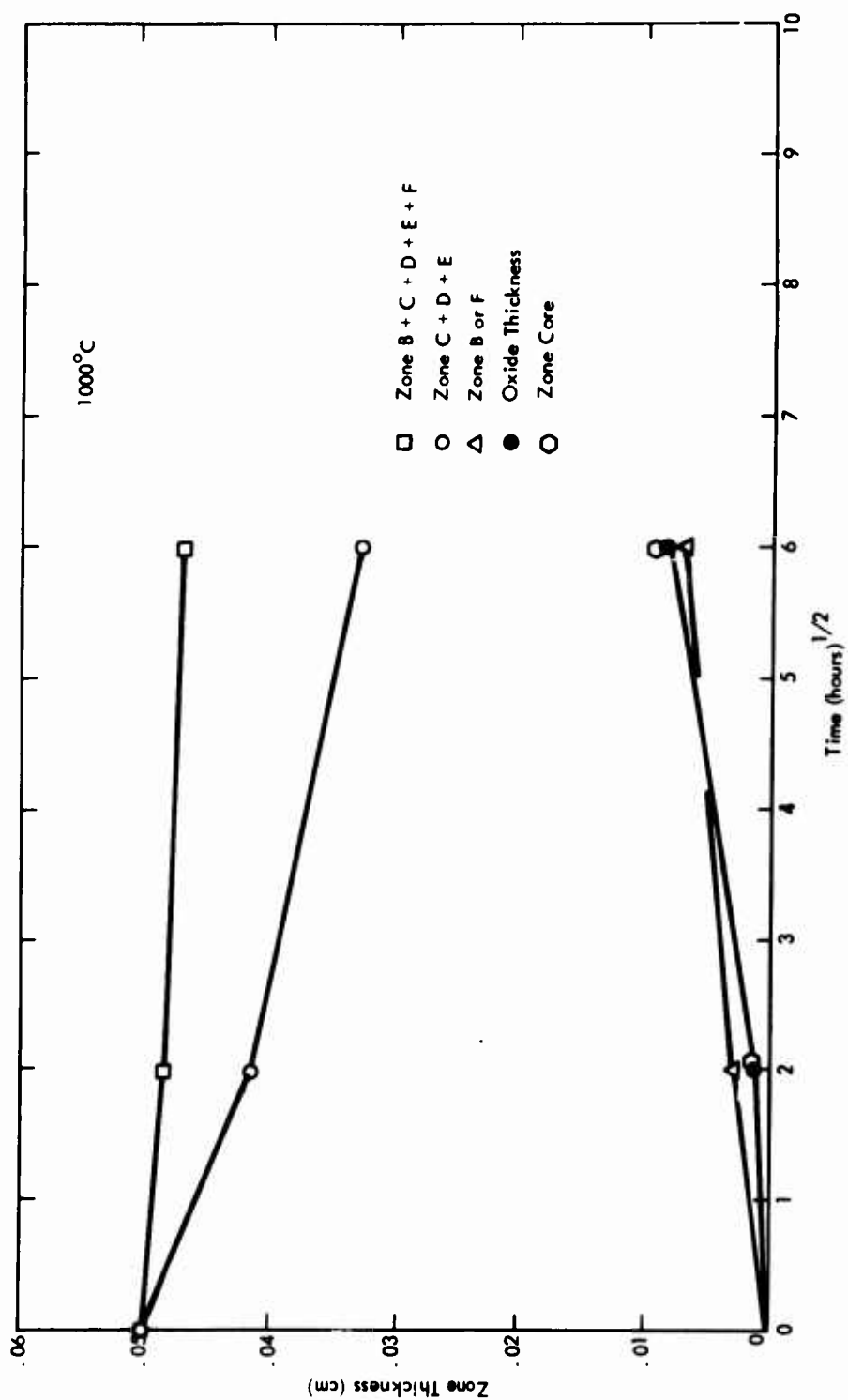


Figure 29. Rate of Growth of Various Zones in B-1 as a Function of Time at 1000°C

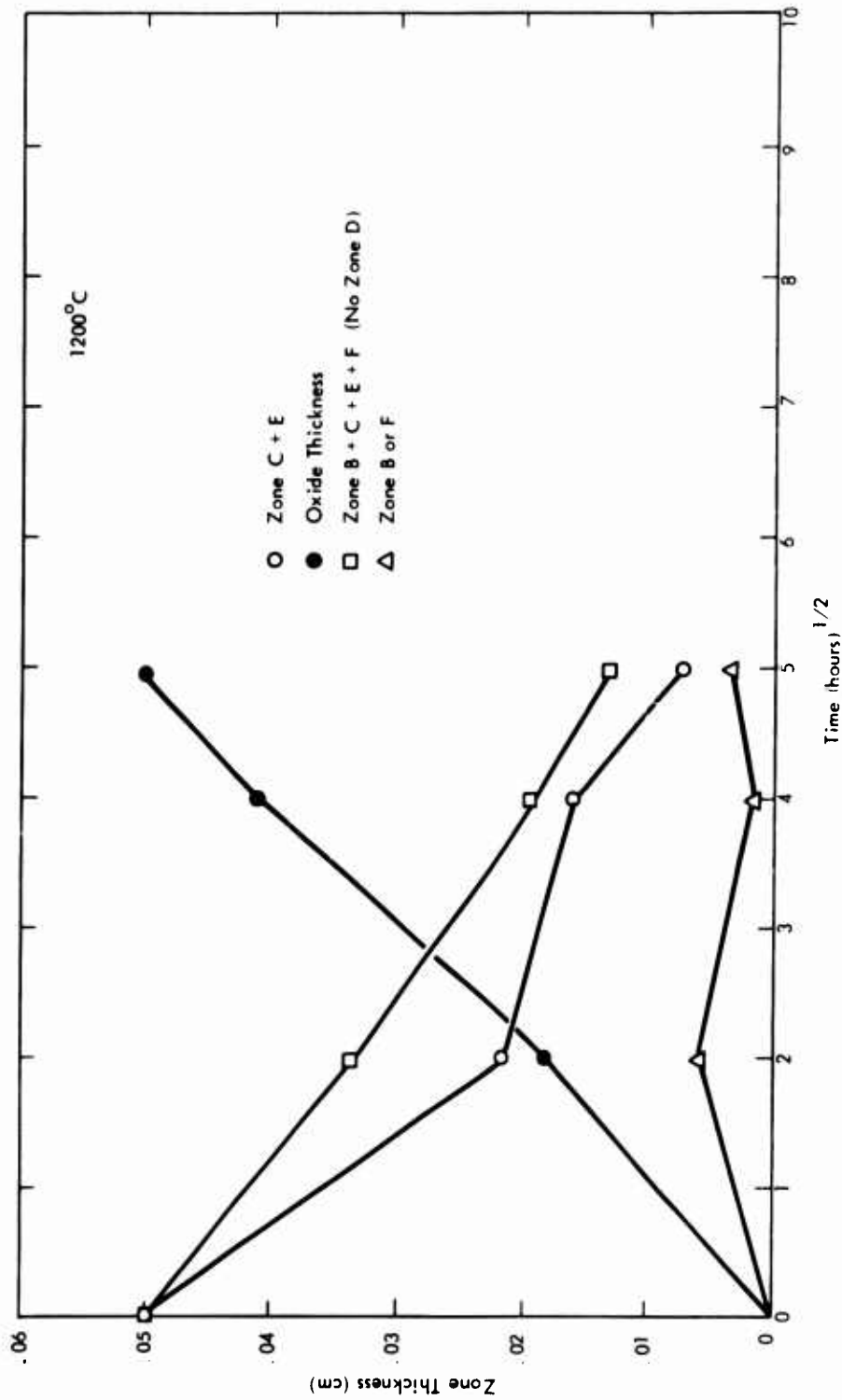


Figure 30. Rate of Growth of Various Zones in B-1 as a Function of Time at 1200°C

For the samples tested at 800°C, it appears that internal oxidation does not occur. Also, the rate of metal loss diminishes after about 4 hours. A plot of $(M(t)/A)^2$ vs time for these temperatures gives a straight line relationship. Figure 31 indicates parabolic behavior or a diffusional controlled process initially. The parabolic oxidation constants are reported in Table 10. For B-1 at 800°C, it appears that a protective oxide layer is controlling the oxidation rate. After 500 minutes the weight gain can be approximated by a linear rate constants of $5.5 \times 10^{-4} \text{ mg/cm}^2/\text{min}$. This linear behavior can be explained by a Loria's-type mechanism⁽³³⁾ where the rate of the reaction is controlled by ionic diffusion through a thin layer of some oxide which remains at a constant thickness. Diffusion through zones B and F, Figure 24, could be rate controlling. Figure 28 indicates that these zones do not change thickness appreciably with time. The oxide scale does, however, grow slowly with time.

At 1000°C the parabolic rate constant for initial oxidation is $k_p = .160 \text{ mg}^2/\text{cm}^4/\text{min}$. The internally oxidized zone C-E thickness increases with time at about the same rate as the zone B-F (Figure 29) as does the oxide layer thickness. Parabolic behavior at this temperature breaks down after 800 minutes as shown in Figure 32 and Figure 23. Break away oxidation occurs; and at 1000°C, a 0.020 inch thick sample is completely consumed after about 80 hours.

Internal oxidation in the zone C-E does not become significant until after about 4 hours.

At 1200°C (Figure 33) and 1260°C (Figure 34) the entire sample is internally oxidized after 4 hours. Parabolic oxidation behavior is noted for the entire oxidation process. The parabolic rate constant for this process is found to be between $4.33 - 5.09 \text{ mg}^2/\text{cm}^4\text{-min}$. Zones B and F are rapidly consumed between 4 and 16 hours at 1200°C. The parabolic behavior at 1200°C - 1260°C indicates that the scale is sufficiently plastic to provide continuous barrier to oxygen transport. At 1000°C, the parabolic oxidation behavior gave way to an apparent break away oxidation behavior probably because the scale was not as plastic at that temperature.

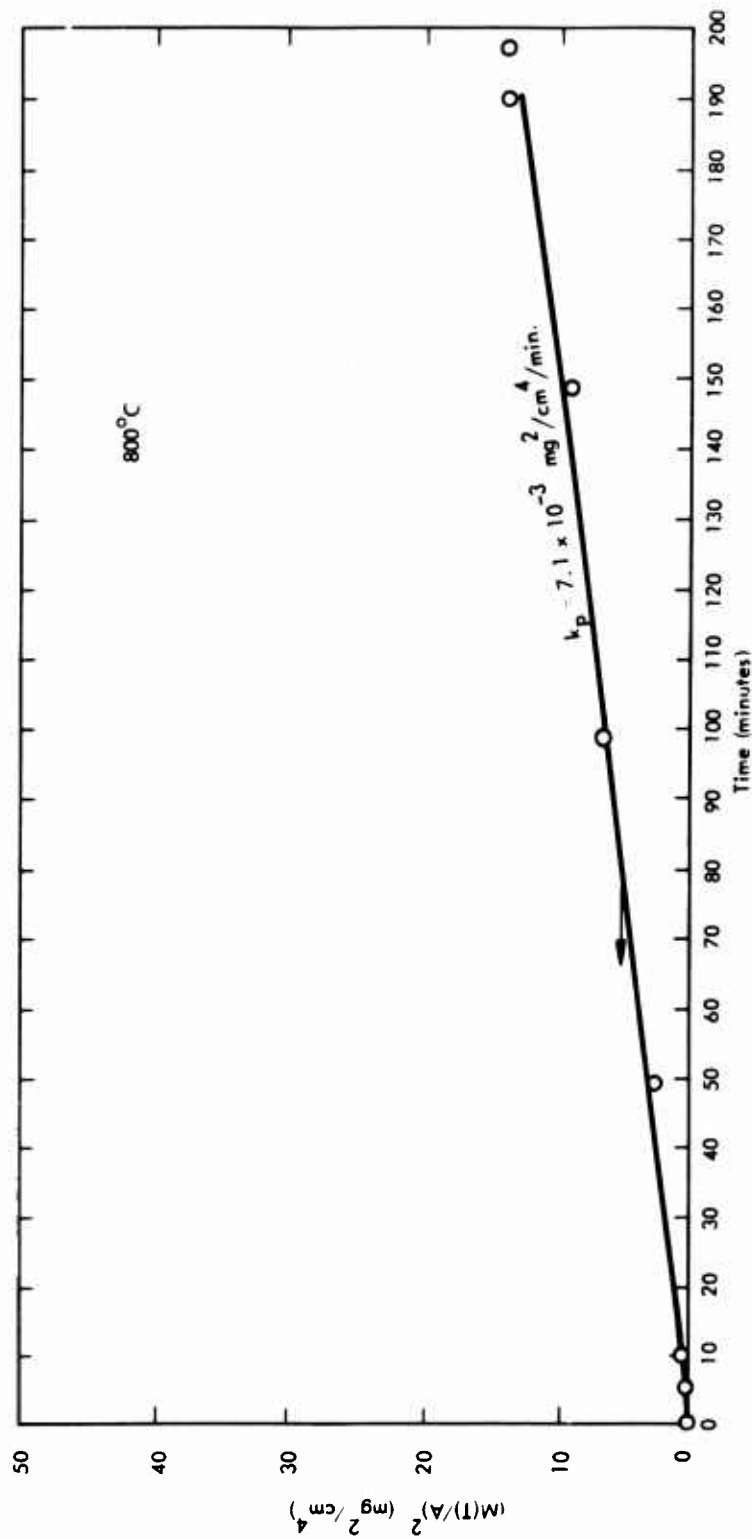


Figure 31. Plot of $(M(t)/A)^2$ vs Time Used to Determine the Parabolic Oxidation Constant for B-1 at 800°C

TABLE 10. Parabolic Oxidation Constants for the Initial Oxidation of B-1 Alloys

Temp. (°C)	k_p $\text{mg}^2/\text{cm}^4\text{-min}$
800	7.1×10^{-3}
1000	1.62×10^{-1}
1200	5.09
1200	4.33
1260	4.86
1260	3.75

$$k_p = 4.42 \times 10^7 e^{-\frac{48,100}{RT}}$$

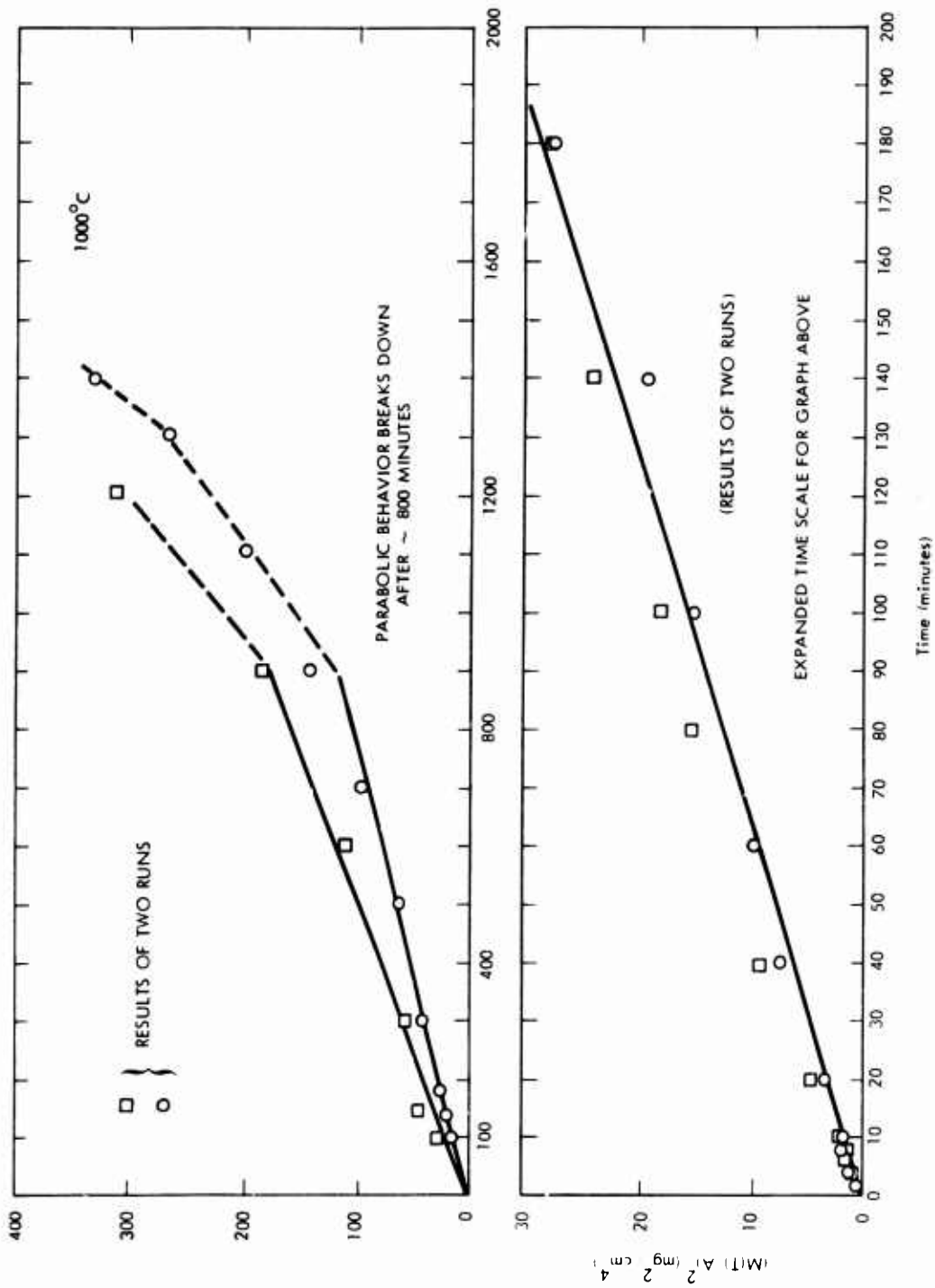


Figure 32. Plot of $(M(t)/A)^2$ vs Time Used to Determine the Parabolic Oxidation Constant for B-1 at 1000°C

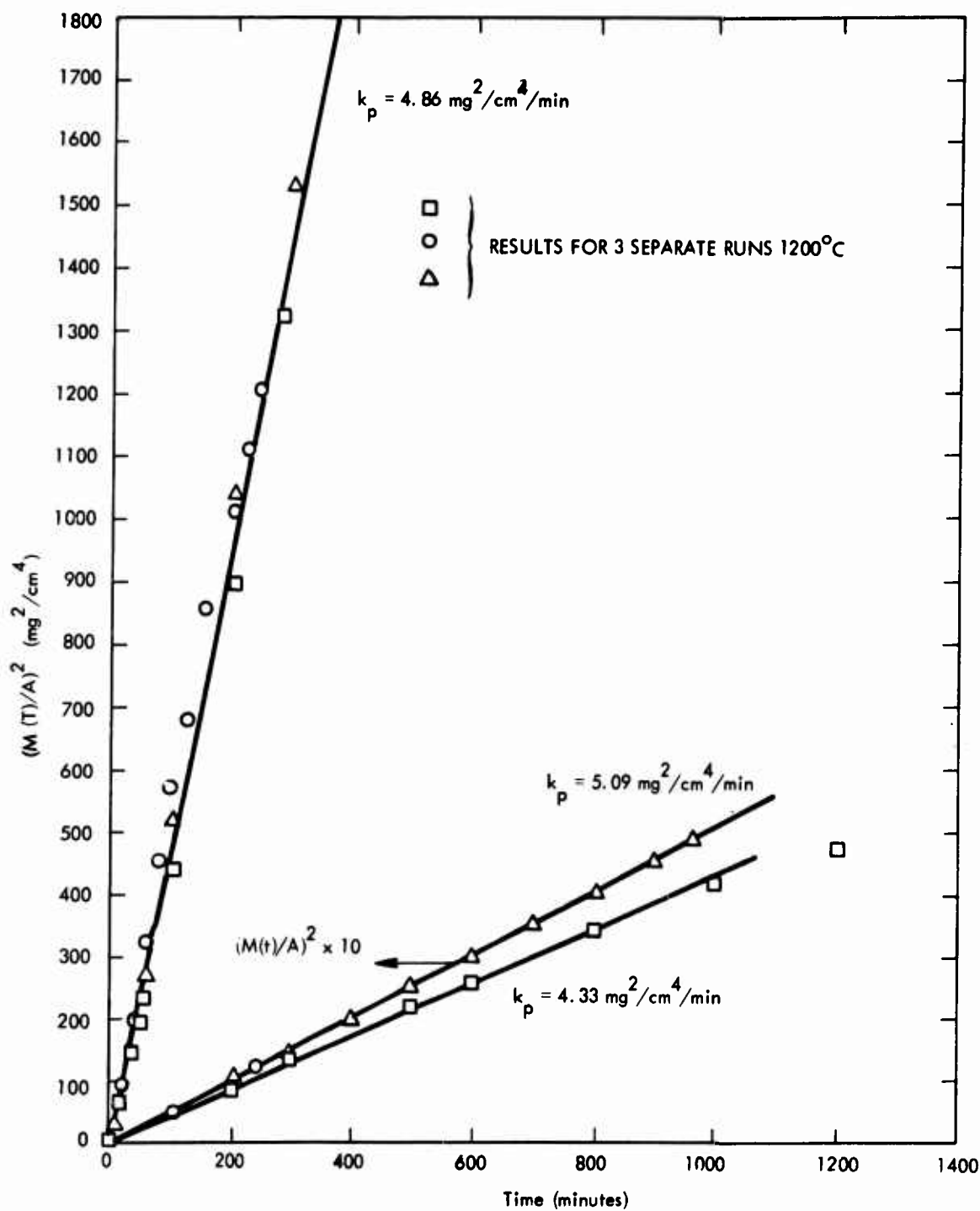


Figure 33. Plot of $(M(t)/A)^2$ vs Time Used to Determine the Parabolic Oxidation Constant for B-1 at 1200°C

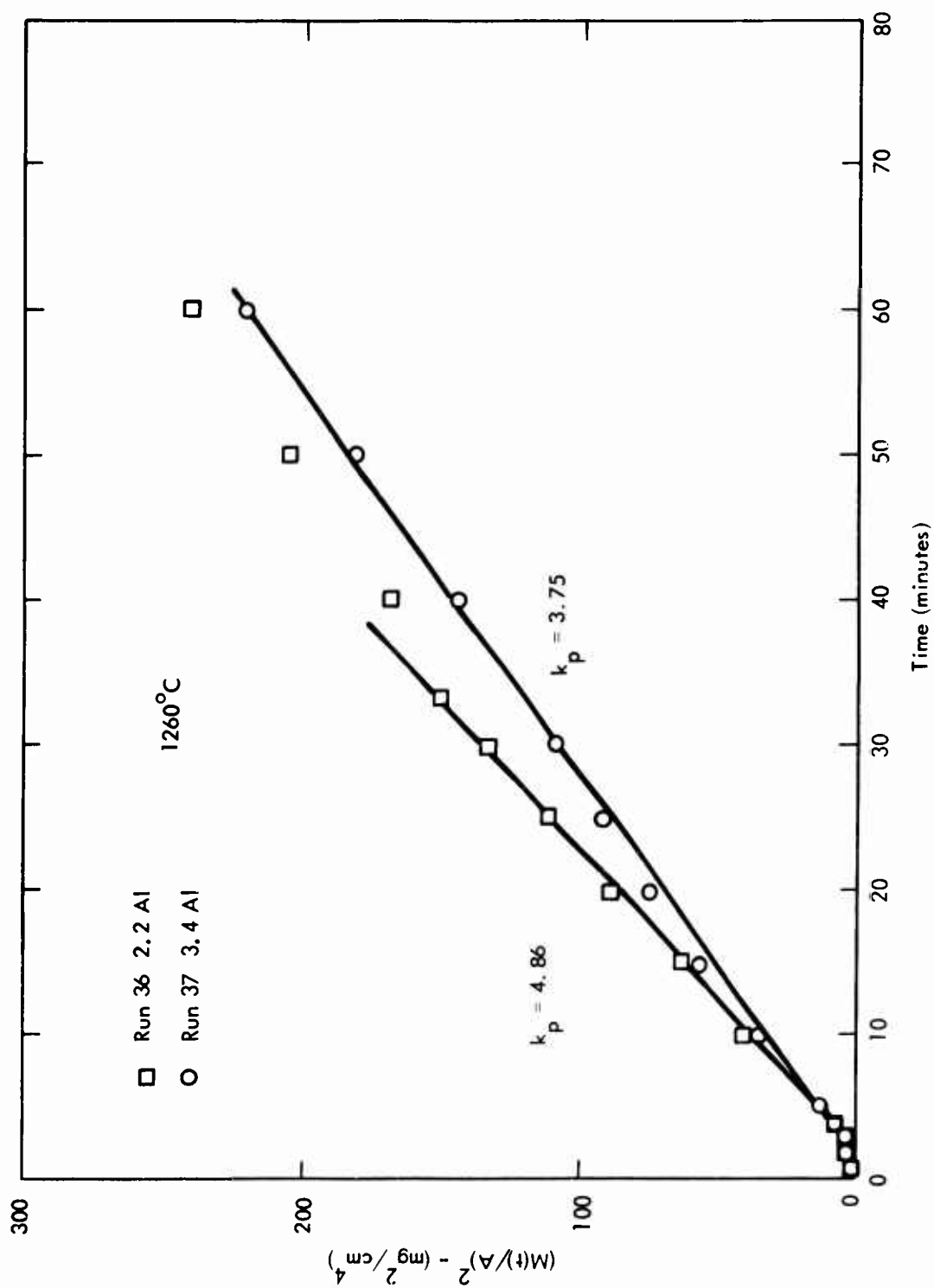


Figure 34. Plot of $(M(t)/A)^2$ vs Time Used to Determine the Parabolic Oxidation Constant for B-1 at 1260°C

X-ray analysis of scales formed on B-1 have indicated that the oxide contains strong lines indicating that TiO_2 is present in oxide. Rapp and Goldberg⁽²⁹⁾ have reported that during the oxidation of Nb-Zr alloys, ZrO_2 particles are present in the oxide, formed from internal oxidation products formed in the metallic phase prior to consumption by the oxide scale.

The parabolic rate constants plotted as a function of $1/T$ are presented in Figure 3.5. The rate constant equation computer fit to these limited number of points gives the relationship

$$k_p = (4.26 \pm 1.65) \times 10^7 \exp\left(\frac{48,100 \pm 9,500}{RT}\right) \text{ mg}^2/\text{cm}^4\text{-min}$$

for the parabolic scaling constant for short times for all of the temperature ranges investigated. At 800°C , the parabolic rate constant becomes linear after several hundred minutes, at 1000°C , the parabolic behavior switches to a break away type oxidation behavior; and at 1200°C , the oxidation behavior is parabolic for the times tested for 0.020 inch thick samples.

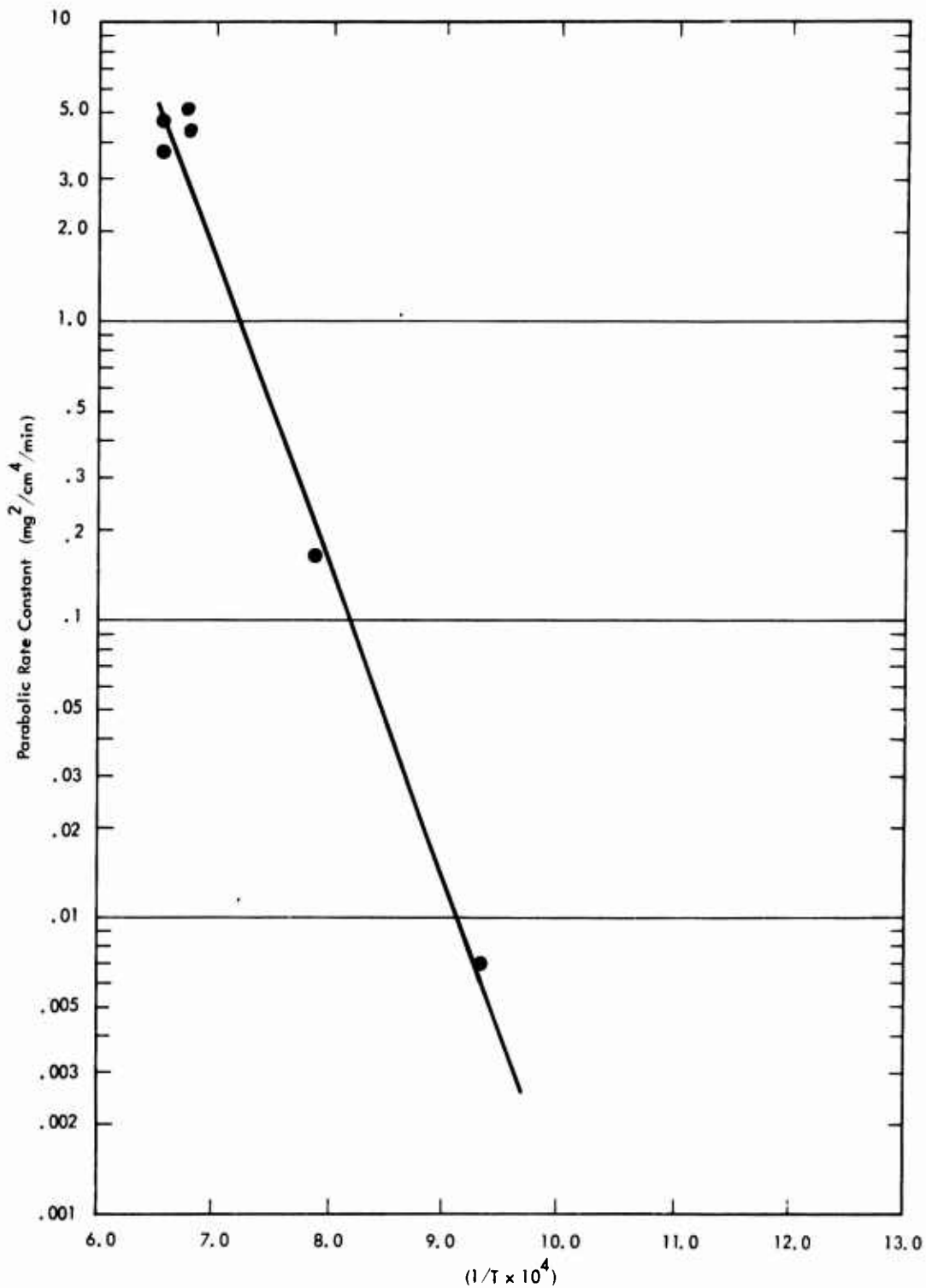


Figure 35. Plot of the Parabolic Rate Constant vs $1/T$ Used to Calculate the Activation Energy for the Initial Diffusion Controlled Oxidation Process Found in B-1 Alloys

V. EFFECTS OF LOW OXYGEN PARTIAL PRESSURE PREOXIDATION EXPOSURE ON THE AIR OXIDATION BEHAVIOR OF Nb

Four pure Nb samples pre-exposed in low oxygen partial pressures (10^{-14} to 10^{-18} atm) at 600–800°C by reaction in purified helium or CO/CO₂ gas mixtures were oxidized in air at 1100°C. The results of these four oxidation exposures are listed in Figure 35. Sample variations in kinetics were observed. Sample No. 29 exhibited the lowest oxidation rate. The initially slow rate of oxidation for the Samples No. 27 and No. 29 during the first 5–7 minutes is similar to that observed for pure niobium in 20 torr oxygen as a result of the autoclave pre-exposure during Phase I of this program⁽¹⁾.

X-ray results of the oxides formed during pre-oxidation exposure of four Nb samples to low oxygen partial pressure is given in Table 11. Although no significant improvement in the overall oxidation rate was observed the initial oxidation kinetics varied significantly enough to warrant a look at the structure of the pre-oxidation products. Both Runs 32 and 34 indicated slower initial oxidation kinetics, and both samples were shown to have the most cubic NbO phase present on the pre-oxidized surface.

This is consistent with the work of Wlodek⁽³⁰⁾ where the effects of 3% Al and 3% V stabilized a protective layer of NbO and caused a significant increase in oxidation resistance within the range of 800 to 1200°C.

Table 11. Oxides Found on Pre-Oxidized Nb Before Air Exposure

Run No.	Pretreatment	X-ray Results (Surface Diffraction)
32	Temperature 635°C He gas 88 min. CO/CO ₂ mixture 32 min. PO ₂ = 10 ⁻²³ atm	Oriented Nb - cubic NbO
33	Temperature 805°C He gas 70 min. CO/CO ₂ 300 min. PO ₂ = 10 ⁻¹⁷ atm	Oriented Nb - cubic NbO - plus one or more of the various Nb ₂ O ₅ patterns - close fit to NbO ₂
34	Temperature 800°C He gas 330 min. PO ₂ = 10 ⁻⁶ atm	Oriented Nb - cubic NbO - plus one or more of the various Nb ₂ O ₅ patterns - NbO stronger than on sample 33
35	Temperature 800°C He gas (cleaned over Ti sponge) PO ₂ = 10 ⁻⁸ atm	Oriented Nb plus a few weak, ill defined peaks or broad, diffuse "humps"

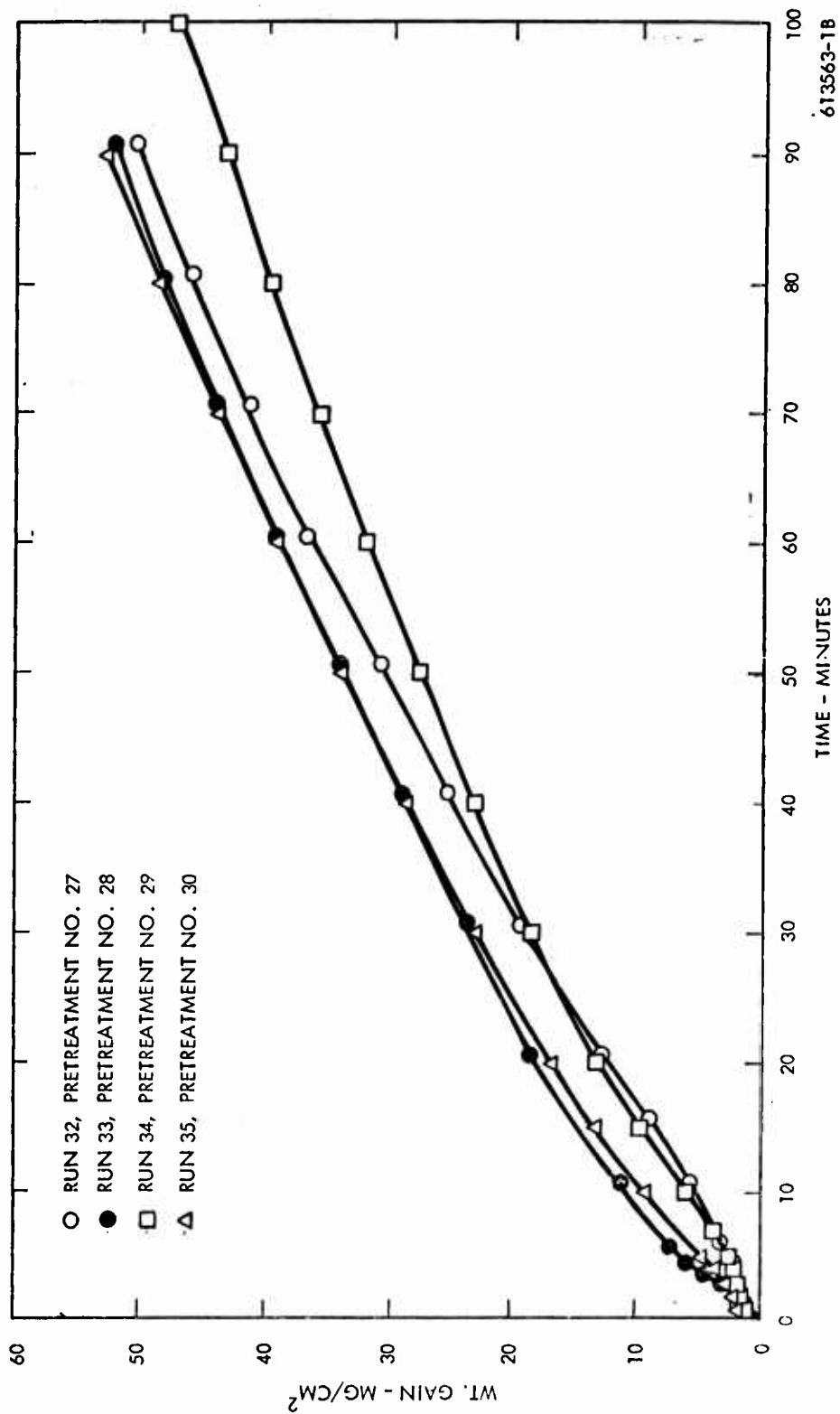


Figure 36. Effect of Preexposure on the Air Oxidation of Pure Nb.

VI. CONCLUSIONS

1. The diffusion coefficients of oxygen in the niobates $\text{TiO}_2\text{-Nb}_2\text{O}_5$ and $\text{HfO}_2\text{-Nb}_2\text{O}_5$ are too large for these oxides to be considered as diffusion barriers for the oxidation protection of Nb alloys.
2. $\text{Al}_2\text{O}_3\text{-Nb}_2\text{O}_5$ exhibits no measurable deviations from stoichiometry. $\text{NiO-Nb}_2\text{O}_5$ exhibits no measurable deviations from stoichiometry until partial oxygen pressures reach 10^{-13} atm or lower.
3. The oxidation mechanism of the Nb based alloy B-1 was studied. A parabolic rate constant for initial oxidation of the alloy was determined.

$$k_p = \left[(4.24 \pm 1.6) \times 10^{-7} \right] \exp \left[\frac{48,000 \pm 9,500 \text{ cal}}{RT} \right] \text{mg}^2/\text{cm}^4\text{-min}$$

At 800°C a very slow linear oxidation process controls the oxidation rate of B-1. At 1000°C the long time oxidation behavior is linear to break away, and a 0.020 mil sample is consumed in 80 hours.

4. Pre-oxidation of Nb at reduced oxygen partial pressures to form NbO affected the kinetics of subsequent air oxidation behavior.

VII. REFERENCES

1. Svedberg, R. C., "Modification and Control of Oxide Structures on Metals and Alloys", WANL-PR(XXX)-001
2. Ibid, p. 54.
3. Berard, M. F., "Diffusion in Ceramic Systems; A Selected Bibliograph", IS-448, May 1962
4. Brett, J., and Seigle, L. L., "The Diffusional Limitations in High Temperature Protective Oxide Coatings", Met. Soc. Conf. Vol. 41, Gordon & Breach, New York, 1967, p. 1019.
5. Douglass, D. L., "Oxidation of Metals," Vol. 1, 127 (1969)
6. Goldschmidt, H. J., "Interstitial Alloys," Plenum Press, New York, 1967, pp. 419-422.
7. Compilation of Diffusion Data, Published by Diffusion Information Center, 22447 Lake Road 205D, Cleveland, Ohio 44116
8. Kubaschewski, O., and Hopkins, B. E., "Oxidation of Metals and Alloys", Butterworths, London, 1967, p. 14
9. Sheasby, J. S., Smeltzer, W. W., and Jenkins, A. E., J. Elect. Chem. Soc. Vol. 115, (1968), p. 338.
10. Kofstad, P., and Anderson, P. J., J. Phys, Chem. Solids, V. 21, p. 280 (1961)
11. Kopstad, P., J. Phys, Chem. Solids, V. 23, p. 1571 (1962)
12. Jannick, P. F., and Whitmore, D. H., J. Chem. Phys. V. 37, p. 2750, (1962)
13. Blumenthal, R. N., Moser, J. B., and Whitmore, D. H., J. Am. Ceram. Soc., V. 48, p. 617 (1965)
14. Bransky, I., Tallan, N. M., Wimmer, J. M., and Gviski, M., J. Am. Ceram. Soc., V. 54, No. 1, Jan. 1971
15. Levin, R. L., Wagner, J. B., Jr., Trans. AIME, V. 233 (1) p. 159 (1965)
16. Price, J. B., and Wagner, J. B., Jr., Z. Phys, Chem. (Frankfurt and Main), V. 49, p. 257, (1966)
17. Walters, L. C., and Grace, R. E., J. Phys, Chem. Solids. V. 28, p. 245, (1967)
18. Campbell, R. H., Koss, and Keeffe, M. O., "Mass Transport in Oxides", ed. J. B. Wachtman, Jr., and A. D. Franklin; Nat. Bur. Stand. (US), Spec. Publ., 296, (1968)

REFERENCES (Cont'd.)

19. Lay, K. W., J. Amer. Ceram. Soc., V. 53, p. 369 (1970)
20. George, W. L., Grace, R. E., J. Phys. Chem. Solids, V. 30, 889 (1969)
21. Sheasby, J. S., Smeltzer, W. W., and Jenkins, A. E., J. Electrochem. Soc. V. 115, p. 338 (1968)
22. Crank, J., The Mathematics of Diffusion, Oxford Univ. Press, London, 1956
23. Wagner, J. B., Jr., Ib.d. No. 18, p. 65
24. Schäfer, H., Berguer, D., Gruehn, R., Z. Anorg. Allgem. Chem. V 365, 31 (1969)
25. Streiff, R., Poulton, D. J., Smeltzer, W. W., Oxid. of Metals, V.3, No. 1 (1971)
26. Kofstad, P., J. of Less Common Metals, V. 14, 153 (1968)
27. Sheasby, J. S., Cox, R., J. of Less Common Metals, V. 15, p. 129 (1968)
28. Wadsley, A. D., Acta Cryst, V. 14, p. 660 (1961)
29. Rapp, R. A., and Goldberg, G. N., Trans. AIME, V. 236, p. 1619 (1966)
30. Wlodek, S. T., Columbium Metallurgy, ed. by D. E. Douglass and F. W. Kunz, Met. Soc. Conf. V. 10, Interscience, New York, 1961, p. 553
31. Comie, J. A., Goodspeed, R. C., Development of Ductile Oxidation Resistant Columbium Alloy, AFML-TR-69-64, July 1969
32. Private Communication, R. L. Ammon, WANL
33. Lories, L., Compt. Rend., V. 231, p. 522 (1950)

APPENDIX A

DATA COMPILATION

The data gathered during these experiments are tabulated in Appendix A. The first two columns of the data sheets are the experimental data, time in seconds, and corrected weight loss in milligrams. The third column is the quantity $-\log (1 - M(t)/Q)$ when plotted as a function of time; the slope of this plot is used to determine the values of D for various oxides ; $M(t)/Q$ in the fourth column is the ratio of the amount of oxygen lost at the specified time and divided by the total amount lost during the equilibration. The fifth column is a tabular of the weight loss per area for the sample (mg/cm^2). The square of this value plotted as a function of time is used to evaluate the value of D for the initial

TABLE A-1. Weight Losses for Nb_2O_5 Between the Oxygen Partial Pressure Range of 4.35×10^{-2} to 3.7×10^{-12} atm at 967°C

TIME-SEC	WT-LOSS	$\text{LOG}(1-\text{M(T)}/\text{O})$	$\text{M(T)}/\text{O}$	$\text{M(T)}/\text{A}$
60	$2.3\text{E}-2$	-.124053	.116667	$4.07112\text{E}-3$
120	$6.4\text{E}-2$	-.310155	.266667	$9.30555\text{E}-3$
180	$9.6\text{E}-2$	-.510326	.4	$1.39583\text{E}-2$
240	.116	-.660357	.433333	$1.63663\text{E}-2$
300	.128	-.76214	.533333	$1.86111\text{E}-2$
360	.136	-.836242	.566667	$1.97743\text{E}-2$
420	.14	-.875469	.583333	$2.03559\text{E}-2$
480	.144	-.916291	.6	$2.09375\text{E}-2$
750	.168	-1.20397	.7	$2.44271\text{E}-2$
1080	.18	-1.38629	.75	$2.61714\text{E}-2$
1380	.198	-1.74297	.825	$2.8739\text{E}-2$
1980	.204	-1.39712	.85	$2.96614\text{E}-2$
2580	.216	-2.30259	.9	$3.14062\text{E}-2$
3180	.224	-2.70805	.933333	$3.25694\text{E}-2$
3780	.232	-3.4012	.966667	$3.37326\text{E}-2$
4380	.236	-4.09434	.983333	$3.43142\text{E}-2$
4980	.223	-2.39573	.95	$3.3151\text{E}-2$
5580	.22	-2.48491	.916667	$3.19873\text{E}-2$

Reproduced from
best available copy.

TABLE A-2. Weight Losses for Nb_2O_5 Between the Oxygen Partial Pressure Range of 3.7×10^{-12} to 6.45×10^{-15} atm at 967°C

TIME-SEC	WT-LOSS	$\text{LOG}(1-M(T)/G)$	$M(T)/G$	$M(T)/A$
120	2.8E-2	-5.24465E-2	5.10949E-2	4.07118E-3
180	9.3E-2	-.185978	.169708	1.35221E-2
240	.152	-.324861	.277372	2.21007E-2
300	.216	-.50114	.394161	3.14062E-2
360	.264	-.657301	.481752	3.83854E-2
420	.368	-1.11332	.671533	5.35069E-2
480	.408	-1.36463	.744526	5.93229E-2
540	.436	-1.58778	.79562	6.3394E-2
600	.46	-1.82894	.839416	6.68836E-2
660	.472	-1.97554	.861314	6.86284E-2
720	.484	-2.14739	.883212	7.03732E-2
780	.5	-2.43507	.912409	7.26996E-2
840	.512	-2.72276	.934307	7.44444E-2
900	.532	-3.53369	.970803	7.73524E-2
1800	.54	-4.22683	.985401	7.85155E-2
2400	.54	-4.22683	.985401	7.85155E-2
3000	.52	-2.97407	.948905	7.56076E-2
3600	.54	-4.22683	.985401	7.85155E-2
4200	.532	-3.53369	.970803	7.73524E-2
4800	.54	-4.22683	.985401	7.85155E-2
5400	.54	-4.22683	.985401	7.85155E-2
6000	.532	-3.53369	.970803	7.73524E-2
7200	.532	-3.53369	.970803	7.73524E-2



TABLE A-3. Weight Losses for Nb₂O₅ Between the Oxygen Partial Pressure Range of 6.45×10^{-15} to 3.3×10^{-17} atm at 967°C

TIME-SEC	WT-LOSS	LOG(1-M(T)/C)	M(T)/C	M(T)/C
60	5.2E-2	-2.93144E-2	2.33839E-2	7.56076E-3
120	.148	-9.58E-2	8.22222E-2	2.15191E-2
180	.242	-.145668	.135556	3.54774E-2
240	.336	-.206614	.186667	4.83521E-2
300	.424	-.268606	.235556	6.16422E-2
360	.512	-.334696	.284444	7.44444E-2
420	.588	-.395515	.326667	8.54947E-2
480	.644	-.442821	.357778	9.36371E-2
540	.68	-.474453	.377778	9.83714E-2
600	.733	-.575353	.437778	.114575
660	.844	-.632734	.468889	.122717
720	.892	-.684298	.495556	.129696
780	.936	-.733769	.52	.136034
840	.976	-.781371	.542222	.14121
900	1.012	-.826044	.562222	.147144
1200	1.028	-.846557	.571111	.14947
1500	1.204	-1.1053	.668333	.175061
1800	1.248	-1.18199	.693333	.181453
2400	1.312	-1.30523	.723333	.190764
3000	1.372	-1.43642	.762222	.199483
3600	1.436	-1.59339	.797778	.203793
4200	1.434	-1.7393	.824444	.215772
6000	1.564	-2.03171	.863333	.227402
7200	1.62	-2.30252	.9	.235547
8400	1.656	-2.52573	.92	.240731
9600	1.663	-2.61274	.926667	.242526
10800	1.692	-2.81341	.94	.246015
12000	1.716	-3.06473	.953333	.249505

Reproduced from
best available copy.

TABLE A-4. Weight Losses for 1.67:1 $\text{TiO}_2\text{-Nb}_2\text{O}_5$ Between the Oxygen Partial Pressure Range of 5.75×10^{-2} to 4.6×10^{-15} atm at 819°C

TIME-SEC	WT-LOSS	LOG(1-M(T)/O)	M(T)/O	M(T)/A
60	8.E-3	-4.00804E-3	4.E-3	1.12419E-3
120	2.E-2	-1.00503E-2	1.E-2	2.81047E-3
180	2.8E-2	-1.40989E-2	1.4E-2	3.93466E-3
480	5.6E-2	-2.83995E-2	2.8E-2	7.86932E-3
780	9.6E-2	-4.91902E-2	4.8E-2	1.34903E-2
1080	.128	-6.61398E-2	6.4E-2	1.7987E-2
1680	.212	-.11205	.106	2.9791E-2
2280	.284	-.153151	.142	3.99087E-2
2880	.348	-.191161	.174	4.89022E-2
3480	.4	-.223144	.2	5.62094E-2
4080	.464	-.263966	.232	6.52029E-2
4680	.512	-.295714	.256	7.1948E-2
5310	.568	-.334075	.284	7.98174E-2
6480	.65	-.393043	.325	9.13403E-2
7680	.732	-.455706	.366	.102863
8880	.812	-.520876	.406	.114105
10080	.86	-.562119	.43	.12085
11280	.93	-.625439	.465	.130637
14280	1.116	-.816445	.558	.156824
17280	1.176	-.886732	.588	.165256
20280	1.316	-1.07294	.658	.184929
23280	1.392	-1.19073	.696	.195609
26280	1.492	-1.37042	.746	.209661
29280	1.574	-1.54646	.787	.221184
32280	1.624	-1.67131	.812	.22821
35280	1.72	-1.96611	.86	.2417
38280	1.8	-2.30259	.9	.258942
41280	1.76	-2.12026	.88	.247321
44280	1.8	-2.30259	.9	.258942
47280	1.824	-2.43042	.912	.256315
50280	1.824	-2.43042	.912	.256315
53280	1.86	-2.65926	.93	.261374

TABLE A-5. Weight Losses for 1.67:1 $\text{TiO}_2\text{-Nb}_2\text{O}_5$ Between the Oxygen Partial Pressure Range of 4.6×10^{-15} to 6.06×10^{-18} atm at 819°C

TIME-SEC	WT-LOSS	$\text{LOG}(1-\text{M(T)/O})$	M(T)/O	$\Delta\text{C(T)/O}$
60	3.2E-2	-6.95933E-2	6.72262E-2	4.42675E-3
120	5.6E-2	-1.125163	.117647	7.36932E-3
180	8.4E-2	-1.124156	.176471	1.13049E-2
240	.132	-1.324776	.277311	1.35491E-2
300	.168	-1.435313	.352941	2.36085E-3
360	.2	-1.545017	.420163	2.31047E-2
420	.224	-1.635939	.470583	3.14773E-2
480	.248	-1.736072	.521003	3.48408E-2
540	.252	-1.753772	.522412	3.54112E-2
600	.268	-1.82738	.563025	3.76603E-2
660	.263	-1.82742	.563025	3.76603E-2
720	.273	-1.877151	.584034	3.90655E-2
780	.284	-1.907922	.596639	3.99087E-2
840	.292	-1.950432	.613445	4.10322E-2
900	.3	-1.994934	.630252	4.21571E-2
1200	.34	-1.25276	.714236	4.7773E-2
1500	.352	-1.34514	.739496	4.94643E-2
1800	.368	-1.48329	.773109	5.17127E-2
2400	.392	-1.7346	.823529	5.50352E-2
3000	.404	-1.83375	.848739	5.67715E-2
3600	.42	-2.14007	.882353	5.90199E-2
4200	.428	-2.29422	.90916	6.01441E-2
4800	.44	-2.5819	.92437	6.18303E-2
5400	.444	-2.69968	.932773	6.23924E-2
6000	.452	-2.98736	.94953	6.35166E-2
7200	.452	-2.98736	.94953	6.35166E-2
8400	.472	-4.77912	.991597	6.63271E-2
9600	.472	-4.77912	.991597	6.63271E-2

Reproduced from
best available copy.

TABLE A-6. Weight Losses for 1:67:1 TiO₂-Nb₂O₅ Between the Oxygen Partial Pressure Range of 6.06×10^{-18} to 4.9×10^{-20} atm at 819°C

TIME-SEC	WT-LOSS	LOG(1-M(T)/O)	M(T)/O	M(T)/A
60	7.2E-2	-.113329	.107143	1.01177E-2
120	.112	-.182322	.166667	1.57386E-2
180	.144	-.241162	.214286	2.02354E-2
240	.168	-.287682	.25	2.3608E-2
300	.192	-.336472	.285714	2.69805E-2
360	.216	-.387766	.321429	3.03531E-2
420	.24	-.441833	.357143	3.37256E-2
480	.26	-.489235	.386905	3.65361E-2
540	.272	-.518794	.404762	3.82224E-2
600	.288	-.559616	.428571	4.04708E-2
660	.3	-.591364	.446429	4.21571E-2
720	.316	-.635328	.470238	4.44054E-2
780	.332	-.681313	.494048	4.66538E-2
840	.344	-.717245	.511905	4.83401E-2
900	.36	-.767255	.535714	5.05885E-2
1200	.384	-.847298	.571429	5.3961E-2
1500	.472	-1.21194	.702381	6.63271E-2
1800	.504	-1.38629	.75	7.08239E-2
2400	.552	-1.72277	.821429	7.7569E-2
3000	.568	-1.86587	.845233	7.98174E-2
3600	.584	-2.03292	.869048	8.20657E-2
4200	.596	-2.17953	.886905	8.3752E-2
4800	.616	-2.48491	.916667	8.65625E-2
5400	.62	-2.55901	.922619	8.71246E-2
6000	.628	-2.72607	.934524	8.82488E-2
7200	.628	-2.72607	.934524	8.82488E-2
8400	.624	-2.63906	.928571	8.76867E-2
9600	.612	-2.41591	.910714	8.60004E-2
10800	.624	-2.63906	.928571	8.76867E-2
12000	.632	-2.82138	.940476	8.83109E-2
15000	.668	-5.12397	.994048	9.33697E-2

TABLE A-7 Weight Losses for 2.85:1 HfO₂-Nb₂O₅ Between the Oxygen Partial Pressure Range of 6.6×10^{-16} to 8.42×10^{-19} atm at 786°C

TIME-SEC	WT-LOSS	LOG(1-M(T)/O)	M(T)/O	M(T)/A
60	1.2E-2	-8.70114E-2	8.33333E-2	1.62013E-3
120	2.4E-2	-.132322	.166667	3.24035E-3
180	3.2E-2	-.251314	.222222	4.32047E-3
240	4.8E-2	-.405465	.333333	6.4807E-3
300	5.6E-2	-.492477	.388889	7.56082E-3
360	6.8E-2	-.63908	.472222	9.18099E-3
420	7.6E-2	-.750306	.527778	1.02611E-2
480	8.E-2	-.81093	.555556	1.03012E-2
540	8.E-2	-.81093	.555556	1.03012E-2
600	8.E-2	-.81093	.555556	1.03012E-2
660	8.4E-2	-.875469	.583333	1.13412E-2
720	8.8E-2	-.944462	.611111	1.13813E-2
780	8.8E-2	-.944462	.611111	1.13813E-2
1080	8.E-2	-.81093	.555556	1.03012E-2
1380	7.2E-2	-.693147	.5	2.72105E-3
1680	7.6E-2	-.750306	.527778	1.02611E-2
2280	8.4E-2	-.875469	.583333	1.13412E-2
2880	8.E-2	-.81093	.555556	1.03012E-2
3480	9.6E-2	-1.09361	.666667	1.22614E-2
4080	.108	-1.38629	.75	1.45816E-2
4680	.124	-1.97408	.861111	1.67418E-2
5280	.136	-2.89037	.944444	1.8368E-2
5880	.132	-2.48491	.916667	1.73219E-2
7080	.14	-3.58352	.972222	1.82022E-2
8280	.116	-1.63761	.805556	1.56617E-2
9480	.14	-3.58352	.972222	1.82022E-2
10680	.132	-2.48491	.916667	1.73219E-2
14880	.14	-3.58352	.972222	1.82022E-2

Reproduced from
best available copy.

TABLE A-8 Weight Losses for 2.85:1 HfO₂-Nb₂O₅ Between the Oxygen Partial Pressure Range of 8.42×10^{-19} to 8.69×10^{-22} atm at 786°C

TIME-SEC	WT-LOSS	LOG(1-M(T)/G)	M(T)/G	M(T)/A
60	4.E-3	-3.07716E-2	3.0303E-2	5.40058E-4
120	1.6E-2	-.129212	.121212	2.16023E-3
180	2.8E-2	-.238411	.212121	3.78041E-3
240	4.4E-2	-.405465	.333333	5.94064E-3
300	5.2E-2	-.500775	.393939	7.02076E-3
360	6.E-2	-.606136	.454545	8.10088E-3
420	6.4E-2	-.663294	.484848	8.64093E-3
480	6.8E-2	-.723919	.515152	9.18099E-3
540	7.2E-2	-.788457	.545455	9.72105E-3
840	9.2E-2	-1.19392	.69697	1.24213E-2
1140	.108	-1.70475	.818182	1.45816E-2
1440	.124	-2.80336	.939394	1.67418E-2
2040	.128	-3.49651	.969697	1.72819E-2
2640	.124	-2.80336	.939394	1.67418E-2
3240	.124	-2.80336	.939394	1.67418E-2
3900	.116	-2.11021	.878788	1.56617E-2
4440	.116	-2.11021	.878788	1.56617E-2
5040	.1	-1.41707	.757576	1.35015E-2
5640	8.4E-2	-1.0116	.636364	1.13412E-2
6840	8.8E-2	-1.09861	.666667	1.18813E-2
8040	.104	-1.5506	.787879	1.40415E-2
9240	.12	-2.3979	.909091	1.62018E-2
10440	.12	-2.3979	.909091	1.62018E-2

TABLE A-9 Weight Losses for 2.85:1 HfO₂-Nb₂O₅ Between the Oxygen Partial Pressure Range of 3.1×10^{-2} to 8.11×10^{-12} atm at 983°C

TIME-SEC	WT-LOSS	LOG(1-M(T)/C)	M(T)/C	M(T)/A
60	2.8E-2	-.492477	.333339	3.78041E-3
120	4.E-2	-.81093	.555556	5.40058E-3
180	5.2E-2	-1.23093	.722222	7.02076E-3
240	6.E-2	-1.79176	.833333	8.10038E-3
300	6.E-2	-1.79176	.833333	8.10038E-3
360	6.E-2	-1.79176	.833333	8.10038E-3
420	6.E-2	-1.79176	.833333	8.10038E-3
480	6.4E-2	-2.19722	.833339	8.64093E-3
540	6.4E-2	-2.19722	.833339	8.64093E-3
600	7.2E-2			

Reproduced from
best available copy.



TABLE A-10 Weight Losses for 2.85:1 HfO₂-Nb₂O₅ Between the Oxygen Partial Pressure Range of 8.11×10^{-12} to 2.24×10^{-14} atm at 983°C

TIME-SEC	WT-LOSS	LOG(1-M(T)/O)	M(T)/O	M(T)/A
120	2.4E-2	-.141412	.131868	3.24035E-3
180	3.6E-2	-.2204	.197802	4.86053E-3
240	4.4E-2	-.276753	.241758	5.74064E-3
300	6.E-2	-.399986	.32967	8.10033E-3
360	7.2E-2	-.503526	.395604	9.72105E-3
420	9.6E-2	-.749659	.527473	1.29614E-2
480	.1	-.797287	.549451	1.35015E-2
540	.112	-.955511	.615385	1.51216E-2
600	.12	-1.07687	.659341	1.62018E-2
660	.128	-1.21502	.703297	1.72819E-2
720	.14	-1.46634	.769231	1.8902E-2
780	.156	-1.94591	.857143	2.10623E-2
840	.164	-2.31363	.901099	2.21424E-2
900	.176	-3.41225	.967033	2.37626E-2
1200	.18	-4.51086	.989011	2.43026E-2
1500	.18	-4.51086	.989011	2.43026E-2
1800	.164	-2.31363	.901099	2.21424E-2
2400	.172	-2.90142	.945055	2.32225E-2
3000	.158	-2.02595	.868132	2.13323E-2
3600	.152	-1.80281	.835165	2.05222E-2
4200	.144	-1.56642	.791209	1.94421E-2
4800	.148	-1.67765	.813187	1.99322E-2
5400	.156	-1.94591	.857143	2.10623E-2
6000	.156	-1.94591	.857143	2.10623E-2
7200	.156	-1.94591	.857143	2.10623E-2
8400	.15616	-1.95208	.858022	2.10839E-2
9600	.156	-1.94591	.857143	2.10623E-2
10800	.148	-1.67765	.813187	1.99322E-2
12000	.152	-1.80281	.835165	2.05222E-2
15000	.148	-1.67765	.813187	1.99322E-2
18000	.16	-2.11296	.879121	2.16023E-2
21000	.156	-1.94591	.857143	2.10623E-2
24000	.16	-2.11296	.879121	2.16023E-2

Reproduced from
best available copy.

TABLE A-71 Weight Losses for 2.85:1 $\text{HfO}_2\text{-Nb}_2\text{O}_5$ Between the Oxygen Partial Pressure Range of 2.24×10^{-14} to 7.98×10^{-17} atm at 980°C

TIME-SEC	WT-LOSS	$\text{LOG}(1-\text{M(T)}/\text{O})$	$\text{M(T)}/\text{O}$	$\text{M(T)}/\text{A}$
60	3.6E-2	-5.35842E-2	5.21739E-2	4.86053E-3
120	.104	-.163372	.150725	1.40415E-2
180	.16	-.263315	.231884	2.16023E-2
240	.208	-.358748	.301449	2.8083E-2
300	.244	-.436373	.353623	3.29436E-2
360	.276	-.510826	.4	3.7264E-2
420	.328	-.645047	.475362	4.42343E-2
480	.356	-.725551	.515942	4.80652E-2
540	.342	-.684489	.495652	4.6175E-2
600	.428	-.968347	.62029	5.77862E-2
660	.444	-1.03136	.643478	5.99465E-2
720	.456	-1.08137	.66087	6.15667E-2
780	.482	-1.19915	.698551	6.5077E-2
840	.496	-1.26883	.718341	6.69672E-2
1200	.504	-1.31094	.730435	6.80474E-2
1500	.52	-1.40089	.753623	7.02076E-2
1800	.548	-1.58086	.794203	7.3988E-2
2400	.576	-1.80049	.834783	7.77684E-2
3000	.576	-1.80049	.834783	7.77684E-2
3600	.58	-1.83621	.84058	7.83085E-2
4200	.596	-1.9934	.863768	8.04687E-2
4800	.608	-2.12997	.881159	8.20889E-2
5400	.624	-2.34704	.904348	8.42491E-2
6000	.636	-2.54771	.921739	8.58673E-2
7200	.66	-3.13549	.956522	9.1096E-2
8400	.672	-3.64632	.973213	9.07823E-2
9600	.672	-3.64632	.973213	9.07823E-2
10800	.684	-4.74493	.991304	9.235E-2
12000	.688	-5.84355	.997101	9.282E-2

Reproduced from
best available copy.

TABLE A-12 Weight Losses for 2.85:1 HfO₂-Nb₂O₅ Between the Oxygen Partial Pressure Range of 4.6×10^{-2} to 1.2×10^{-8} atm at 1192°C

TIME-SEC	WT-LOSS	LOG(1-M(T)/O)	M(T)/O	M(T)/A
60	4.E-3	-1.50379E-2	1.49254E-2	5.40053E-4
120	6.E-2	-.253449	.223881	3.10088E-3
180	.103	-.515813	.402985	1.45816E-2
240	.144	-.770705	.537313	1.94421E-2
300	.148	-.803495	.552239	1.99822E-2
360	.148	-.803495	.552239	1.99822E-2
420	.156	-.872488	.58209	2.10623E-2
480	.16	-.908856	.597015	2.16023E-2
540	.16	-.908856	.597015	2.16023E-2
600	.16	-.908856	.597015	2.16023E-2
660	.172	-1.02664	.641791	2.32225E-2
720	.18	-1.11365	.671642	2.43026E-2
1020	.22	-1.71979	.320826	2.97032E-2
1320	.172	-1.02664	.641791	2.32225E-2
1620	.172	-1.02664	.641791	2.32225E-2
2220	.204	-1.4321	.761194	2.7543E-2
2820	.212	-1.56564	.791045	2.86231E-2
3420	.216	-1.63974	.80597	2.91632E-2
4020	.224	-1.8068	.835821	3.02433E-2
4620	.232	-2.00747	.865672	3.13234E-2
5220	.232	-2.00747	.865672	3.13234E-2
5820	.24	-2.25878	.895522	3.24035E-2
7020	.264	-4.20469	.985075	3.56439E-2

Reproduced from
best available copy.

TABLE A-13 Weight Losses for 2.85:1 HfO₂-Nb₂O₅ Between the Oxygen Partial Pressure Range of 1.2×10^{-8} to 2.92×10^{-11} atm at 1192°C

TIME-SEC	WT-LOSS	LOG(1-M(T)/O)	M(T)/O	M(T)/A
60	.124	-.242425	.215278	1.67418E-2
120	.248	-.563094	.430556	3.34836E-2
180	.316	-.795426	.548611	4.26646E-2
240	.36	-.980829	.625	4.86053E-2
300	.4	-1.18562	.694444	5.40058E-2
360	.428	-1.3589	.743056	5.77862E-2
420	.448	-1.50403	.777778	6.04865E-2
480	.468	-1.67398	.8125	6.31868E-2
540	.48	-1.79176	.833333	6.4807E-2
600	.488	-1.87877	.847222	6.58871E-2
660	.484	-1.83432	.840278	6.53471E-2
720	.484	-1.83432	.840278	6.53471E-2
720	.484	-1.83432	.840278	6.53471E-2
840	.488	-1.87877	.847222	6.58871E-2
900	.492	-1.92529	.854167	6.64272E-2
1200	.496	-1.97408	.861111	6.69672E-2
1500	.492	-1.92529	.854167	6.64272E-2
1800	.492	-1.92529	.854167	6.64272E-2
2400	.492	-1.92529	.854167	6.64272E-2
3000	.512	-2.19722	.888889	6.91275E-2
3600	.504	-2.07944	.875	6.80474E-2
4200	.516	-2.26176	.895833	6.96675E-2
4800	.504	-2.07944	.875	6.80474E-2
5400	.524	-2.40486	.909722	7.07476E-2
6000	.556	-3.36038	.965278	7.50631E-2
7200	.572	-4.96981	.993056	7.72283E-2

Reproduced from
best available copy.